AN INVESTIGATION OF THE MANUFACTURABILITY OF TUNGSTEN-COPPER FOR USE IN A COMPACT RECUPERATOR

W. Koekemoer
(B.Eng.)
12323144

Dissertation submitted in partial fulfillment of the degree

Master of Engineering

at the Potchefstroom Campus of the North-West University.

Supervisor: Prof. J Markgraaff
November 2008
Potchefstroom

Keywords

Compact recuperator, tungsten-copper, high temperature materials, recuperator design, "elkonite®", printed circuit heat exchanger®.

Abstract

A substantial raise in recuperator effectiveness has been established in the past by improving the fabricating and joining configurations regarding the manufacturing of compact recuperators. Further advancement of state-of-the-art recuperators requires providing for increased temperatures and pressures. This can only be achieved by incorporating high temperature materials into the recuperator design. Although many high temperature materials have been identified in past research, less of these can be utilized in new concepts due to difficulties regarding fabricating and joining. However recently, in an independent study, a tungsten-copper alloy was identified through detailed material selection methods as a suitable material for high temperature applications. The validity of tungsten-copper regarding fabricating and joining, to establish a leak tight structure still needs to be demonstrated.

The aim of the study is to carry out a comprehensive review of existing recuperator technologies and design methodologies as well as to investigate the manufacturability of tungsten-copper for use in a recuperator design of limited size. More specifically, the objectives entail the following: (1) The comprehensive review of existing recuperator technologies and recuperator design methodologies, (2) The design and fabrication of a recuperator of limited size using tungsten-copper as a heat transfer material and (3) The determination of the feasibility of fabrication of the design and the applicability of the selected W-Cu alloy in the design.

The fabrication technique that is presented in the design entailed the use of 2mm tungsten carbide drill bits to machine the correct recuperator profile, while the recuperator unit was joined by utilizing a mechanical fastening system. Although diffusion bonding was initially identified as the ideal joining technique for the recuperator of this research,

restrictions and limitations relating to the use of diffusion bonding has lead to the identification of a fastening system as the technique used. Evaluation of the fabricated recuperator revealed that several factors were outside the initially specified values, *inter alia* the flatness tolerance of recuperator plate geometries and machined slots precision. These factors contributed to a leaking recuperator structure when tested. The most likely contributing factors for the latter relate to non-conforming tolerances achieved in the fabricated design, residual stresses induced by the machining process as well as design issues relating to the recuperator plate geometries.

The design and fabrication of a recuperator of limited size using tungsten-copper as a heat transfer material, requires re-evaluation. Similar work will ensure a design of a high quality when provision is made for advanced surface finishing of machined parts (notably the recuperator plate geometries), slight modifications to the design as well as stress relieving of machined components for the purpose of eliminating any residual stresses that might be present.

Sleutelwoorde

Kompakte hitteruiler, wolfram-koper, hoë temperatuur materiale, hitteruiler ontwerp, "elkonite®".

Uittreksel

'n Beduidende styging in hitteruiler effektiwiteit is in die verlede gedemonstreer deur die verbetering van masjinerings- en hegtingstegnieke betrokke by die vervaardiging van kompakte hitteruilers. Verdere ontwikkeling en vordering van hierdie tegnologie kan slegs plaasvind indien hoër temperature en drukke in die hitteruiler omgewing geakkommodeer kan word. Om laasgenoemde te bewerkstellig, moet hoë werkverrigting en hoë temperatuur materiale geinkorporeër word in hitteruiler ontwerpe. Hoewel menige materiale in die verlede geïdentifiseer is vir hoë temperatuur toepassings, kan net 'n handvol van dié materiale gebruik word vanweë die ongunstige eienskappe t.o.v. vervaardiging en hegting. In 'n onlangse onafhanklike studie is 'n wolfram-koper legering geïdentifiseer as 'n uiters geskikte materiaal vir hoë temperatuur toepassings d.m.v. gedetailleerde materiaalseleksie metodes. Die geldigheid van die wolfram-koper legering t.o.v. vervaardiging en hegting moet egter nog gedemonstreer word.

Die doel van die studie is om 'n omvangryke oorsig van huidige hitteruiler tegnologieë tesame met hitteruiler ontwerp metodologieë weer te gee asook om die vervaardigbaarheid van wolfram-koper (W-Cu), vir gebruik in 'n kompakte hitteruiler, te ondersoek. Meer spesifiek, was die volgende doelwitte van belang: (1) die weergee van 'n omvangryke oorsig / hersiening van huidige hitteruiler tegnologieë tesame met hitteruiler ontwerp metodologieë (2) die ontwerp en vervaardiging van 'n hitteruiler van beperkte grootte deur gebruik te maak van W-Cu as die hitteoordrag materiaal asook (3) die evaluering van die uitvoerbaarheid van die vervaardiging van die ontwerp tesame met die toepaslikheid van die wolfram-koper allooi in die ontwerp.

Masjinering van die hitte-oordrag profiel van die kompakte hitteruiler is gedoen deur gebruik te maak van 2mm wolfram karbied boorpunte. Hegting van die eenheid is

bewerkstellig deur 'n verbindingsraam te gebruik. Alhoewel hegting deur middel van diffusie aanvanklik geidentifiseer is as die beste hegtingstegniek vir die betrokke studie is 'n verbindingsraam gebruik vanweë beperkinge ten opsigte van befondsing en toerusting beskikbaarheid. Evaluering van die vervaardigde hitteruiler het verskeie faktore onthul wat afgewyk het van die waardes wat aanvanklik gespesifiseer is. Hierdie afwykings behels onder andere die platvlak toleransie tussen die hitteruiler plate en die presisie van die gemasjineerde groewe vir afseëling. Afwyking van hierdie faktore het tot gevolg gehad dat die hitteruiler gelek het tydens toetsing. Die waarskynilke aspekte wat bydrae tot laasgenoemde sluit die volgende in: (1) afwyking van toleransies in die vervaardigde ontwerp, (2) resspannings wat veroorsaak is deur masjinering van hitte oordrag profiele asook (3) ontwerp aspekte met betrekking tot die hitte oordrag plate. .

Die ontwerp en vervaardiging van 'n kompakte hitteruiler vanuit die voorgestelde wolfram-koper legering moet geherevalueer word. In gelyksoortige werk sal gevorderde oppervlak afwerking van gemasjineerde parte (merkbaar vir die hitteruiler plate), geringe veranderinge aan die ontwerp van die hitteruiler sowel as spanningsverligting van die ontwerp materiaal 'n ontwerp van 'n hoë gehalte verseker.

Acknowledgements

This dissertation has become part of my life in the past four years, in both good and 'not so many good' ways (my wife can bear witness to that!). But now even more I am overjoyed to have completed this dissertation and to close down this 'phase' of my life. I am extremely grateful toward the following people for inspiring me in their own unique ways and helping me to complete this project:

- All thanks and praise to God for the strength He gave me and still gives me. Thank you for taking me through this experience and for all the people You brought onto my path during the progress of this project.
- My wife Eileen, for always listening to my minute problems and for always shedding an objective light on issues that seem dull and grey to me. You are truly special and inspirational and thank you for always loving me unconditionally.
- To my supervisor, Professor Johan Markgraaff, not only for giving me guidance with this project but also for other opportunities you have afforded me that helped me grow into the person I am today. It is truly appreciated.
- To THRIP, for making my study possible from a financial point of view. Thank you.
- To M-Tech Industrial for affording me the opportunity to join your workforce late in 2005 and allowing me to gain valuable experience whilst completing my studies. I will forever be grateful.
- My friends in music, Kristoff, Retief, Lindri, and everyone else at Duet/Kruispunt whom I had the privilege of making and recording music with. It was truly a blast and also instrumental with regards to 'stress relieving' in the final months of this project. Thank you.
- My Mother, Father and Brother whom I love dearly and thank for every opportunity, big or small, that was afforded to me. Thank you for all your unconditional love and support.

Table of Contents

List of Tables

List of Figures

Abbreviations and Acronyms

A	-	Heat Transfer Surface Area
A_f	-	Fin Surface Area
A_{ff}	-	Free flow area
5W3	-	Tungsten-copper – 'Elkonite'
C	-	Fluid capacity rate
C/C	-	Carbon Fiber Reinforced Carbon
Cp	-	Specific heat
CVD	-	Chemical Vapor Deposition
E	-	Young's Modulus
EDM	-	Electrical Discharge Machining
EES®	-	Engineering Equation Solver®
f	-	Fanning friction factor
h	-	Heat transfer coefficient
HAZ	-	Heat Affected Zone
IHX	-	Intermediate Heat Exchanger
k	-	Thermal conductivity
K	-	Secondary losses
L	-	Length
l_c	-	Clamping Length
LBM	-	Laser Beam Machining
LMTD	-	Log Mean Temperature Difference method
$\dot{m}$	-	Mass flow rate
NTU	-	Number of Transferred Units
Nu	-	Nusselt number
P	-	Perimeter of fin
PG	-	Pyrolytic Graphite
Pr	-	Prandlt number
PCHE	-	Printed circuit heat exchanger
PSR	-	Primary Surface Recuperator

q	-	Heat transfer
R	-	Resistance against heat transfer
R''_f	-	Fouling Factor
R_{tot}	-	Total thermal resistance to heat transfer
R_w	-	Wall Resistance against heat transfer
Re	-	Reynolds number
SS	-	stainless steel
t	-	Wall/Fin thickness
T	-	Temperature
UA	-	Overall heat transfer coefficient
V_c	-	Impact Point Velocity
V_d	-	Detonation Velocity
W-Cu	-	Tungsten-copper alloy
ε-NTU	-	Effectiveness-NTU method

Greek symbols

α	-	Heat transfer surface area density / compactness
ρ	-	Density
ΔP	-	Pressure drop
ΔT	-	Temperature drop
ε	-	Effectiveness
η_o	-	Overall surface efficiency of a finned surface

Subscripts

c	-	Cold side
e	-	Outlet
h	-	Hot side
i	-	Inlet

1 INTRODUCTION

1.1 Introduction

The development of compact recuperators in the last two decades has been the most important technological advance with respect to improved performance of closed-cycle gas turbines. Recuperator effectiveness went from a restrained 80% for large conventional recuperators in the early 1980's to about 95% with the introduction of the recently developed compact recuperators, depending on the heat duty involved [1]. Research has shown that many methods were implemented in the past to increase recuperator effectiveness with the main goal of improving the performance of closed-cycle gas turbines. These methods can primarily be divided into 2 categories:

- increasing the compactness of recuperators; and
- high temperature material considerations.

The compactness of a recuperator refers to the ratio of heat transfer surface area of the recuperator to the volume of the recuperator, otherwise known as the surface-area density. A larger effectiveness is attributed to a recuperator if its surface-area density is high. A recuperator is regarded as being 'compact' if the surface-area density exceeds a value of $700m^2/m^3$. The higher the surface-area density of a recuperator, the smaller its footprint area becomes for a specified heat output, thus making it ideal for turbogenerator designs constrained by size [2].

By increasing the surface-area density of a recuperator, the inherent porosity of the structure as a whole is also increased. The higher the porosity of the structure, the more difficult it becomes to create a leak tight, high integrity structure. Due to the latter, challenges regarding design, manufacturing and joining have been encountered in establishing a recuperator with a

high surface-area density. Some institutions have made promising developments regarding this issue, though. Recent developments in compact recuperator technology has given birth to the Printed Circuit Heat Exchanger® and the Marbond® Heat Exchanger, incorporating surface-area densities in excess of $2{,}500m^2/m^3$ and $10{,}000m^2/m^3$ respectively. The manufacturing configuration involved with these units entails a "chemical etching and diffusion bonding" process which is very costly [3]. Compact recuperators manufactured by these means deliver a surprisingly high effectiveness as well as high structural integrity of the recuperator over various ranges of temperatures and pressure differentials. Other research has also shown the efficiency of the diffusion bonding process in the successful manufacture of other similar recuperators [4]. Thus, a substantial raise in recuperator effectiveness has been established by improving the fabricating and joining configurations when manufacturing a recuperator with a high surface-area density.

Further advancement of state-of-the-art recuperators requires providing for increased temperatures and pressures. This can only be done by incorporating high temperature materials into the recuperator design. Although many high temperature materials have been identified in past research, not many of these can be utilized in new concepts as efficient recuperator materials, due to difficulties as far as fabricating and joining are concerned. A perfect example is ceramic materials, which enables high temperature operation but can be ruled out primarily due to its difficulty to fabricate and to convert to shape. Nickel-based alloys have an excellent creep-range limit of ±750-800°C, but are also limited by fabrication techniques [1]. A definite gap evidently exists between high temperature materials for use in high temperature applications and its manufacturability (or lack thereof).

In an independent study, Van Greuning [5] identified tungsten-copper as a viable material for use in high temperature applications, more specific with regard to compact recuperators. According to Van Greuning's study, tungsten-copper has excellent thermal and structural characteristics, provided by the copper and tungsten in the alloy respectively, which would be ideal for use in specialized high temperature- and high pressure applications [5].

The scope of Van Greuning's study entailed two aspects: firstly the design of a compact recuperator through the use of finite element methods and secondly the systematic and detailed selection of applicable materials for the design, which included tungsten-copper, through material selection software and procedures. The validity of tungsten-copper regarding fabricating and joining to establish a leak tight structure for use in a high temperature environment, still remains to be demonstrated.

The aim of this study is to carry out a comprehensive review of existing recuperator technologies and design methodologies and to investigate the manufacturability of tungsten-copper for use in a recuperator design of limited size. More specifically, the objectives entail the following:

- The comprehensive review of existing recuperator technologies and recuperator design methodologies.
- The design and fabrication of a recuperator of limited size using tungsten-copper (W-Cu) as a heat transfer material.
- Determination of the feasibility of fabrication of the design and the applicability of the selected W-Cu alloy in the design.

Any opportunities for further study in this regard will also be suggested.

2 LITERATURE SURVEY

2.1 Introduction

A thorough investigation and review of available recuperator technologies as well as certain related fields is necessary in order to determine the methods for establishing a recuperator relevant to this study.

This literature survey therefore presents a detailed review of the following aspects:

- **Existing recuperator technologies.** Discussion of certain important aspects from a formidable knowledge base that is relevant to this study.
- **Relevant materials and manufacturing technologies.** Existing and new recuperator materials together with applicable fabrication and joining technologies are discussed.
- **Recuperator design methodologies.** An overview of certain methodologies used in recuperator design as well as an in depth view of the recuperator design methodology used in this study.

2.2 Existing Recuperator Technologies

A formidable knowledge base relating to existing recuperator technology is available, offering valuable information pertaining to this review. In the following section, existing recuperator technologies are discussed in terms of the function of a recuperator, major heat transfer surface geometries, effective recuperator requirements for this day and age and more recent developments concerning recuperators, i.e. an in-depth look at compact recuperators.

2.2.1 What is a Recuperator?

A recuperator is defined as any device that recovers waste heat from exhaust gases for use in another process through a series of heat transfer profiles or surface geometries. The waste heat derived from these exhaust gases is generally used to preheat the compressed air in a gas turbine engine before it enters the fuel burner stage. By increasing the compressed air inlet temperature, less energy is needed to preheat the gases before combustion takes place, which makes the system in question inherently more efficient.

Existing modern recuperator expertise ranges extensively, from a primary surface recuperator manufactured in Germany in the 1970's to the more recent Printed Circuit Heat Exchanger® (PCHE) and the Marbond® Heat Exchanger concepts as developed by Heatric Inc. and Chart-Marston Inc respectively. These recuperator units incorporate only some of the available heat-transfer surface geometries for its design. From this wide variety of surface geometries available for high efficiency compact heat exchangers, only 3 types are of primary significance pertaining to this study:

- Primary surface recuperator (PSR).
- Plate-fin recuperator.
- Tubular geometries. [6]

2.2.2 Heat Transfer Surface Geometries

The ultimate goal for recuperator designers has been to engineer a recuperator based on a stack of corrugated plates that represent the entire heat transfer matrix with headering and manifolds [7]. This concept of thin-walled corrugated sheets in a recuperator is known as a

primary surface recuperator (PSR). Modern manufacturing methods (laser cutting, welding) have after many years made the concept of a PSR a reality. The PSR displays the following primary attributes;

- A surface geometry that is ±100% effective.
- Demonstrates an effectiveness of larger than ±80%.
- Sealing of passageways can easily be accomplished by welding, eliminating the need for time-consuming, expensive high temperature furnace brazing operations.

What makes this type of heat transfer surface geometry so significant, is the fact that it is one of only a handful that has successfully displayed its viability to high volume production. A total of approximately 15,000 primary surface recuperator units have been implemented in the AGT-1500 Army battle tanks [7]. A study in the late 1970's conducted by two German engineers, Dr. Manfred Kleeman & Dr. Siegfried Foerster, also displayed the flexibility of the PSR for high volume automated production in the form of an automated stamping and folding process of a continuous foil stock. Not only is the PSR flexible concerning high volume production but it also displays good performance and structural integrity at a low cost potential [6].

The **plate-fin recuperator** name implies the involvement of primary and secondary surfaces in the recuperator and is similar to the PSR with regard to the way it is assembled. A recuperator is put together in sandwich form from a series of flat sheets and corrugated fins by means of furnace brazing to form an integral unit. By using primary and secondary heat transfer surfaces, a much higher surface-area density can be obtained. Overall, this type of recuperator delivers a much higher heat transfer coefficient and increased compactness relating to the other two mentioned here. Although fouling was a common problem in this type of recuperator surface, it has shown substantial improvement in terms of structural integrity over the years. One problem worth mentioning here is the considerable amount of time and capital required by furnace brazing [2] (the process implemented to fabricate this type of recuperator). This negatively impacts the purpose of producing a minimum cost heat exchanger.

Since it would be inconsistent not to mention, reference is finally given to **tubular geometries.** This type of recuperator is known for its high cost but it comprises excellent pressure maintaining capability and finds its use in many vehicular applications.

The basic characteristics of these afore-mentioned geometries are stated in Table 2.1 for comparison purposes [8]. In the recuperator utilization graph displayed in Figure 2-1 [7], it can be seen that initially plate-fin geometries were utilized more often since the origin of recuperator technology. From the mid 1970's however (origin of PSR technology), primary surface geometries have enjoyed the most attention, retaining a steep climb regarding recuperator deployment in the last decade. The latter is followed closely by the plate-fin- and tubular geometries respectively.

Heat exchanger type	Primary Surface	Plate-fin	Tubular
Surface geometry	Formed plates	Offset fin secondary	Tube
Type of construction	Welded	Brazed	Braze, welded
Flow configuration	Counterflow	Counterflow	Cross-counterflow
Effectiveness, %	>90	>90	<85
Surface compactness, m^2/m^3	2000	2000	900
Thermal density, MW/m^3	15	15	10
Flexibility toward high volume production	Excellent	Good	Possible
Potential use for recuperated gas turbine	Yes	Yes	Possible

Table 2.1: *Comparison of plate-fin, tubular and primary surface recuperator types.* Modified after Utriainen [8].

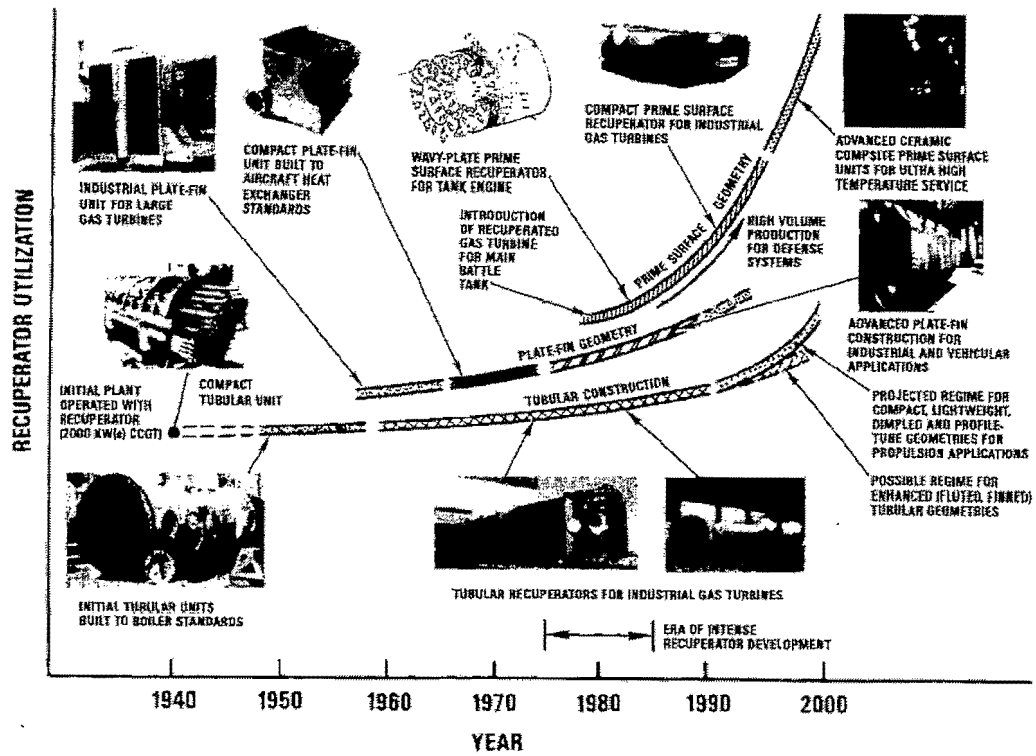

Figure 2-1: *Gas turbine recuperator evolution.* Modified after McDonald & Wilson [7].

Successful implementation of the recuperator surface geometries mentioned above into recuperator units, has been limited in the past due to several unwanted qualities - poor reliability of the recuperator structure, bulky size/weight of the recuperator and high cost of the recuperator. Recuperators needed to be more effective in terms of heat transfer, size and weight. This induced a reassessment of the recuperator requirements needed in a demanding environment, with the goal to ultimately increase cycle efficiency and decrease total turbo generator cost. These requirements and the introduction thereof into recent compact recuperator concepts are elaborated upon next.

2.2.3 Effective Recuperator Requirements

The requirements set out in a preliminary design of an effective recuperator should be fronted by a high thermal effectiveness (including high thermal conductivity and high heat transfer area) of the recuperator and low cost implications. Other important characteristics that should also be taken into account include high performance potential, compact size, light weight and proven structural integrity. Recuperators with effectiveness between 91% and 98% can lead

to an effective increase in gas turbine efficiency of ±38% [6]. A more detailed summary of these requirements for a gas turbine recuperator is given in Table 2.2.

Criteria Fields	Microturbine recuperator requirements
Major design criteria	• Low heat exchanger cost. • Meet demanding microturbine performance and economic goals. • High recuperator reliability.
Performance	• High recuperator effectiveness (η> 90%). • High thermal conductivity. • High thermal transfer. • Low pressure loss (delP< 5%). • Good part load performance.
Surface geometry	• Plate-fin surface geometry. • High surface compactness. • Superior thermal-hydraulic characteristics.
Fabrication	• Minimum number of matrix parts. • Continuous/automated fabrication process. • Welded sealing (eliminate need for furnace brazing). • Adaptable to high volume production methods. • Utilize heat exchanger industry experience (e.g. automobile radiators).
Type of construction	• Compact and light weight matrix. • Integral manifolds/headers. • Matrix envelope flexibility (annular or platular).
Cost	• No basic material wastage (zero scrap). • Minimum (or zero) labor effort. • Standardization. • Materials selection for particular duty. • Unit cost goal not to exceed 1.5 times material cost.
Integrity	• Resistant to thermal cycling. • Remain leak tight for engine life.

Table 2.2: *Microturbine recuperator requirements serving as outline for evaluation of recuperator design.* Modified after McDonald [6].

The requirements noted in Table 2.2 will subsequently be used as a framework for comparison to past and present recuperator technology. Most of these requirements have been successfully introduced into recent compact recuperator designs, which are addressed in the following section.

2.2.4 Compact Recuperators

Compact heat exchangers (CHE's) are becoming increasingly important in industrial processes. According to Reay [9] compact heat exchangers, while accounting for between 5% and 10% of the ± $15 billion world-wide market for heat exchangers, are seeing their sales increase by 10% per annum, compared to the 1% for all types of heat exchangers. This is due to a number of benefits compact heat exchangers offer:

- Improved efficiency due to closer approach temperatures.
- Smaller volume and weight of the recuperator.
- Lower installed cost.
- Improved safety and a radical approach to plant design.

The size of a compact recuperator is one of the primary aspects to be considered in the design configuration, since it generally has a large impact on its manufacturing cost as well as the transportation and installation of the unit. Since the size of the recuperator depends on its heat transfer surface area, one can compare the heat exchangers to one another by determining their respective surface-area densities. Gezelius [10] defines the surface-area density as the total heat transfer area divided by the volume of the heat exchanger (measured in m^2/m^3). The higher the value of a unit's surface-area density, the smaller and lighter it becomes for a specific output, which in turn reduces the cost involved. The unit is then classified as a compact heat exchanger when the surface area density value exceeds $700m^2/m^3$ [10]. More conventional heat exchangers display much lower surface-area densities ranging between $100m^2/m^3$ and $300m^2/m^3$. Compact heat exchangers can incorporate surface-area densities of up to $10{,}000m^2/m^3$, with design trends still increasing compactness and heat transfer properties. This high compactness implies an appreciable reduction in material cost and ease of installation which makes it an ideal choice for use in advanced gas turbines.

Comparison of the performance characteristics of most compact heat exchanger types is given in Table 2.3. As can be seen in Table 2.3, optimal heat exchanger compactness values (ranging from $200m^2/m^3$ to $10{,}000m^2/m^3$) are achieved in the form of the PCHE- and Marbond exchangers with compactness values of respectively $5{,}000m^2/m^3$ and $10{,}000m^2/m^3$.

Type of Heat Exchanger	Compactness (m^2/m^3)	Stream Types	Materials	Temperature Range (°C)	Max Pressure (bar)	Cleaning Methods	Corrosion Resistance	Multi stream capability	Multi pass capability
Plate and Frame (gaskets)	= > 200	Liquid-liquid, Gas-liquid, 2-phase	S/S, Ti, Incoloy, Hastelloy, graphite, polymer	-35 to +200	25	Mechanical	Good	Yes	Yes
Partially welded plate	= > 200	Liquid-liquid, Gas-liquid, 2-phase	S/S, Ti, Incoloy, Hastelloy,	-35 to +200	25	Mechanical, Chemical	Good	No	Yes
Fully welded plate (Alfarex)	= > 200	Liquid-liquid, Gas-liquid, 2-phase	S/S, Ti, Ni-alloys	-50 to +350	40	Chemical	Excellent	No	Yes
Brazed plate	> 200	Liquid-liquid, 2-phase	S/S	-195 to +220	30	Chemical	Good	No	No
Bavex plate	200 – 300	Liquids, Gases, 2-phase	S/S, Ni, Cu, Ti, Special steels	-200 to +900	60	Mechanical, Chemical	Good	In principle	Yes
Platular plate	200	Liquids, Gases, 2-phase	S/S, Hastelloy, Inconel	= > 700	40	Mechanical	Good	Yes	Yes
Compabloc plate	= > 300	Liquids	S/S, Ti Incoloy	= > 300	32	Mechanical	Good	Not usually	Yes
Packinox plate	= > 300	Liquids, Gases, 2-phase	S/S, Ti, Hastelloy, Inconel	-200 to +700	300	Mechanical	Good	Yes	Yes
Spiral	= > 200	Liquid-liquid, 2-phase	C/S, S/S, Ti, Incoloy, Hastelloy	= > 400	25	Mechanical	Good	No	No
Brazed plate fin	800 – 1,500	Liquids, Gases, 2-phase	Al, S/S, Ni alloy	Cryogenic to +650	90	Chemical	Good	Yes	Yes
Diffusion Bonded plate fin	700 – 800	Liquids, Gases, 2-phase	Ti, S/S	= > 550	> 200	Chemical	Excellent	Yes	Yes
Printed Circuit (PCHE)	200 – 5,000	Liquids, Gases, 2-phase	S/S, Ni, Ni alloys, Ti	-200 to +900	> 400	Chemical	Excellent	Yes	Yes
Polymer (e.g. channel plate)	450	Gas-liquid	PVDF / PP	= > 150	6	Water wash	Excellent	No	Not usually
Plate and shell	-	Liquids	S/S, Ti	= > 350	70	Mechanical	Good	No	Yes
Marbond	10,000	Liquids, Gases, 2-phase	S/S, Ni, Ni alloys, Ti	-200 to +900	> 400	Chemical	Excellent	Yes	Yes

Table 2.3: *Summary of the principal features of a range of compact heat exchanger types (s/s – stainless steel).* Modified after Reay [9].

These two concepts involve truly innovative designs which incorporate high effectiveness with low weight of the recuperator unit. Although these two heat exchanger types are still in their infancy regarding utilization in gas turbines, they will eventually penetrate the compact heat exchanger market. The need in general now is to establish a low cost manufacturing method for producing these compact heat exchangers.

Although compact recuperators display very favourable properties, there is one concern for potential CHE users which involves fouling. Fouling occurs due to the presence of particulates in the working fluid and the subsequent creation of discontinuities in the flow channels of the heat exchanger caused by the uninterrupted flow of the working fluid [10]. This especially arises for gas-liquid applications, where the fluid present agglomerates any particles and creates "dead-spots" in the micro channels of the heat exchanger where particles would be prone to adhere to the passage wall and subsequently create serious fouling problems. Conversely, gas-gas applications do not incorporate this problem due to the lack of moisture present as a result of the compact heat exchangers' high operating temperature. Although compact heat exchangers offer a variety of benefits, users of this technology should rather consider incorporating working fluids that do not contain any particulates. If the heat exchanger environment is of such a nature that particles are always present, the design of the heat exchanger should allow for more clearance in the flow channels to ensure that no agglomeration of particles take place.

These two innovative recuperator designs (i.e. the PCHE- and Marbond Recuperators) will be evaluated in the following section to firmly establish a basis for the more recent developments regarding compact recuperator technology.

2.2.5 Recent Developments in Compact Recuperator Technology

2.2.5.1 Printed Circuit Heat Exchanger (PCHE)

Qualitative description of a PCHE

This new concept has only recently been introduced into the market by its sole vendor Heatric Inc.. Virtually no mention of PCHE's are given in available heat exchanger literature due to it being a relatively new concept. The definition of a printed circuit heat exchanger is inherent to the way it is manufactured. The manufacturing process entails a chemical etching and diffusion bonding process. In the first step of the manufacturing process, fluid passages are photochemically etched into both sides of a metal plate. A series of milled plates are then stacked and joined by means of diffusion bonding[1]. Diffusion bonding allows the plates to be joined so that the bond acquires the same strength as the parent metal being used. The latter is established by grain growth that eliminates the interface at the joint [3]. Figure 2-2 and Figure 2-3 give a schematic layout of the assembling process and a section view of the printed circuit semi-circular profile respectively.

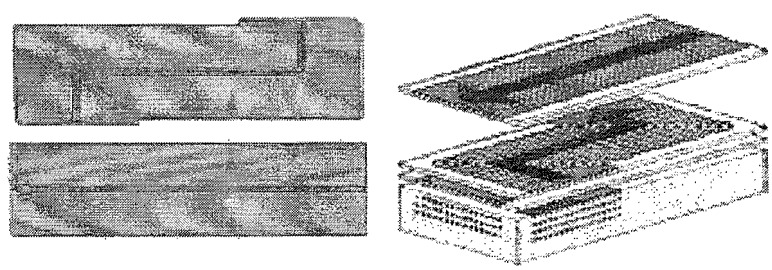

Figure 2-2: *Orientation of fluid passages etched out photochemically and method of assembly.* [3]

Figure 2-3: *Cross-section of semi-circular channels. Grain growth during diffusion bonding occurs in such a manner that the interface between the two original plates is eliminated.* [3]

[1] *Manufacturing process details supplied by Heatric™ (Heatric™ Homepage, 2005)*

The printed circuit heat exchanger design offers a unique combination of innovative manufacturing technology and potential range of application. Since the characteristics of PCHE's encompass compactness and operation at exceedingly high temperatures and high pressures, it has applications in a variety of other unit operations including reactors, mass transfer and mixers.

The concept of a printed circuit heat exchanger would ideally match the profile of a recuperator that qualifies itself in terms of automated manufacturing and high volume production. Having a high heat transfer surface area density of up to $5{,}000 m^2/m^3$ [3], it clearly has an advantage over its competitors in terms of material usage and size. The feasibility of this concept has been determined by Gezelius [10], which is elaborated upon in the next section.

Comparison to Conventional Heat Exchangers

Gezelius [10] compiled a study in conjunction with Heatric Inc. wherein direct comparisons between the printed circuit heat exchanger and other conventional heat exchangers were made to confirm the advantages of PCHE's. The respective heat exchangers were designed to meet the same requirements and the conventional heat exchangers comprised of a shell-and-tube IHX[2], a helical IHX and a compact plate-fin IHX. Gezelius concluded the following, amongst others:

- For a shell-and-tube IHX:
    - The standard heat exchanger performance parameters (specific performance and surface-area density) of the PCHE was clearly superior to that of the shell-and-tube IHX, having a volume of roughly between 9 and 16 times smaller than its bigger counterpart.
    - The circulator power required for the PCHE was slightly higher than that of the shell-and-tube IHX, but could probably be ascribed to the PCHE not being fully optimized for the particular comparison.
    - Modifying the PCHE's design to incorporate the same required circulator power still delivered a heat exchanger with a total volume significantly lower than that of its bigger counterpart.
- For a helical IHX:

[2] *Intermediate Heat Exchanger*

- The secondary pressure drop (with respect to the secondary fluid) through the PCHE is between 9 – 16 times less than that for a helical IHX and in turn requires less circulator power for the secondary loop. Inlet- and outlet losses are not taken into account for the PCHE, but Gezelius assures that, even with allowance being made for the latter, the secondary pressure drop would still be significantly lower.
- The size of the PCHE with regard to the helical IHX is very small, including a total heat transfer surface area of 4,234m^2 in a cubic volume of 1.6m^3, thus demonstrating high compactness and high effectiveness.
- The PCHE also displays excellent performance parameters, having a surface-area density of approx. 77 times larger than that of the helical IHX. Also, halving the primary pressure drop delivers only a minor increase in heat exchanger face- and flow area.

- For a compact plate-fin IHX:
  - The PCHE has similar primary and secondary pressure drops, thus enabling a design which incorporates maximum reduced volume of the heat exchanger. On the contrary, the compact plate-fin IHX having a secondary pressure drop three times higher than its primary pressure drop could not be optimally reduced in volume due to the latter constraint.
  - The 1.0mm channel diameter PCHE delivers a specific performance approximately twice as much as that delivered by the compact plate-fin IHX. This is due to the PCHE having half the core volume than that of the compact plate-fin IHX. When compared to a 2.0mm channel diameter PCHE, Gezelius found that the particular PCHE still had the smaller volume compared to the compact plate-fin IHX.
  - Gezelius also states that the thin fins on the compact plate-fin IHX (thickness = ±0.0076mm) may fail due to the excessive temperatures and pressures at which these heat exchangers operate. This problem would not exist for PCHE's since the latter can operate efficiently up to the regions of 50MPa.
- In general, the PCHE has one definite disadvantage over the three previously mentioned heat exchangers: the PCHE has only been commercially produced by Heatric Inc. for the last 20 years whereas the rest have been studied extensively

for the past few decades. Hopefully this is to change in the heat exchanger industry in the years to come.

2.2.5.2 Marbond Heat Exchanger

Recently, Chart-Marston Inc. has developed the Marbond® heat exchanger [11]. The Marbond heat exchanger, boasting high integrity, compactness and being able to operate over a range of temperatures and pressures not met with conventional heat exchangers, is the latest truly innovative design to enter the marketplace. The manufacturing procedure for the Marbond heat exchanger, comprising stacked and bonded together stainless steel plates, entails the same method applied to the printed circuit heat exchanger (i.e. chemical etching and diffusion bonding) and allows for flexibility of design. Construction allows for the use of small passageways (see Figure 2-4), which significantly increases the porosity of the heat exchanger core and subsequently delivers a substantially higher surface-area density than the PCHE. Reay [9] states that a doubling in the porosity of the Marbond heat exchanger, other factors being equal, results in the halving of the volume for a given surface area. This consequently results in a smaller footprint-area relating to the PCHE which equals savings. The volume of the Marbond heat exchanger could be as low as 5% of that of the equivalent shell and tube heat exchanger, making them a cost-effective alternative in many applications. An opened up version of the Marbond heat exchanger is displayed in Figure 2.4. As stated with the PCHE, virtually no mention of the Marbond heat exchanger is given in present literature due to its recent introduction into the market. More comparative studies concerning this heat exchanger will be a valuable addition to existing literature.

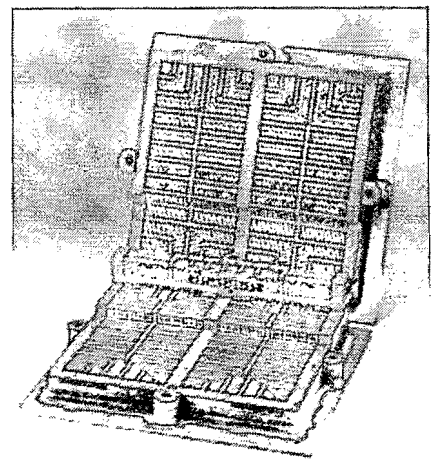

Figure 2-4: *The Marbond compact heat exchanger as developed by Chart-Marston Inc.* [12]

Although a firm basis concerning previous and new recuperator technologies have been established, it is important to realize the vital role that materials and manufacturing expertise fulfill in the realization of a highly effective, cost efficient recuperator. Developmental research must be aimed at establishing the most cost-effective combination of all effective recuperator requirements as discussed in Section 2.2.3 into a recuperator design using the best material and manufacturing process. Elaboration on the materials and manufacturing aspects that go hand in hand with recuperator technology will follow hereafter.

2.3 Materials and Manufacturing Technologies

Applicable materials and manufacturing technologies to be discussed include existing and new recuperator materials, relevant manufacturing procedures and relevant joining procedures.

2.3.1 Existing Recuperator Materials

2.3.1.1 AISI 347 stainless steel

Most recuperators today use AISI 347 stainless steel (SS) as the material in the design. AISI 347 SS is used where gas inlet temperatures reaches 650°C or less, since it possesses relatively good tensile strength and corrosion resistance at this elevated temperature. The corrosion resistance is due to 18% chromium content which forms a protective chromium oxide film on the surface of the alloy. As can be noted from Figure 2-5, a thermal effectiveness approaching 30% is the highest that can be reached by using AISI 347 SS as recuperator material [13].

Depending on the operating conditions applicable to a recuperator design, one of the benefits of using AISI 347 SS as a recuperator material is the formation of a dense adhesive external oxide layer that inhibits the transport of oxygen to the material below the film, thus protecting the alloy from excessive oxidation damage. This protective layer can however increase at a faster rate if it is subjected to higher temperatures. This in turn can lead to oxide spallation and chrome depletion which ultimately leads to an effective decrease in the cross section of the recuperator material and consequent failure of a recuperator such as the PSR due to creep (see Figure 2-6). It is therefore important to

regulate the temperature at which AISI 347 SS will operate [15]. If higher temperatures are required in the turbo generator design, it is unavoidable to conduct a new material selection for materials with significantly better properties.

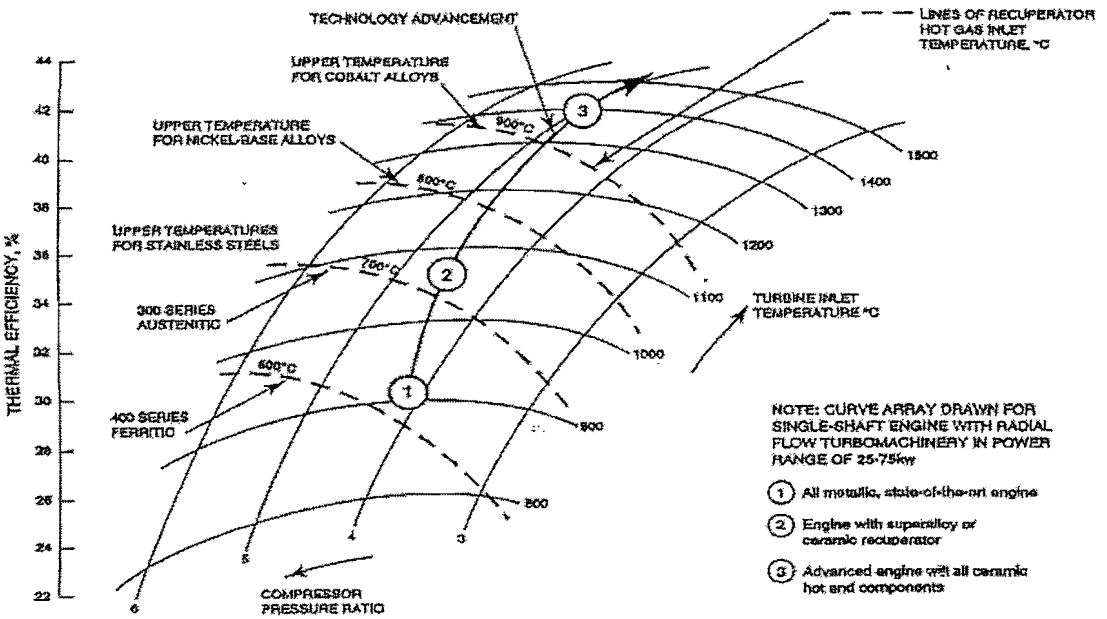

Figure 2-5: *The impact of major parameters on the performance of small gas turbines.* Modified after Pint et al. [14].

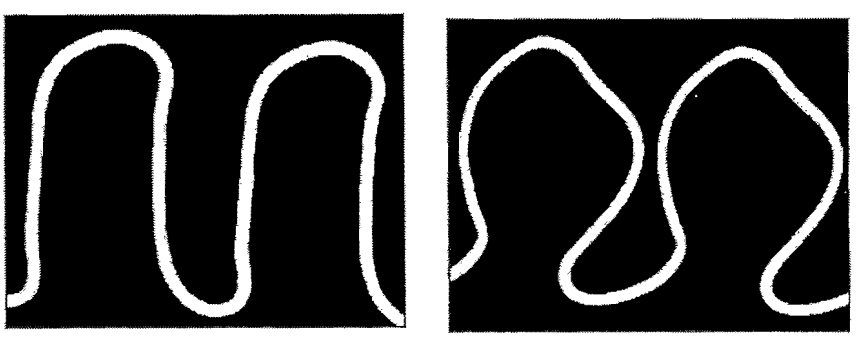

Figure 2-6: *Excessive creep (right) can close up the flow channels in a PSR air cell.* Modified after Maziasz et al. [15].

2.3.1.2 *Other metallic alternatives*

For increased temperature service, a higher nickel content alloy may be used. Maziasz et. al. [15] investigated materials to be used at 700°C and 760°C that delivered lower cost implications and improved performance at higher temperatures. This was due to the oxidation testing of AISI 347 SS at 650°C in 10% water vapor, which resulted in a very severe attack on the material after only a few thousand hours. These materials included a customized super 347 stainless steel which incorporates a projected increase in recuperator hot gas inlet temperature to approximately 750°C. By gaining this temperature rise, an increase in low pressure micro turbine efficiency of up to 33% can be established. It is unknown, however, whether the implementing of this material in recuperator design will be successful since all the fundamental properties are not yet defined [15].

By using an Inconel 625 alloy, an efficiency of up to 35% can be realized. The latter would be a viable alternative if the material costs were low but Inconel 625 prices up to 5 times more than AISI 347 SS. In their paper on the subject, Natesan et. al. [16] identified Fe-Cr-Ni-alloys such as Alloy 800H and austenitic stainless steels as ideal recuperator materials. They also identified nickel based alloys (617, Hastelloy X and Hastelloy XR) for components that are exposed to helium coolant at temperatures of up to 900°C. The latter materials *inter alia* feature in the platular plate- and the Packinox® plate heat exchangers which are very costly.

2.3.1.3 *Ceramic alternatives*

Beside these materials, ceramics have also been investigated for use in a variety of gas turbine applications. McDonald [7] suggests that the ultimate performance potential of microturbines can eventually only be realized if a high temperature ceramic heat exchanger is put into operation. In order to fabricate ceramic recuperators, two critical decisions must be made. The first is the selection of the ceramic material to be used and the second the selection of the construction method to be used. The review of the activities in ceramic recuperation shows that no one material has been used consistently [13]. These materials include cordierite, nitride bonded SiC, phosphate bonded SiC, alumina chromia and magnesia chromia. With the exception of some, these materials are

no longer considered for high temperature operations since no one material meets the required specifications for today's high temperature applications, which include the following:

- Low thermal expansion.
- High thermal shock resistance.
- Good oxidation and corrosion resistance.
- High temperature strength.
- Good creep resistance.
- Ease of fabrication [13].

It is of crucial importance to accommodate all the above-mentioned aspects into the recuperator design when a ceramic is considered. This must be done in such a way that an economically feasible concept emerges. The most important aspect of these involves the ceramics' manufacturability. One can therefore immediately rule out ceramics for this purpose since its potential for minimum cost and continuous fabrication have not yet been demonstrated in existing literature. This doesn't mean that future work with regard to this field should be avoided. In actual fact development concerning ceramic recuperators should be pursued all the more, but for the purpose of this study it is only included for the sake of completeness.

The following section evaluates new and viable material concepts when trying to set up the most cost-effective approach for establishing higher recuperator effectiveness.

2.3.2 New Recuperator Materials

The material types to be discussed in the following section involve pyrolytic graphite (PG), carbon reinforced carbon composites (C/C composites) and tungsten-copper (W-Cu). It is important to realize that these materials are not evaluated only for their properties but also essentially for their adaptability to use in the application of a recuperator. These materials will be evaluated by *inter alia* looking at their characteristics, manufacturability, joining abilities and finally availability.

2.3.2.1 PYROID® pyrolytic graphite[3]

PYROID® pyrolytic graphites (PG) are specialized, "five-nine" purity, chemical vapor deposited (CVD), carbon products grown atom-by-atom with unique thermal, electrical and chemical properties [17]. PG is a unique form of graphite being ultra pure, due to it being synthesized from purified hydrocarbon gases, and close to theoretical density. It also possesses extreme anisotropy due to its layered structure, resulting in thermal conductivity properties firstly similar or higher to copper in the plane of the layered structure and secondly lower than alumina brick in the planes perpendicular to the layered structure. PG can have a thermal conductivity as high as 2,000W/m.K (i.e. 5 times the value for copper) in the plane of the layered structure. Not only the thermal conductivity properties but also the material's electrical and chemical properties are enhanced in the direction of the layered structure, delivering characteristics far more superior than that of conventional graphites. Low particulates, the result of proprietary finishing processes, and chemical resistance to fluorine based gases provide solutions to problems in plasma and semi-conductor etching systems.

With PG performing exceptionally well at high temperatures (stable up to 2,200°C) it is an ideal material selection for special thermal management applications, including heat sinks. The most important characteristics concerning PG are displayed in Table 2.4. Graphite is an attractive material for elevated temperature use in inert atmosphere and ablative environments (high temperature use in impure environments with traces of air will lead to severe oxidation). Graphite displays favorable properties at these high temperatures including a high sublimation temperature, improved strength with increasing temperature up to a point (about 2,000°C), thermal stress resistance and chemical inertness. However in its bulk forms of polycrystalline graphite and pyrolytic graphite, its utility for many applications has been limited by low strain to failure, flaw sensitivity, anisotropy, variability in properties and fabrication difficulties associated with large sizes and complex shapes. If this material is selected, the design must take these difficulties into account and consequently allow for the effective use of PG as recuperator material.

[3] *As cited on the Minteq web site on www.minteq.com/our-products/minteq-pyrogenics-group/pyroidR-pyrolytic-graphite/ (2005)*

A discussion on C/C composites, a technology developed initially to improve on certain aspects of conventional graphites such as manufacturing graphite materials in truly structural forms will now follow.

Property	Value	Unit
Density	2.18 – 2.22	g/cc
Flexural strength (a,b)	120	MPa
Tensile strength (a,b)	80	MPa
Compressive strength (a,b)	100	MPa
Young's Modulus (a,b)	20,000	MPa
Thermal Expansion (a,b) (c)	0.5×10^{-6} 20×10^{-6}	K^{-1} K^{-1}
Thermal Conductivity (a,b) (c)	300 3.5	W / m –K W / m -K
Electrical resistivity (a,b) (c)	0.5×10^{-3} 0.5	ohm – cm ohm - cm
Crystal structure	Hexagonal	
Melting point (Atmosphere)[4]	Sublimes at 3650°C	
Impurities		
Total	0.01max	%
Metallic	10	ppm

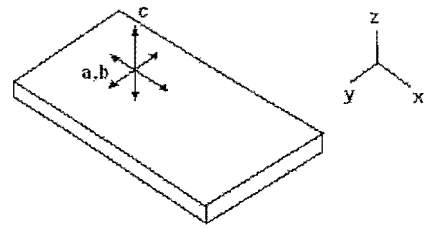

Table 2.4: *Important characteristics of PG.* [17]

2.3.2.2 C/C composites

C/C composites are materials that consist of carbon fibers embedded in a carbonaceous matrix. The original C/C composites were produced using two-directional (2-D) reinforcements in the form of low modulus rayon precursor carbon and graphite fabrics. The woven fiber preform is coated with the matrix material using *chemical vapor infiltration* to provide initial structure to the material. At first the matrix material was derived from pyrolyzed high char yield thermosetting resins such as phenolic. After depositing a thin layer of matrix on the fibers, the material is impregnated with a thermoset polymer resin and then heat treated in an inert atmosphere. This resin infusion process is repeated several times in order to increase the density of the matrix. At each

[4] The melting point of PG when the ambient pressure is one atmosphere (1 bar)

step the heating turns the resin into a carbon matrix of increasing density. Repeating the procedure several times reduces the porosity of the material as the resin is forced into the pores of the matrix. The final product is a carbon fiber reinforced anisotropic carbon matrix composite that has a high strength to weight ratio. The material is used in applications for temperatures well above 1,000°C. In fact, the strength of C/C composites increases with increasing temperature up to 2,200°C because of the improved coupling between fiber and matrix. It should be noted that the rates of increase in strength from room temperature to elevated temperatures are lower for C/C Composites than for graphite. Compared to graphite, however, C/C is 10 to 20 times stronger in the plane of the fabric reinforcements.

Values of thermal conductivity in the plane of the fiber structure range between 50 and 180W/m.K, while values in the plane perpendicular to the fibers are between 5 and 30W/m.K. High performance carbon products with properties encompassing those of conventional graphites and carbon composites have also been developed by SGL Carbon Group, having thermal conductivity properties of 260 and 500 W/m.K respectively. C/C products are usually machined wet with hard metals or diamond tools. If there are a large number of workpieces and their contours are suitable, water-jet cutting can also be recommended.

One of two major problems that C/C composites display (similar to graphites), involves its directionality. Because of the latter's 2-D reinforced structure, the material exhibits very low values of strength and thermal conductivity in the direction perpendicular to the reinforcement, which is a serious drawback. If directionality was the only drawback, then solving the problem would entail the implementation of multidirectional substrates [18]. All the most important properties of the composite (i.e. thermal, mechanical and physical properties) can be controlled by the appropriate design of substrate parameters. These parameters include fiber orientation, volume fraction of fibers in required directions, fiber spacing, substrate density, yarn packing efficiency and fiber selection [19]. However, another major problem that C/C composites display entails high temperature oxidation, which begins at a temperature threshold of 370°C for unprotected materials. Most C/C products are also very susceptible to high temperature corrosion. Unless oxidation inhibitors are introduced into the composite and an inert atmosphere is provided for the material to function in, high temperature oxidation is inevitable.

Van Greuning [5] identified the tungsten-copper alloy otherwise known as Elkonite® as ideal for application in a high-temperature recuperator due to its excellent structural and thermal properties at elevated temperatures as well as its capabilities of ensuring improved performance when integrated with the ideal performance characteristics of compact heat exchangers. More specifically, he identified the grade of tungsten-copper generally referred to as Elkonite 5W3® as an ideal material which is consequently used in the manufactured recuperator of this research. It is essential that an evaluation of this proposed material, in the light of its properties and adaptability to use in a recuperator concept, is also included.

2.3.2.3 Tungsten-copper (Elkonite 5W3®)

Tungsten-copper (hereafter referred to as W-Cu), composite materials being produced by *inter alia* the infiltration of a porous tungsten structure [20], are materials that combine the thermal conductivity properties of copper with the high strength and high temperature properties of tungsten. Tungsten is the main component of these alloys, and is mainly responsible for the composite's high density (between 17 and 18.5g/cm^3) and its brittle behaviour at room temperature. The copper on the other hand serves as a binder matrix which holds together the brittle tungsten grains and lends ductility to the composite for machining purposes. Table 2.5 gives an overview of the most important properties of the composite 5W3.

Properties	Metric
Physical Properties	
Density (kg/m^3)	1400-1700
Mechanical Properties	
Hardness, Rockwell B	95
Flexural Modulus (GPa)	0.965
Electrical Properties	
Electrical Resistivity (ohm-cm)	3.59e-006
Thermal Properties	
Thermal Conductivity (W/mK)	140-275
Coefficient of Thermal Expansion (@ 20°C) (ppm/°C)	9.4
Melting Point (°C)	1080-3410
Solidus (°C)	1080
Liquidus (°C)	3410

Table 2.5: *Important characteristics of tungsten-copper composite 5W3.*

As a high performance material, W-Cu is characterized by high electrical and thermal conductivity, low thermal expansion and high wear resistance. Both elements of the composite possess excellent attributes concerning thermal conductivity. With individual values of thermal conductivity for high conductivity copper and tungsten being 391 and 166W/m.K respectively and an overall value ranging between 140-275W/m.K it is an excellent material selection for special heat management applications. This is apparent when the properties of firstly both elements and secondly the composite at elevated temperatures are analyzed. Looking at Figure 2-7 which shows the temperature dependence of some metals, one sees that with increasing temperature the thermal conductivity of high conductivity copper and tungsten decreases. Opposing this is the temperature dependence of W-Cu stated in Figure 2-8, where a unique attribute of the composite is revealed. One sees that an increase in temperature up to roughly 600°C is accompanied with an increase in thermal conductivity properties of the composite. Past this temperature region, the value of the thermal conductivity property starts to decrease similar to Figure 2-7. This unique property of W-Cu provides good grounds for the material to be used in applications where this temperature range is maintained. The thermal expansion of W-Cu also varies with a variation in the weight percentage of copper, with the coefficient of thermal expansion of copper being 4 times larger than that of tungsten.

Various methods for fabricating W-Cu to reach near theoretical density involve fabrication by thermo-mechanical method, sintering under ultra high pressure, fabricating by mechano-thermochemical methods and sintering of nano-structured powders [5]. Machining of W-Cu can be done using cemented carbide tools.

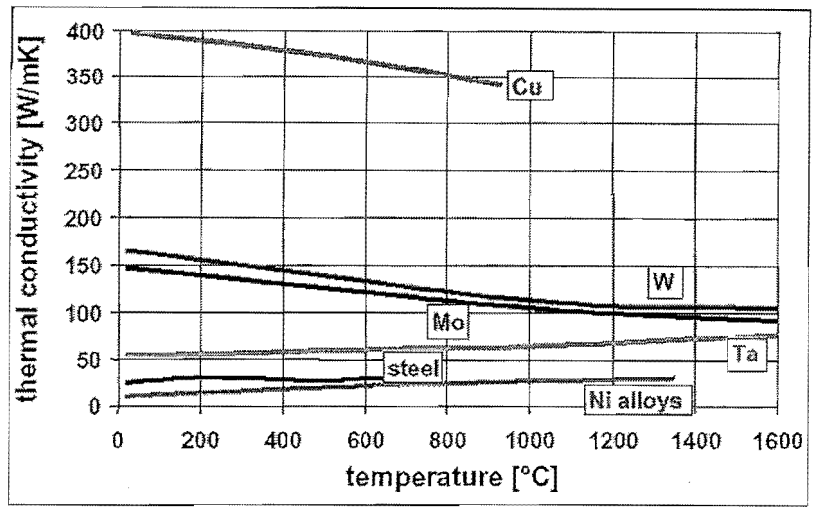

Figure 2-7: *Temperature dependence of thermal conductivity of some metals.* [5]

The only prominent concern that arises when evaluating W-Cu's properties, relates to its high density. Its density of $17 g/cm^3$ in effect means that a relatively small structure of W-Cu will possess a large weight-to-volume ratio, which indirectly puts a constraint on the recuperator effectiveness that can be reached and in turn the total economic feasibility. Despite this aspect, W-Cu still possesses excellent properties to be used as recuperator material in the design.

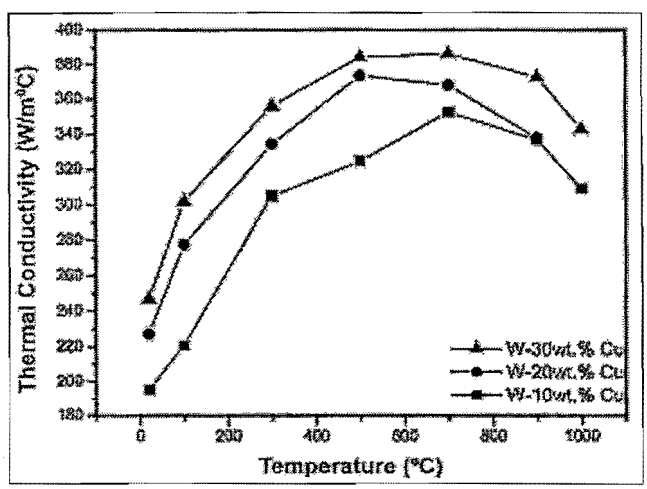

Figure 2-8: *Temperature dependence of thermal conductivity of W-Cu.* [5]

2.3.3 Applicable Manufacturing Procedures

When designing high temperature and pressure components, great care should be taken in the selection of the appropriate manufacturing procedures for establishing the components

and overall assembly. This selection referred to is primarily driven by the characteristics of the component material. Relevant manufacturing processes that would be ideal for use in manufacturing a recuperator using W-Cu as the base material are evaluated together with their risks.

2.3.3.1 Laser Beam Machining (LBM)

Laser Beam Machining is a high energy machining process in which the work material is melted, vaporized and/or combusted by a narrow beam of coherent light [21]. This process, which does not require a vacuum, is used to machine a variety of metallic and non-metallic materials. The non-metallic materials include ceramics, plastics, composites, wood, glass and rubber. Laser cutting is used to produce intricate two-dimensional shapes in work pieces made out of materials such as sheet metal and paper up to 15 mm thick with high cutting speeds. Small precision cuts and holes with small tolerances can also be produced by this process. Even the creation of small channels in ceramic substrates for cooling and identification purposes has been established by means of laser scribing. Figure 2-9 to 2-11 give a schematic layout of the LBM process and demonstration of the intricate parts that can be produced by means of laser beam machining.

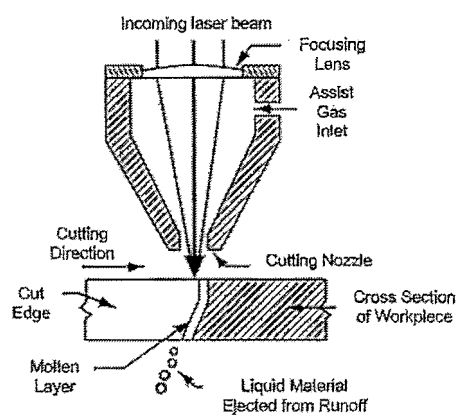

Figure 2-9: *Schematic Illustration of the Laser Beam Machining Process.* [21]

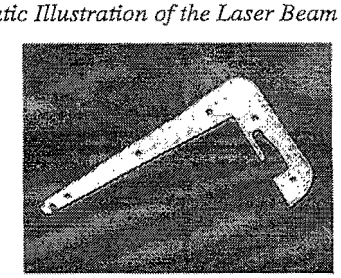

Figure 2-10: *Example of parts produced by means of Laser Beam Machining - a CO2 laser cut medical part.* [21]

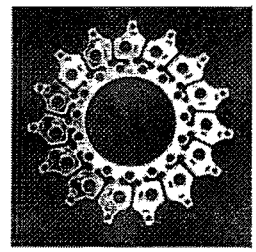

Figure 2-11: *Example of parts produced by means of Laser Beam Machining- a 6061-T6 CO2 laser cut part.* [21]

The LBM process is suitable for use in the following cases:

- The processing of difficult-to-machine materials such as hardened metals, ceramics and composites.
- Processing of materials with low reflectivity, thermal diffusivity and thermal conductivity, since the efficiency of the LBM process is dependent on a material's thermal and optical properties.
- Processes where cleanliness is required.

This process usually produces a rough and heat-affected area on the machined piece, which in critical applications will have to be removed or heat treated.

Geometrical capabilities that can be achieved by this process are as follows:

- Typical work piece thickness being machined range from 1.27mm to 20.32mm.
- The width of the cut, i.e. kerf width, typically ranges from 0.0762mm to 0.508mm.
- Achievable tolerances are quite close, often to within 0.0254mm of the part geometry.
- The typical surface finish resulting from laser beam cutting may range from 3.175μm to 6.35μm.

Process limitations and impediments that LBM poses are as follows:

- It is a time-consuming process. For a specific work piece width and profile width (to be machined), for example 2mm, the LBM process will only be able to machine these widths in increments of 20μm, thus making this specific process extremely time consuming and impractical.

- This is one of the most costly methods to use in the manufacturing of recuperator plate profiles.

Due to the above-mentioned limitations, this technique has not been implemented in the design of the mini-channel recuperator. Other promising methods will be addressed next.

2.3.3.2 Spark Erosion Machining / Electrical Discharge Machining

Electrical discharge machining (or EDM) is a machining method primarily used for hard metals or those that would be impossible to machine with traditional techniques. EDM is a non-traditional method of removing material by a series of rapidly recurring electric arcing discharges between an electrode (the cutting tool) and the work piece, in the presence of an energetic electric field [22]. The EDM cutting tool is guided along the desired path very close to the work but it does not touch the piece. Consecutive sparks produce a series of micro-craters on the work piece and remove material along the cutting path by melting and vaporization. The particles are washed away by the continuously flushing dielectric fluid.

One critical limitation, however, is that EDM only works with materials that are electrically conductive. EDM can cut small or odd-shaped angles, intricate contours or cavities in extremely hard steel and exotic metals such as titanium, Hastelloy, Kovar, Inconel and carbide [23]. Each spark involved in the EDM process produces a temperature of between 10,000-20,000°C. Consequently, the workpiece is subjected to a heat affected zone (HAZ), the top layer of which comprises recast material. The thickness, composition and condition of this layer depend on the discharge energy and the make-up of the workpiece, tool electrode and dielectric fluid, and both hard and soft surface layers can be produced despite perceived wisdom that the recast layer is always hard. With ferrous workpiece materials, the recast layer typically appears white and amorphous when viewed under a microscope, and is prone to tensile residual stress and microcracking [24].

An electrical discharge machine (see Figure 2-12) is considered to be the most precision-oriented manufacturing process and is widely used for creating simple and complex shapes and geometries [25]. EDM machining is favoured in situations where high

accuracy of work and low production quantities are required. Tables 2.6 and 2.7 give an indication of the dimensional accuracy and the surface finish achievable with EDM.

Dimensional Accuracy	+/- 0.0005 inches per inch	+/- 0.0127 mm per 25.4mm
Comments	Profile accuracy of 0.0003 is obtainable with cutting path.	

Table 2.6: *A layout of the dimensional accuracy achievable with the Electrical Discharge Machining (EDM) Process.*

Surface Finish	16 Ra is achievable, 64 or higher Ra is typical and less expensive
Comments	Surface Finish features created by EDM have an "orange peel" appearance

Table 2.7: *A layout of the surface finish achievable with the Electrical Discharge Machining (EDM) Process.*

There are two basic types of EDM: wire and probe (die sinker). Wire EDM is used primarily to cut shapes through a selected part or assembly. With a wire EDM machine, if a cutout needs to be created, an initial hole must first be drilled in the material, then the wire can be fed through the hole to complete the machining. Probe (die sinking) EDMs are generally used for complex geometries where the EDM machine uses a machined graphite or copper electrode to erode the desired shape into the part or assembly. Sinker EDM can cut a hole into the part without having a hole pre-drilled for the electrode.

Design considerations to take into account when considering the use of EDM are as follows:

- The surface-finish for the part must be relaxed if feasible, to allow the manufacturer to produce a part with fewer passes, at a higher current level and a higher metal-removal rate.
- The part must be designed or prepared in such a way that the amount of stock removed by EDM is relatively small which will significantly reduce the amount of time and cost for each part.

Although this method may seem very feasible, it has not been considered for the fabrication of the mini channel recuperator due to its limited production rate. EDM is most widely used in the making of prototypes (aerospace and automobile industries) where production quantities are relatively low. For cost and time purposes, it has been

decided to machine the mini channel recuperator profiles using more conventional techniques which are elaborated upon in the chapter conclusion.

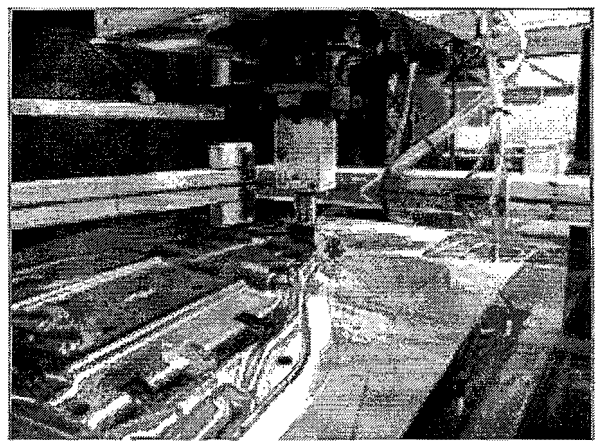

Figure 2-12: *Photo of the Electrical Discharge Machine.* [22]

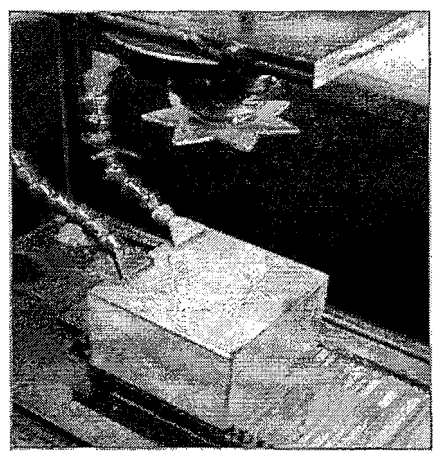

Figure 2-13: *Photo of the electrical discharge machine showing master electrode at top, badge die workpiece at bottom, oil jets at left (oil has been drained). Initial flat stamping will be "dapped" to give a curved surface.* [22].

2.3.4 Applicable Joining Procedures

The selection of the appropriate joining method is driven by *inter alia* the pressure and temperature environment, working fluid, etc. Relevant joining procedures that would be ideal in producing the recuperator are evaluated below, together with the risks involved for each.

2.3.4.1 Explosive Welding

The explosion bonding process, also known as "cladding by the explosion welding process", is a technically based industrial welding process [26]. As with any other welding process, it complies with well understood, reliable principles. The process uses an explosive detonation as the energy source to produce a metallurgical bond between metal components. It can be used to join virtually any metals combination, both those that are metallurgically compatible and those that are known as non-weldable by conventional processes [27]. Explosive welding was first recognized as a possibility in 1957 in the United States of America when it was observed that metal sheets being explosively formed occasionally stuck to the metal dies. The process has since been developed fully with large applications in the manufacturing industry.

Explosive welding is a solid state joining process. When an explosive is detonated on the surface of a metal, a high pressure pulse is generated. This pulse propels the metal at a very high rate. If this piece of metal collides with another piece of metal at an angle, welding may occur. For welding to occur, a jetting action is required at the collision interface. This jet is the product of the surfaces of the two pieces of metals colliding. This cleans the metals and allows two pure metallic surfaces to join under extremely high pressure. The metals do not commingle, they are atomically bonded. Due to this fact, any two metals may be welded to eachother (i.e.- copper to steel; titanium to stainless). At the collision point, the newly created clean metal surfaces impact at high pressures of several GPa. Figure 2-14 shows the explosive welding process [28].

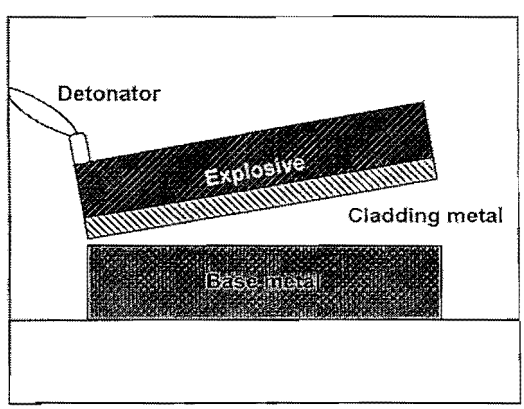

(a)
Cladding metal is positioned above base metal with a specific clearance in between, and explosives are charged on the surface of the cladding metal.

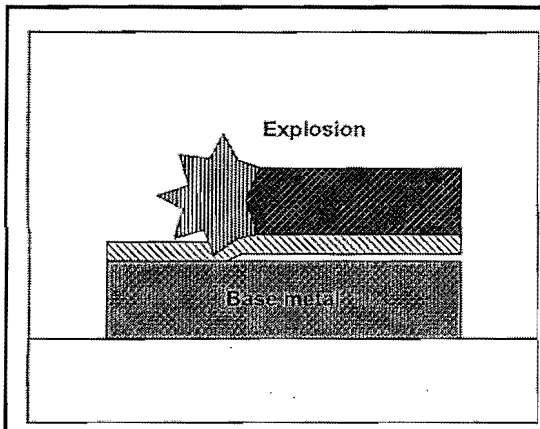

(b)
The explosives are detonated, and as the detonation front moves across the cladding metal, the energy generated by the explosion presses the cladding metal onto the base metal at an extremely high speed, fluidizing the collision front of both metals. This fluidized metal forms a "metal jet", as oxides, nitrides, and absorbed gases are removed from the bonding surfaces, exposing clean metal surfaces to collide.

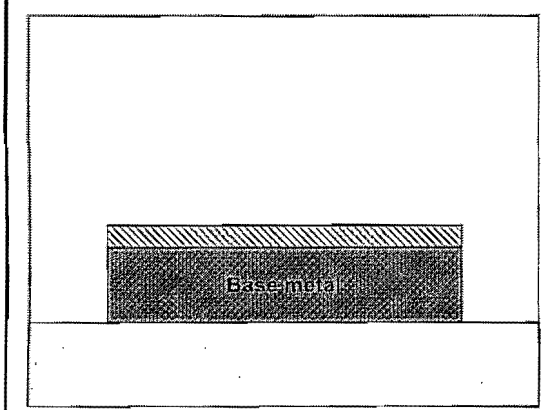

(c)
Activated surfaces of the metals are brought together with such force that the surface molecules are brought close enough to bond together by inter atomic attraction. The detonation front travels so quickly that bonding is completed before heat transmission is able to occur.

Figure 2-14: *Explosive cladding procedure explained.* [28]

From Figure 2-14, the following terminology should be noted:

- The cladding metal (also called the cladder) is the plate, which is in contact with the explosive. It is typically the thinner component.
- The base metal is the plate onto which the cladding metal is being bonded.
- The stand-off distance is the separation distance between the cladding metal and the base metal when fixtured parallel to each other prior to the bonding operation.
- Explosives – situated on top of the cladding metal.

Furthermore, this process can clad one or more layers onto one or both faces of a base metal, with the potential for each to be a different metal type or alloy. Due to its use of explosive energy, the process occurs extremely fast, and unlike conventional welding processes, parameters cannot be fine-tuned during the bonding operation. The bonded product quality is assured through selection of proper process parameters, which can be

well controlled. These include material surface preparation, plate separation distance prior to bonding, and explosive load, velocity, and detonation energy. Selection of parameters is based upon the mechanical properties, mass, and acoustic velocity of each component metal being bonded. Optimum bonding parameters, which result in consistent product quality, have been established for most metals combinations. Parameters for other systems can be determined by calculation using established formulas.

Although there is much heat generated in the explosive detonation, there is no time for heat transfer to the metals. The result is an ideal metal-metal bond without melting or diffusion. The proper impact parameters for a specific metal combination are dependent upon the metal types, thickness and mechanical properties. Selection of the proper parameters is critical to assure a strong, high quality, ductile bond.

The impact conditions are associated by the equation:

$$Vp = 2\,Vc \sin(\beta / 2)$$

Since the plates are parallel, the impact point velocity, Vc, is equal to the detonation velocity Vd. Explosive detonation velocity, Vd, (2,000 to 3,500 m/s) is an independent variable selected to achieve required impact conditions. Stand-off distance is an independent variable selected to achieve required impact conditions. The impact angle β is a dependent variable, controlled by Vd and the standoff distance. It is typically 5 to 25 degrees. The plate collision velocity at the impact point, Vp, is typically in the 250 to 500m/s range, with the specific value being dependent upon metal types,their physical and mechanical properties and chemical compatibility [26].

Unfortunately limitations concerning the use of explosive cladding exist. Explosive cladding deforms the metals at very high rates (104 up to 105sec-1). The metals must be ductile enough to undergo this deformation without cracking. Limits usually accepted are a minimum elongation of 15% and a notch toughness value above 30J at bonding temperature. Most common engineering metals meet these criteria and are readily bondable. Dissimilar metal explosion bonded joints are applied anywhere a designer needs to make a high-quality transition between metals. Typical uses include ultra-high vacuum joints between aluminum, copper and stainless steel, corrosion resistant claddings

on mild steel substrates, and alloy aluminum joined to low-expansion rate metals for electronic packages. Powder metal products such as Glidcop™ and Al-SiC can be joined to wrought metal without thermal excursions. Difficult metals such as beryllium, Al-Be alloys and rhenium have also been joined with explosion bonding.

As with previously mentioned procedures, a high element of risk exists relating to the explosive bonding of the profiled recuperator plates. Explosive bonding in itself provides little risk in terms of compromising a design in a scenario where the design consists of two flat surfaced parts. There is little, if any, room for warpage of surfaces when two flat surfaces are bonded to each other by means of explosive bonding. When the surfaces consist of profiled channels, though, as with the mini-channel recuperator, the risk of warping the existing profiles becomes greater. The probability of the profiled channels warping during the bonding process is substantial due to the high instantaneous temperature and pressure generated by the bonding process. Although certain factors limit the scale of this study, this method of establishing a high integrity assembly cannot be ruled out. This aspect should be evaluated in further studies.

2.3.4.2 Diffusion bonding

Diffusion bonding is a solid state joining technique by which coalescence of clean, close-fitting parts is obtained through a combination of pressure and heat [29]. Solid State diffusion bonding is obtained by applying heat, well below the melting temperature of the metals, a static pressure which does not cause a macroscopic plastic deformation in the material, and a time required to form a metallurgical bond with atomic diffusion process. The diffusion bonding process creates strong and seamless joints between similar and dissimilar materials, without the use of secondary phases, solvents or liquids and is used for aluminum alloys, high strength steels and titanium alloys in the aerospace industry to produce complex and inaccessible joints without localized distortion [30].

Quality factors involved with diffusion bonding involve *inter alia* the following [29,31]:

- Bonding temperature – The bonding temperature is typically 50-70% of the melting point of the most fusible metal in the process.

- Bonding pressure – The bonding pressure should be great enough to avoid deformation of the joint interface as well as to remove oxide films. Insufficient pressure will leave unfilled voids in the joint interface.
- Bonding time – Applying joining pressure for too long will change chemical composition of the applicable material.
- Bonding surface finish - Flat, smooth and clean mating surfaces are required to establish high quality joints.
- Bonding environment - Diffusion bonding is normally conducted in a protective atmosphere.

The potential applications of diffusion bonding are as follows:

- Specialized joining applications where preservation of the solid state is important
- Joining of dissimilar materials
- Joining of materials having high temperature service capability - The generally higher cost of diffusion bonding becomes justifiable when fabricating components for high temperature service [29]. An example of a diffusion bonded specimen is given in Figures 2.15 and 2.16.

Figure 2-15: ***Diffusion bonded Zirconia sample. Bond is at mid-plane around sample.*** [31]

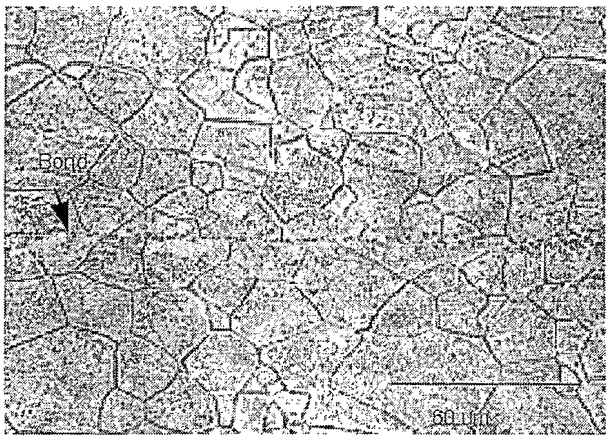

Figure 2-16: ***Diffusion bonding at atomic level.*** [31]

The cost of diffusion bonding equipment varies considerably. It can be an expensive and time consuming process with total expenses dependant upon the applicable joining temperatures & pressures, purity of the atmosphere during bonding as well as the size of the components to be joined. For economic reasons, this process will probably not see broad application in the same sense that ordinary fusion welding techniques are now utilized. It will be employed to an increasing degree in making high strength joints where optimum properties at temperature are required [29].

Diffusion bonding is a specialized joining process that will offer notable advantages compared to other joining techniques if used as the identified joining technique to establish the recuperator of this research. A high strength joint created by means of diffusion bonding will not deform any of the heat transfer profiles and will also ensure integrity and strength of the joint at elevated temperatures..

2.3.4.3 Mechanical fastening

When considering using a fastening system in a design, it is important to realise the following aspects:

(a) The designer should have a thorough understanding of joints.

(b) The basics of fastening systems should be understood to ensure that the joint (wherin the fastening system is utilised) does not open unintentionally, thus compromising the function of the joint.

Table 2.8 provides a detailed indication of the relation of the fastener material to the specific working environment involved. Some of these specific environments are of primary importance when considering the application of the W-Cu mini-channel recuperator. Two important aspects to take into account when considering fastening systems in a design involves the reactive loading of fasteners and the thermal effect on fasteners, the latter being the most important aspect that governs the selection of fasteners and fastener material in a fastening system. This will be elaborated upon next.

Number	Characterization of Environment	Examples of materials for high strength screws and bolts
1	Dry and Temperature < ± 300ºC	Low alloyed- or carbon steel (C35, C45, 35B2, 20Mn5, 42CrMo4), painted or other corrosion protection coating suitable for this temperature range.
2	Humid + (salt) solution + temperature < ± 300ºC	Low alloyed- or carbon steel (C35, C45, 35B2, 20Mn5, 42CrMo4), enhanced corrosion protection coating suitable for this temperature range.
3	High temperature up to ± 600ºC	High alloy steel with Cr-, Ni- or Mo-content (42CrMo4, 42CrMo5-6, X5CrNi18-10, X22 Cr MoV12-1), ferritic or austenitic.-
4	High temperature over ± 600ºC	Heat resistant steels with high Cr-content and alloyed elements Ti, Nb, (10CrNiMoMnNbVB15-10-1, X6 NiCrTiMoVB25-15-2); Ni-base alloys (NiCrTiAl20).
5	Low temperatures under ± -50ºC	Austenitic steels with sufficient Cr- and Ni- content (X5CrNi18-10, X2CrNiMoN17-13-3).
6	Long term appearance requirements	Screws made of stainless steel (X5CrNi18-10), chemical inert materials like titanium (TiAlV6-4), steel with multilayer coatings.
7	Chemical reactive components like magnesium, lithium as clamped part or nut thread component	Screws made of component material, screws made of passivating/chemical inert metals, steel with multilayer coatings.
8	Fastening of light metal components, e.g. made from aluminum or magnesium	Screws made of aluminum (AA 6013, AA 6056, AA 7075; matching of corrosive behaviour and high thermal expansion coefficient).
9	Small volume and extreme lightweight designs	Highest screw strength over 1400 MPa up to +/- 2000 MPa (use in aviation- and aerospace industry, special production requirements necessary and high contact pressures must be acceptable; 38NiCrMoV7-3, X2NiCoMo18-8-5) or lightweight materials for screws (TiAlV6-4, tensile strength +/- 1100 MPa.

Table 2.8: *Fundamental selection of screw material and screw surface.* Modified after Friedrich [32].

Reactive loading during operation

The time-dependent effect on fasteners during its lifetime of use is referred to as the reactive loading on fasteners. This reactive loading consists of chemical reactions (i.e. all kinds of corrosion) or aging (embrittlement of materials, e.g. by heat/radiation or radioactive effects with defect generation in grain structure of materials). The primary aspect of concern is corrosion, since almost all technical materials have corrosive behavior which should be taken into account when designing a fastening system to be utilized in a recuperator assembly. Aspects that play an integral part in determining the limitations for the fastening system (relating to corrosion) include working pressure, operating temperature and the fluid utilized in the recuperator [32].

Thermal loading during operation

Often, a threaded fastening system must be used at different temperatures. For example, a scenario might present itself where fasteners that is to be used at an elevated temperature (T_1) must be fastened at room temperature (T_2). If the screw material and the material of the clamped part have different thermal properties (Young's Modulus; E_p, E_s) or different thermal expansion coefficients (α_p, α_s) or if the properties are temperature dependent in the range of temperatures applied, the preload applied to the fastener varies (i.e. the threaded fastening system is tightened and thus subjected to a preload, which will be referred to hereafter as F_i). This variation in F_i can be significant. Consequently, it is the task of the design engineer at hand to check that the thermal loading of the particular threaded fastening system does not lead to preload overload (due to preload increase) or preload reduction (due to decrease of clamping force) [32].

This change in preload will be referred to hereafter as δF_p. The change in the preload can be positive or negative. It is positive if the Young's Moduli of the screw and the clamped part respectively are constant and the thermal expansion coefficient of the clamped part is larger than that of the screw ($\alpha_p > \alpha_s$). The latter is typical of threaded fastening systems with light metal parts and steel screws. This positive change in the preload can result in a screw failure (due to static fracture of the screw by yielding/plastification). A negative change in the

preload on the other hand ($\alpha_p < \alpha_s$) can result in component separation and finally in a fatigue failure of the screw. This change in the preload of a fastening system is illustrated in equation (2.1).

$$\Delta F_p = \frac{l_c \Delta T(\alpha_p - \alpha_s)}{\left(\delta_{st1}\frac{E_{st1}}{E_{st2}} + \delta_{pt1}\frac{E_{pt1}}{E_{pt2}}\right)} \qquad (2.1)$$

Where l_c is the clamping length of the fastener system, E_{t1} and E_{t2} the modulus of the material (part or screw) at temperatures T_1 and T_2 respectively, ΔT the temperature difference involved and $\delta_{s/p}$ the resilience of the screw / part involved [32]. Equation (2.1) gives a good indication of what can be done to minimize the preload in a fastening system:

- Minimizing the thermal expansion mismatch (i.e. α_p - α_s).
- Reducing the temperature difference (ΔT).
- Maximizing, for the given clamping length, both the resiliencies δ_s and δ_p.

By implementing equation (2.1) into design, an accurate value of stress addition or stress loss in a joint containing a fastening system, due to operations at elevated temperature, can be calculated. Sufficient provision for the above-mentioned scenario can then be made in the design by the design engineer.

2.4 Recuperator Design Methodologies

Common methods used to design recuperators involve the Log Mean Temperature Difference- (LMTD) and the Effectiveness-NTU methods (ε-NTU) [5]. According to Incropera et.al. [33], the LMTD method is a simple method to employ when designing a recuperator if the fluid temperatures are known and the outlet temperatures are specified or readily determined from the energy balance expressions. However, if only the inlet temperatures are known, it is preferable to use an alternative approach in analyzing the heat exchanger design at hand, termed the Effectiveness-NTU method. The following section will analyze the ε-NTU method in detail.

2.4.1 Heat Exchanger Analysis: ε-NTU method

The rating of a recuperator concerns the evaluation of the performance of a fully specified heat exchanger to do a job. The rating of a heat exchanger does not imply the best possible utilization of the given exchanger. It simply evaluates whether or to what degree a given job can be performed within the constraints of the flow rates, heat duty, fouling resistance, and the allowable pressure drop. The effectiveness of a heat exchanger may be defined as the ratio of the actual heat transfer to the maximum possible heat transfer, i.e.

$$\varepsilon = \frac{q}{q_{\max}} \tag{2.2}$$

The effectiveness of a counterflow heat exchanger in general is considered to be better than any other heat exchanger configuration since a smaller surface area for the same fluids is required to achieve the same heat transfer [34]. In theory, the maximum heat transfer one could achieve with a counterflow arrangement is achieved by implementing equation (2.3):

$$q_{\max} = (\dot{m} Cp)_{\min} (T_{h,i} - T_{c,i}) \tag{2.3}$$

where $\dot{m}$ refers to the massflow of the fluid, Cp to the fluid specific heat, $T_{h,i}$ to the inlet temperature of the hot working fluid and $T_{c,i}$ to the inlet temperature of the cold working

fluid. The minimum product of $(\dot{m}\,Cp)$ in equation (2.3) is needed since the fluid with the lowest value for $(\dot{m}\,Cp)$ undergoes the maximum possible temperature difference. Consequently, the maximum possible heat transfer can occur. For convenience, the heat capacity rates are defined as follows:

$$C_c = m_c Cp_c \text{ and } C_h = m_h Cp_h, \tag{2.4}$$

where $C_c = C_{min}$ if $C_c < C_h$

or $C_h = C_{min}$ if $C_h < C_c$.

In the latter equation, the subscripts c and h refer to the cold and hot fluid streams respectively. By incorporating equations (2.2) and (2.3), the actual heat transfer rate may be readily determined from the following expression:

$$q_{actual} = \varepsilon (mCp)_{\min} (T_{h,i} - T_{c,i}) \tag{2.5}$$

According to Incropera et.al. [33], expression (2.6) applies for any heat exchanger. Here, C_{min}/C_{max} (also denoted by C_r) is equal to C_c/C_h or C_h/C_c depending on the relative magnitudes of the hot and cold fluid heat capacity rates.

$$\varepsilon = f(NTU, \frac{C_{\min}}{C_{\max}}) \tag{2.6}$$

The *number of transfer units (NTU)* is a dimensionless parameter and indicates the relative heat transfer surface area. The latter is defined as

$$NTU = \frac{UA}{C_{\min}} \tag{2.7}$$

where UA is the overall heat transfer coefficient.

2.4.2 Overall Heat Transfer Coefficient

According to Incropera et.al. [33], the determination of the overall heat transfer coefficient is an essential, and sometimes one of the most uncertain parts of any heat exchanger analysis. The overall heat transfer coefficient is related to the total thermal resistance to heat transfer between two fluids according to expression (2.8).

$$UA = \frac{1}{R_{tot}} \tag{2.8}$$

The total thermal resistance (R_{tot}) is determined by the following:

- The conduction and convection resistances between fluids separated by a composite plane.
- The fouling factor (R_f), i.e. when heat transfer surfaces are subject to fouling by fluid impurities, rust formation, or deposition of fluid films (distinguish between $R_{f,c}$ and $R_{f,h}$ for the cold- and hot fluid stream fouling factors in equation (2.9)).
- The thermal resistance experienced due to the wall material between fluids namely R_w, which is a function of thermal conductivity – the basis for selecting W-Cu as the appropriate heat transfer material.

With the inclusion of surface fouling and fin effects, the overall heat transfer coefficient may be expressed by equation (2.9) as follows;

$$\frac{1}{UA} = \frac{1}{(\eta_o hA)_c} + \frac{R''_{f,c}}{(\eta_o A)_c} + R_w + \frac{1}{(\eta_o hA)_h} + \frac{R''_{f,h}}{(\eta_o A)_h} \tag{2.9}$$

In the above equation, h and A represents the fluid heat transfer coefficient and the total heat transfer area respectively, while η_o is termed the overall surface efficiency or the temperature effectiveness of a finned surface. The overall surface efficiency is defined by

$$\eta_o = 1 - \frac{A_f}{A}(1 - \eta_f) \tag{2.10}$$

where A_f is equal to the entire surface area of a fin and η_f is the efficiency of a single fin. η_f can be calculated as follows;

$$\eta_f = \frac{\tanh(mL)}{mL} \tag{2.11}$$

with

$$m = \sqrt{\left(\frac{hP}{kA_c}\right)} \tag{2.12}$$

In equation (2.11), L is identified as being the length of a single fin. In equation (2.12), P is defined as the perimeter of the fin, k as the thermal conductivity of the fin material and A_c is the cross section area involved. It is defined such that, for the hot or cold surface without fouling, the heat transfer rate is equal to equation (2.13).

$$q = \eta_o hA(T_b - T_\infty) \tag{2.13}$$

where T_b is the base surface temperature and A is the total surface area (fin plus exposed base area) [33].

2.4.3 ε-NTU Relations

The effectiveness of a particular heat exchanger (ε) is often tabulated as a function of C_r and NTU (as seen from equation (2.6)). These ε-NTU relations for various configurations of heat exchangers are summarized in Table 2.9.

The primary aim in the thermal design of heat exchangers is to determine the necessary surface area required to transfer heat at a given rate for given fluid temperatures and flow rates [35]. The latter is facilitated by employing the overall heat transfer coefficient, UA, in the fundamental heat transfer relation

$$q = UA\overline{\Delta T} \tag{2.14}$$

where $\overline{\Delta T}$ is an average effective temperature difference for the entire heat exchanger.

Flow Configuration	Effectiveness Equation	Equation
Parallel flow	$\varepsilon = \frac{1-e^{-NTU(1+C_r)}}{1-C_r}$	(2.15)
Counterflow	$\varepsilon = \frac{1-e^{-NTU(1-C_r)}}{1-(C_r)e^{-NTU(1-C_r)}}$	(2.16)
Cross-flow (Both streams unmixed)	$\varepsilon = 1-e^{-NTU}$	(2.17)
Cross-flow (Both streams mixed)	$\varepsilon = \frac{NTU}{\frac{NTU}{(1-e^{-NTU})}+(C_r)\frac{NTU}{(1-e^{-NTU(C_r)})}-1}$	(2.18)
Cross-flow (Stream C_{min} unmixed)	$\varepsilon = \frac{1}{C_r}(1-e^{-C_r(1-e^{-NTU})})$	(2.19)
Cross-flow (Stream C_{max} unmixed)	$\varepsilon = 1-e^{\left(\left(\frac{1}{C_r}\right)\left(1-e^{-NTU(C_r)}\right)\right)}$	(2.20)

Table 2.9: *Summary of recuperator effectiveness equations for various flow configurations.* Modified after Pitts & Sissom [35].

2.4.4 Pressure Drop Equations

Pressure drop in fluid flow is energy that is lost. In engineering practice, the pressure drop in pipes and ducts can be calculated from

$$\Delta p_{0,L} = \left(\frac{fL}{D_H} + \sum K\right)\frac{|\dot{m}|\dot{m}}{2\rho A^2_{ff}} \qquad (2.21)$$

with A_{ff} the free flow area, D_H the hydraulic diameter, L the length, f the so-called *Darcy-Weisbach* friction factor and ΣK the sum of the secondary loss factors due to elbows, T-pieces, valves, etc. The *Darcy-Weisbach* equation is valid for non-circular ducts when the geometric diameter is replaced by the hydraulic diameter D_h defined by:

$$D_h = \frac{4A}{P_w} \tag{2.22}$$

where A is the cross-sectional area and P_w is the wetted duct perimeter (i.e. the perimeter touched by the fluid). The friction factor is a function of the Reynolds number (Re) in the pipe and the relative roughness of the surface finish ε/D_H. The Reynolds number can be calculated as follows:

$$\mathrm{Re} = \left| \frac{\dot{m}}{\mu} \frac{D_H}{A_{ff}} \right| \tag{2.23}$$

with μ the viscosity of the gas in the pipe. The friction factor obtained is calculated for laminar flow (Re < 2000) from

$$f = \frac{C}{\mathrm{Re}} \tag{2.24}$$

with $C = 64$ for round ducts and pipes, $C = 57$ for square ducts and $C = 96$ for very flat rectangular-shaped ducts [36]. For turbulent flow ($5 \times 10^3 < \mathrm{Re} < 10^8$ with $10^{-6} < \varepsilon/D_H < 10^{-2}$), the friction factor may be calculated from

$$f = 0.25 \left(\log \left(0.27 \frac{\varepsilon}{D_H} + \frac{5.74}{\mathrm{Re}^{0.9}} \right) \right)^{-2} \tag{2.25}$$

2.5 Conclusion – Literature Survey

After the detailed investigation and review of available recuperator technologies with its related fields, the author has identified the following methods for establishing the recuperator of this research:

- For manufacturing, a conventional machining procedure will be used. Due to financial aspects and practicality, manufacturing of heat transfer profiles by means of tungsten carbide drill bits has been selected as the preferred manufacturing method.

- Diffusion bonding has been selected as the most applicable/feasible method for implementation into the recuperator design to ensure a high structural integrity of the recuperator assembly.

- The design methodology for the recuperator will be based on the ε-NTU method. Motivation for this is elaborated upon in the design limitations noted here after.

3 THERMAL DESIGN OF THE RECUPERATOR

3.1 Introduction

The objective of this chapter is to describe the design of the recuperator of limited size produced from W-Cu. Design calculations were carried out using EES® as the equation solver given predetermined conditions and constraints (operational and dimensional).

3.2 Recuperator Core Design

3.2.1 Implementation of Design Methodology

Heat exchanger design problems can be twofold of nature [33]. One scenario is where most input parameters are known, i.e. fluid inlet temperatures and flow rates together with a desired hot or cold outlet temperature. The design problem is then one that consists of selecting the appropriate heat exchanger type and ideal size of the heat transfer area that would be sufficient to achieve the desired outlet temperature. The second scenario is applicable to the specific design at hand. The heat exchanger type and size is known (the reason for this will be discussed in the following section) and the objective is to determine the heat transfer rate and fluid temperatures for a pre-determined massflow and inlet temperature. For the latter, the ε-NTU method is commonly employed, and has also been employed in the current design. By implementing the ε-NTU-method, the tricky iterative nature of using the LMTD-method can be eliminated. The NTU and C_{min}/C_{max} values may be computed if the heat exchanger type, size and flow rates to be implemented are known as input. Consequently, the effectiveness of the heat exchanger can be determined by the

applicable equation, where after values for the heat transfer rate and outlet temperatures can be determined.

3.2.2 Design Specific Limitations

Several factors, of primary and secondary importance, played a role in constraining the designed recuperator's size. These were as follows:

- Primarily the cost of the specific grade of tungsten-copper used in the manufactured recuperator was the limiting factor, which consequently imposed a tight budget and a recuperator constrained by size.
- Machining costs encountered in machining the heat transfer profile of the recuperator was of secondary importance, but also limiting regarding the size of the recuperator.

These factors constrained the recuperator size to some extent. Aspects concerning the size of the recuperator profile geometry, plate geometry and profile geometry length are defined in the following section.

3.2.3 Core Design

3.2.3.1 Profile Geometry

When referring to the profile geometry of the recuperator, reference is given to the geometry of a recuperator channel that would serve as path for fluid flow. Part of the information needed as input into the thermal design included the size of the profile geometry intended for use. These basic values for single cell geometry are defined in Figure 3.1.

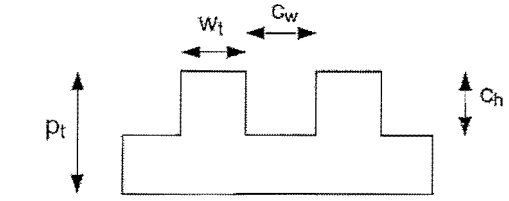

Figure 3-1: *General profile geometry. Both plate geometries possess the same profile geometry but have different layouts.*

3.2.3.2 Plate Geometry

Taking into account previous literature with reference to available recuperator geometries as well as material availability issues, it has been decided to base the recuperator design on that of a micro-channel recuperator, with the schematic representation of the layout shown below. Schematic layouts of firstly the different plate geometries used in the design and secondly the assembly of these profiles are shown in Figure 3-2 and Figure 3-3. This concept incorporates a simple cross-counterflow configuration, where the largest part of the configuration is of a counterflow nature. The exact amount of plates used is determined later in this chapter.

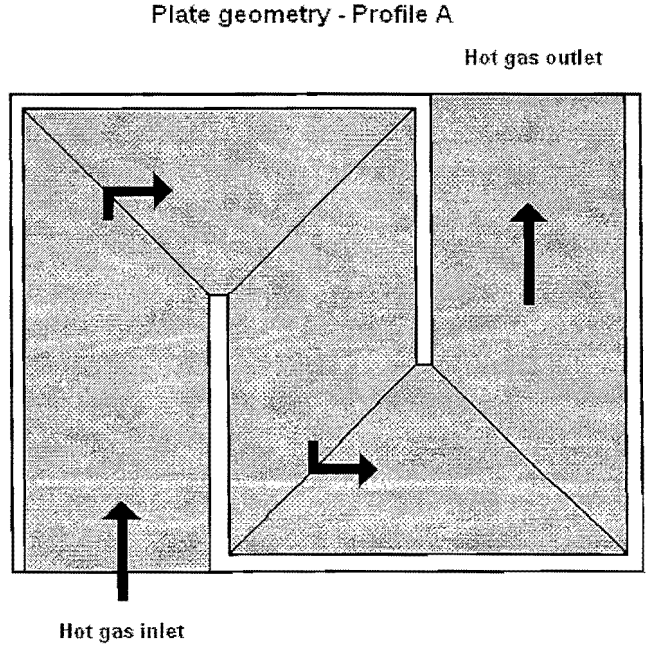

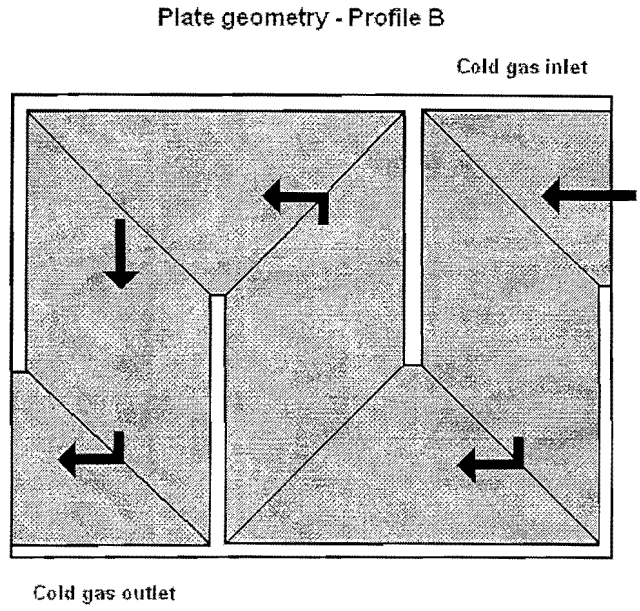

Figure 3-2: *Designed layout of the individual plate geometries. With this design, the maximum surface area is utilized in the heat transfer process and thus the most compactness of the recuperator obtained (i.e. ratio of heat transfer area vs. volume of the recuperator).*

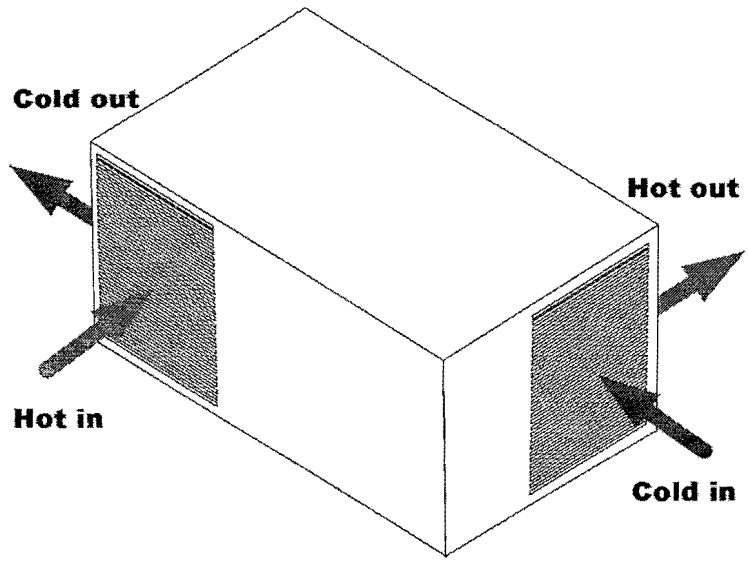

Figure 3-3: *Schematic illustration of the assembled recuperator model consisting of a sequence of the two different geometries*

3.2.3.3 Channel Length

The channels in the recuperator plate geometry are orientated in such a way that the length of each channel would be just as long as the other adjacent channels. For the purpose of this

design, being constrained by size, the value of the channel length has been selected as 300mm.

3.2.4 Thermal Design Input Values

With some dimensional elements of the recuperator being known and by defining values for feasible operational temperatures, pressures as well as optimum mass flows, design calculations relating to the performance of the recuperator of this research were compiled using EES® as the equation solver. Input values decided upon and used in these calculations are shown in Table 3.1. These values were partly modeled around those implemented for the recuperator used in the Pebble Bed Micro Model (PBMM). However, a much smaller mass flow was used due to the size constraint on the recuperator under consideration.

W-Cu Recuperator characteristics	Property value
Profile width (c_w)	2mm
Profile height (c_h)	2mm
Fin thickness (w_t)	1mm
Base thickness ($p_t - c_h$)	1mm
Channel length	300 mm
Channel amount / plate	Tbd
Plate amount	Tbd

Table 3.1 (a): *The initial defined characteristics which are employed in the manufactured W-Cu recuperator.*

Initial operating conditions	Property value
Hot inlet temperature (degrees)	400 ºC
Hot inlet pressure (kPa)	200 kPa
Cold exit temperature (degrees)	20 ºC
Cold exit pressure (kPa)	500 kPa
Hot channel mass flow (kg/s)	0.0001
Cold channel mass flow (kg/s)	0.0001
Fluid	Nitrogen Gas

Table 3.1 (b): *The dimensional and operational conditions decided upon for use in design calculations of the W-Cu recuperator carried out in EES®..*

3.3 Results of Thermal Design

3.3.1 Results of EES Calculations

Design calculations of the recuperator were carried out in EES®. For the complete EES calculation sheet with accompanying results, refer to Appendix A. It is important to remember that the results stated have been carried out for one hot and one cold recuperator channel only. Collective results are stated later on, together with the geometry for the recuperator under consideration.

3.3.1.1 Results for one channel

Results from the design calculations for the hot and cold sides are shown in tabulated form in Table 3.2. A channel effectiveness of 96.6% was derived. By incorporating a channel length

of 300mm and the respective profile size of 2mm x 2mm, a hot- and cold side pressure drop of respectively 16.217% and 2.38% was incorporated. Theoretically, the hot channel exit- and cold channel exit temperatures have been determined as 38.9°C and 382.2°C respectively.

Operating characteristic	Property value
Hot channel mass flow (kg/s)	0.0001
Hot inlet pressure (kPa)	200 kPa
Hot exit pressure (kPa)	167.57 kPa
Delta P_{hot} (%)	16.217 %
Hot inlet temperature (degrees)	400 ºC
Hot exit temperature (degrees)	38.9 ºC
Cold channel mass flow (kg/s)	0.0001
Cold inlet pressure (kPa)	500 kPa
Cold exit pressure (kPa)	488.14 kPa
Delta P_{cold} (%)	2.38 %
Cold inlet temperature (degrees)	20 ºC
Cold exit temperature (degrees)	382.2 ºC
Maximum heat transfer / channel	39.6 W
Actual heat transfer / channel	38.24 W
Effectiveness of recuperator channel	96.6 %

Table 3.2: *Results derived from the equation solver for the recuperator conditions as stated in Table 3.1(a) and (b) for one hot and one cold recuperator channel.*

3.3.1.2 Size limitation of the recuperator

Before the proposed size and amount of W-Cu plates could be determined, it was necessary to weigh up the thermal design of the recuperator against the cost of the material. The golden mean between the right amount of channels per plate in the recuperator design and the cost of the individual tungsten-copper plates also had to be found. For the purpose of this design, it was decided that:

- A total of 52 heat transfer channels, for the hot and cold sides respectively, would be selected for the design.

- With the latter in place, a workable plate size was decided on, at approximately 100mm x 140mm x 3mm.
- Each tungsten-copper plate would then house 13 heat transfer channels.
- A total amount of eight plates would be needed in the design of the W-Cu recuperator.
- The total cost of the eight plates amounted to R15,000.00.

3.3.2 Design/Fabrication Specifications

The design and fabrication specifications of the recuperator were determined by incorporating the W-Cu plate size and amount of plates available with the results stated in Table 3.2. These specifications are shown in Table 3.3. Profiles A and B would each incorporate 52 channels through the 8 plates of the recuperator unit, totaling up to 104 channels. Also stated in Table 3.3 is the *heat transfer area to recuperator volume* ratio of the proposed unit which is shown to be $371.43 m^2/m^3$. The theoretical achievable heat transfer amounts to ± 2 kW for the whole recuperator unit.

The results derived from these calculations have been used to generate a virtual 3D model of the mini-channel recuperator presented in this research. This model, created in Solidworks®, has been used for fabrication purposes and the detailed manufacturing drawings created from this model are attached in Appendix B.

Operating characteristic for recuperator	Property value
Channel amount per plate – profile A	13 channels
Channel amount per plate – profile B	13 channels
Profile A plates (qty)	4 plates
Profile B plates (qty)	4 plates
Total Heat Transfer Area (m^2)*	0.1248m^2
Total Volume of structure (m^3)*	0.000336m^3
Alpha (m^2/m^3)	371.43m^2/m^3
Hot side mass flow (kg/s)	0.0052
Cold channel mass flow (kg/s)	0.0052
Maximum heat transfer of recuperator	2059.2W
Actual heat transfer of recuperator	1988.48W
Effectiveness of recuperator channel	96.6%

Table 3.3: *Results derived from the equation solver for the whole recuperator unit.*

4 FABRICATION OF THE DESIGNED RECUPERATOR

4.1 Introduction

This chapter describes the fabrication of the designed tungsten-copper recuperator as stated in chapter 3, effected by techniques identified in chapter 2.

The heat transfer profiles of the recuperator plate geometries have been established by use of 2mm sized tungsten carbide drill bits and using CNC machining based on the dimensions of the virtual models generated. Although it was concluded in chapter 2 that diffusion bonding was ideal for use in the recuperator of this research, the availability of diffusion bonding equipment as well as restrictions in funding has lead to the identification of a fastening system as an alternative joining method that was used in this study. Manufacturing drawings attached in Appendix B have been supplemented to reflect the incorporation of a fastening system as joining method into the recuperator assembly. Ideally the components making up the recuperator core can be diffusion bonded and should be investigated in future work.

4.2 Mini-channel Recuperator Components

Figure 4-1 shows the virtual 3D model of the assembly of recuperator components as generated in Solidworks®. Components that make up the assembly can be grouped as follows:

- Recuperator plate profile A
- Recuperator plate profile B
- Channel Sealants
- Fastening system and frame
- Integrated header box and headers

Detailed views and designations of all recuperator components can be seen in assembly drawing (5W3-FR01-01) attached in Appendix B (inclusive of the newly incorporated fastening system). Details regarding the fabrication of these components are elaborated upon next.

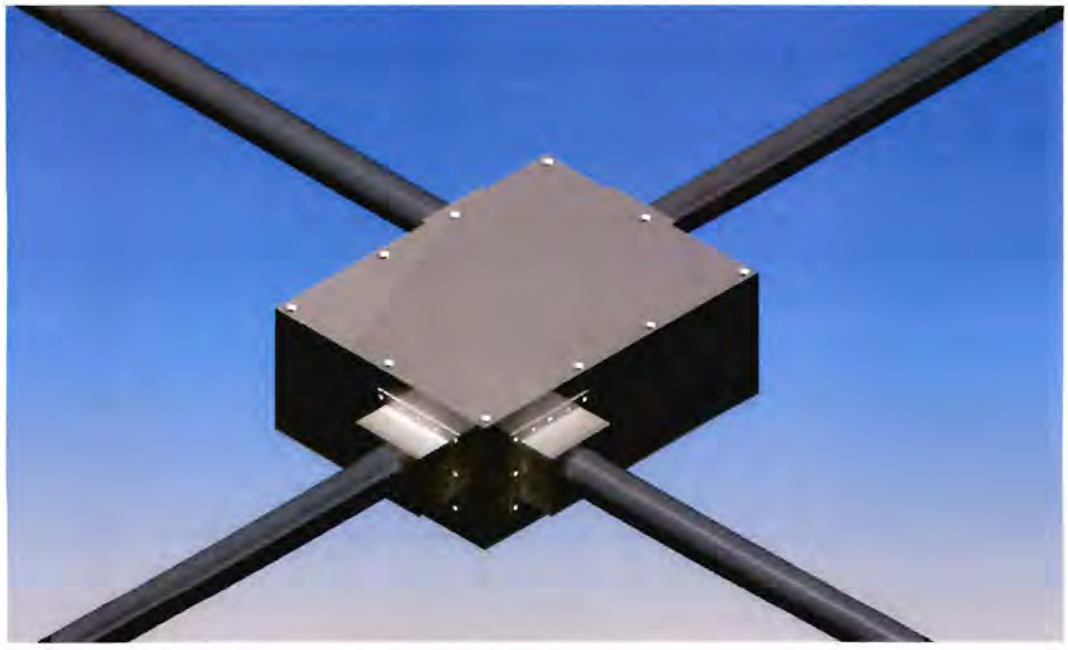

Figure 4-1: *Schematic illustration of the mini-channel recuperator assembly.*

4.2.1 Recuperator Plate Geometries A & B

The recuperator plate geometries are the foundation of the mini-channel recuperator in terms of functionality of the recuperator. The more heat transfer surface area available on the plates per unit volume, the larger the degree of effectiveness obtained from the recuperator as a whole. Some fabrication specifications that were outlined in chapter 3 of this document and used in fabrication entailed the following:

- Channel dimensions - 2mm x 2mm x 300mm.
- Channel amount - 13 channels/plate.
- Flow configuration - majority counterflow

Figure 4-2 shows the implementation of all above mentioned aspects into plate geometries A and B (Figure 4-2 (a), left and right respectively). By incorporating these plate geometries, a surface-area density of 371.43m^2/m^3 was achieved. Four sets of plate geometries A and B have been joined to each other to form the recuperator unit (partly assembled recuperator unit showed in Figure 4-2 (b)). The dimensions of the partly assembled unit are 100mm x 140mm x 24mm.

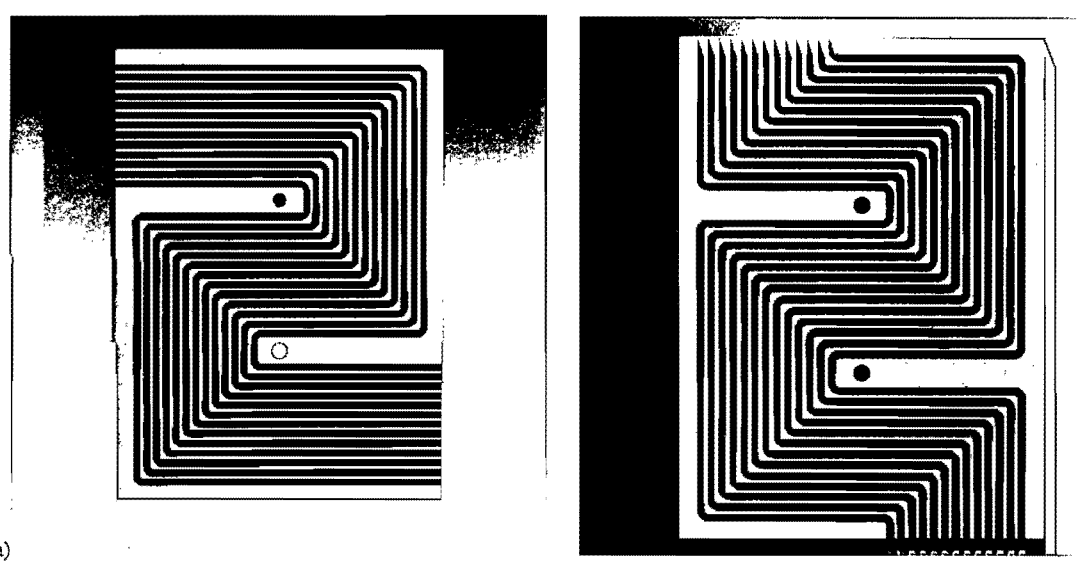

(a)

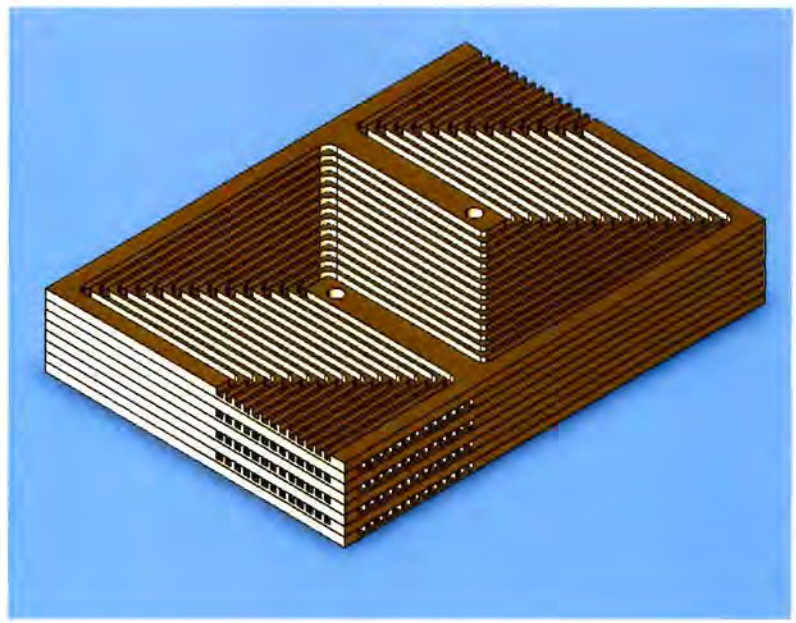

(b)

Figure 4-2: *(a) Schematic Illustration of recuperator plate geometries A (top left) and B (top right) implemented in the (b) partly assembled recuperator unit (bottom).*

Channels from plate geometry A serves as a medium for the higher temperature fluid, while profile B serves as a medium for the lower temperature fluid. As mentioned earlier, machined profiles have been established by use of 2mm sized tungsten carbide drill bits and CNC machining based on the dimensions of the virtual models generated. With the orientation of the header inlets and outlets on the series of plate geometries as such, header sections were easily attached to the assembled unit.

Aspects that were of primary concern in assembling the recuperator plate geometries by means of the newly identified fastening system involved the following:

- Possible leakage of working fluid in the horizontal plane of the recuperator unit, i.e. between adjacent W-Cu plate geometries.
- Possible leakage of working fluid at the corners of the assembled unit (from high pressure side to low pressure side).

0.1mm thick annealed C23000 (otherwise known as "Red Brass") with a thermal conductivity value of about 160W/m.K was employed as gasket material between the

assembled W-Cu plates to limit any leakage that might occur through the horizontal stacking planes. To some extent, the use of C23000 to seal off the respective plate geometries defeats the application of using W-Cu material in the design. These sheets were used in the design for the sole purpose to seal off recuperator plate geometries when tested for a leak, which would not have been required if the plate geometries were diffusion bonded. Due to restrictions in equipment availability and lack of funding for diffusion bonding, this alternative method of sealing has been used. The use of C23000 as gasket material is illustrated in Figure 4-3.

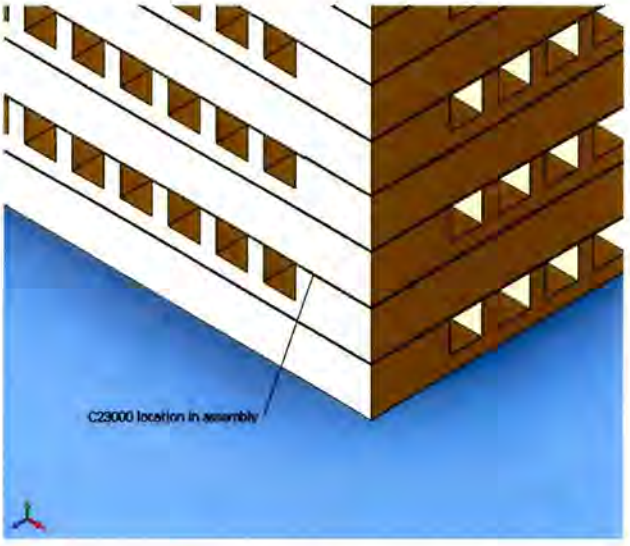

Figure 4-3: *Schematic illustration of the location of the C23000 gasket material used in the assembly of the mini-channel recuperator.*

4.2.2 Fastening System and Frame

4.2.2.1 Initial remarks

A fastening system had to be identified as the joining method for the recuperator of this research to supply the recuperator with sufficient structural integrity needed to work effectively. Overhead requirements to which the fastening system was subjected to were identified, taking into account the previous literature elaborated upon in chapter 2 of this document. These requirements are shown in Table 4.1.

System Requirements	Description / Value
Thermal Expansion Mismatches	Minimized / Eliminated up to 400℃
Assembly Load (*m*)	2,000kg
Minimum Safety Factor	1.5

Table 4.1: *Primary requirements set out by the author for the fastening system implemented in the mini-channel recuperator.*

4.2.2.2 Fastener specifications and calculations

Figure 4-4 gives a schematic illustration of the fastening system implemented into the design. The fastening system incorporates a frame enclosing the top and bottom of the recuperator and held in place by 12 M4 x 42mm bolts. Only 2 of the 12 bolts utilized go through the recuperator unit while the other 10 bolts are positioned directly from the top frame to the bottom frame. The bolt grade and related properties used are specified in Table 4.2.

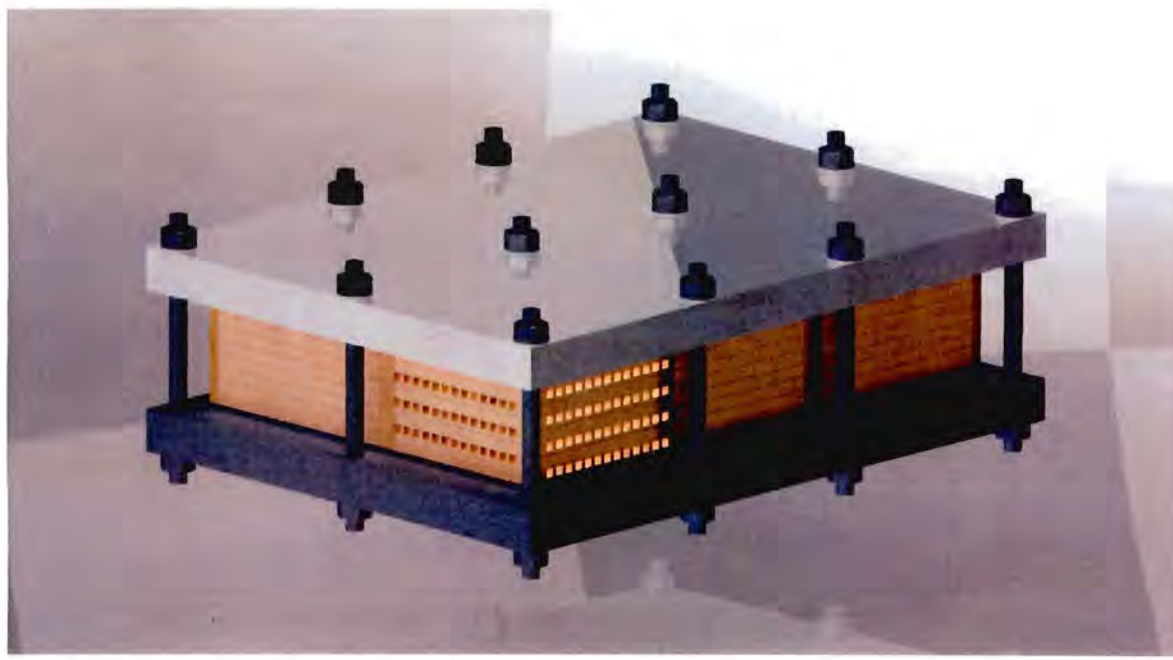

Figure 4-4: *Schematic illustration of the fastening system consisting of the top and bottom clamping frames and the twelve M4 x 42 bolts.*

Criteria/Property	Value
Bolt Grade / Property Class	5.8
Bolt size	M4
Minimum proof strength (S_p in MPa)	380MPa
Tensile stress area (A_t in mm2)	8.78
Number of bolts	12

Table 4.2: *Metric mechanical-property class and other properties for Steel M4 bolts.*

Given the input from Tables 4.1 and 4.2, the twelve M4 x 42 bolts (grade 5.8) in the recuperator assembly were subjected to an axial load (P) of 19620 Newton (see equation (4.1)). This preload was applied to the bolts in the fastener assembly by compressing the recuperator plates evenly to the specified load *m* by means of a hydraulic press. With the load applied, all bolts were consequently hand tightened. By doing this, control over the load experienced by all bolts was effectively exercised.

$$P = mg = (2000kg) * 9.81 = 19620N \tag{4.1}$$

For a joint constant of C=0.32, one bolt in the assembly experiences the following bolt stress:

$$\begin{aligned} \sigma_1 &= F_i + \left(C * \frac{P}{12} \right) \Big/ A_t \\ &= \left(0.32 * \frac{19620}{12} \right) \Big/ 8.78 \\ &= 59.6MPa = \pm 60MPa \end{aligned} \tag{4.2}$$

The value for F_i is virtually zero since the preload has been applied to the bolts in the fastening assembly by means of hydraulic compression of recuperator plates, and hand tightening of bolts. The value of the bolt stress experienced by one bolt as calculated is only a fraction of the minimum proof stress (S_p) as stated in Table 4.2. By incorporating the answer from equation (4.2) into equation (4.3), the safety factor for one bolt was derived when operating at room temperature.

$$SF_{bolt} = SP_{\min} / \sigma_1 = 6.33 \quad (4.3)$$

As can be seen, the safety factor of 6.33 derived from equation (4.3) is more than sufficient when compared to the initial required safety factor of 1.5. It must be mentioned that this case is only valid for the unit at room temperature. The temperature effect on the fastening system will be addressed next.

4.2.2.3 High temperature effect on fastening system

As mentioned in chapter 2 of this document, it was important to take into account the thermal expansion mismatches of all material components involved in the assembly, at the applicable operating temperatures. This had to be done to avoid any load variation in the fastening system at elevated temperatures, if operated, that might cause the recuperator unit to leak. The change (increase/decrease) in the bolt stress experienced by a bolt when used to clamp a parts of different composition for use at elevated temperatures is given by equation (4.4), which is a modified version of equation (2.1) stated earlier on [32].

$$\Delta\sigma_p = \frac{\alpha_p - \alpha_s}{\left(\frac{1}{E_s A_s}\right) + \left(\frac{1}{E_p A_{sub}}\right)} (\Delta T / A_s) \quad (4.4)$$

In equation (4.4), the following terms are referenced:

- α_p and α_s refer to the thermal expansion coefficients of the clamped part and the bolt respectively.
- ΔT refers to the change of temperature experienced by the fastening system.
- E_p and E_s refer to the Young's Moduli of the clamped part and bolt respectively.
- A_s refers to the nominal cross section area of the bolt/screw in mm^2.
- A_{sub} refers to the area of real stress distribution in the clamped part in mm^2.

By using equation (4.4), an accurate estimate of the change in the bolt stress as experienced by the bolts in the fastening system due to temperature effects was made. Changes in bolt stresses up to 400℃ caused by equivalent assembly widths of (i) W-Cu plates (24mm) as well as (ii) C23000 sheets (1mm) when clamped were calculated and are shown in Tables 4.3 to 4.6.

For the W-Cu plates, results are as follows:

Overall thickness of W-Cu plates (mm)	24mm
Real stress distribution area (A_{sub}) (cm^2)	1.556 cm^2
Real stress distribution diameter (D_{sub}) (cm)	1.466 cm

Table 4.3: *Thickness and other properties relating to W-Cu plates in assembly.*

Temp difference (℃)	Thermal stress decrease (MPa)
5	-4.8
10	-9.7
15	-14.5
20	-19.4
25	-24.2
30	-29.1
35	-33.9
40	-38.8
45	-43.6
50	-48.5
55	-53.3
60	-58.2
65	-63.0
70	-67.9
75	-72.7
80	-77.6
85	-82.4
90	-87.3
95	-92.1
100	-97.0
110	-106.7
120	-116.4
130	-126.1
140	-135.8
150	-145.5
160	-155.2
170	-164.9
180	-174.6
190	-184.3
200	-194.0
225	-218.3
250	-242.5
275	-266.8
300	-291.0
325	-315.3
350	-339.5
375	-363.8
400	-388.1

Table 4.4: *Thermal stress decrease caused by equivalent width of W-Cu plates at 5 ℃<T<400 ℃.*

For the C23000 sheets, results are as follows:

Overall thickness of C23000 sheets (mm)	1mm
Real stress distribution area (A_{sub}) (cm^2)	0.714 cm^2
Real stress distribution diameter (D_{sub}) (cm)	1.038 cm

Table 4.5: *Thickness and other properties relating to C23000 sheets in assembly.*

Temp difference (℃)	Thermal stress increase (MPa)
5	1.5
10	3.1
15	4.7
20	6.3
25	7.8
30	9.4
35	11.0
40	12.6
45	14.2
50	15.7
55	17.3
60	18.9
65	20.5
70	22.1
75	23.6
80	25.2
85	26.8
90	28.4
95	29.9
100	31.5
110	34.7
120	37.8
130	41.0
140	44.2
150	47.3
160	50.5
170	53.6
180	56.8
190	59.9
200	63.1
225	71.0
250	78.9
275	86.8
300	94.7
325	102.6
350	110.5
375	118.4
400	126.2

Table 4.6: *Thermal stress increase caused by equivalent width of C23000 sheets at 5 ℃<T<400 ℃*

- For the identified fastening system clamping an equivalent width of W-Cu plates (24mm) at a temperature of 400℃, a decrease in bolt stress of 388MPa was calculated.
- For the identified fastening system clamping an equivalent width of C23000 sheets (1mm) at a temperature of 400℃, an increase in bolt stress of 126MPa was calculated.
- For the fastened assembly of both W-Cu plates and C23000 sheets (equivalent widths at a temperature of 400℃), a decrease in bolt stress of 262MPa was calculated, thus a decrease in bolt stress of 21MPa per bolt.

To counteract this loss of applied load, a positive change in bolt load was required. This has been done by including 2 additional aluminum plates in the fastener assembly (each plate of width 1.6mm), providing the increase in the bolt stress required at elevated temperatures to minimize any thermal expansion mismatches between components in the fastener assembly. The implementation of this in the fabricated recuperator design is shown in Figure 4-5. Calculation of the thermal stress increase caused by an equivalent width (3.2mm) of aluminum plates are also shown in Tables 4.7 to 4.8, after which the final change in bolt stress caused by the fastened assembly at elevated temperatures is noted.

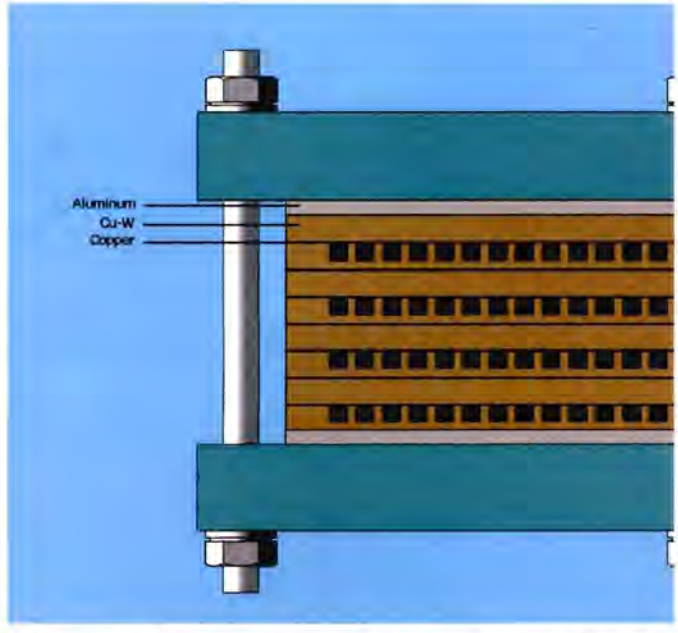

Figure 4-5: *Location of the two additional aluminum plates in the W-Cu structure*

For the Aluminum 3032 plates, results are as follows:

Overall thickness of Al 3032 sheets (mm)	3.2 mm
Real stress distribution area (A_{sub}) (cm^2)	0.901 cm^2
Real stress distribution diameter (D_{sub}) (cm)	1.147 cm

Table 4.7*: Thickness and other properties relating to aluminum plates in assembly.*

Temp difference(℃)	Thermal stress increase (MPa)
5	3.0
10	6.1
15	9.2
20	12.3
25	15.4
30	18.5
35	21.6
40	24.7
45	27.8
50	30.8
55	33.9
60	37.0
65	40.1
70	43.2
75	46.3
80	49.4
85	52.5
90	55.6
95	58.7
100	61.7
110	67.9
120	74.1
130	80.3
140	86.5
150	92.6
160	98.8
170	105.0
180	111.2
190	117.4
200	123.5
225	139.0
250	154.4
275	169.9
300	185.3
325	200.8
350	216.2
375	231.7
400	247.1

Table 4.8*: Thermal stress increase caused by equivalent width of aluminum plates at 5 ℃<T<400 ℃.*

- For the identified fastening system clamping an equivalent width of aluminum plates (3.2mm) at a temperature of 400℃, an increase in bolt stress of 247MPa was calculated.
- For the whole fastened assembly (consisting of W-Cu plates, C23000 sheets as well as aluminum plates - all equivalent widths at a temperature of 400℃), a decrease in bolt stress of 13MPa was calculated, thus a decrease in bolt stress of ~1MPa per bolt.

4.2.3 Integrated Header Box and Headers

The integrated header box has the following primary functions:

- The integrated header box serves as housing for the mini-channel recuperator.
- The header box incorporates all respective headers and additional components into one unit to ensure the integrity of the recuperator.

A schematic illustration of the header box assembly is shown in Figure 4-6.

Figure 4-6: *Schematic illustration of the integrated header box together with headers for the recuperator.*

The integrated header box consists of the following components, also illustrated in Figure 4-7:

- **Header Box Base plate** (indicated by number **5,** Figure 4.7): Serves as the base plate for the whole recuperator unit. All of the side plates of the unit are located on the base plate through the clearance holes situated on the four edges of the base plate. The twelve bolts that protrude from the recuperator frame, are positioned in the bigger diameter blind holes on the same plate.
- **Header Box Side plates** (indicated by numbers **1 and 3,** Figure 4.7): While serving as the base for the recuperator headers, it also incorporates two slots on the left and right sides of the header openings respectively on the recuperator side, for positioning separate stainless steel inserts. Provision is also made to attach the side plates to the top and bottom fastening plates.
- **Slotted Plate Inserts** (indicated by number **4,** Figure 4.7): The purpose of the slotted plate inserts is twofold. Firstly, it locates the recuperator side plates in the correct position relating to the W-Cu plates of the recuperator. Secondly, the inserts seal off the path of the gas in the horizontal direction to a lower pressure environment when gas enters or exits through a header so that the fluid doesn't leak from the high pressure inlet to the low pressure exit of the recuperator. In order to effectively locate the slotted inserts in the recuperator assembly, provision for the inserts has been made in the W-Cu plates by implementing 1mm slots at a 1mm depth at the specified locations. This can be seen in Figure 4.8.
- **Mini-channel Recuperator Headers** (indicated by number **2,** Figure 4.7): The recuperator headers act as the interface of the nitrogen gas lines to the whole recuperator header box.
- **Header Box Top plate** (not shown in figure): The primary purpose of the header box top plate is to seal off the recuperator on the top of the unit, so that no egress of fluid from header entrance to outer environment takes place. It also, as with the bottom base plate, makes provision for locating the header box side plates and the twelve bolts protruding from the recuperator frame.

It is the purpose of the following chapter to evaluate the fabricated recuperator design by various identified means.

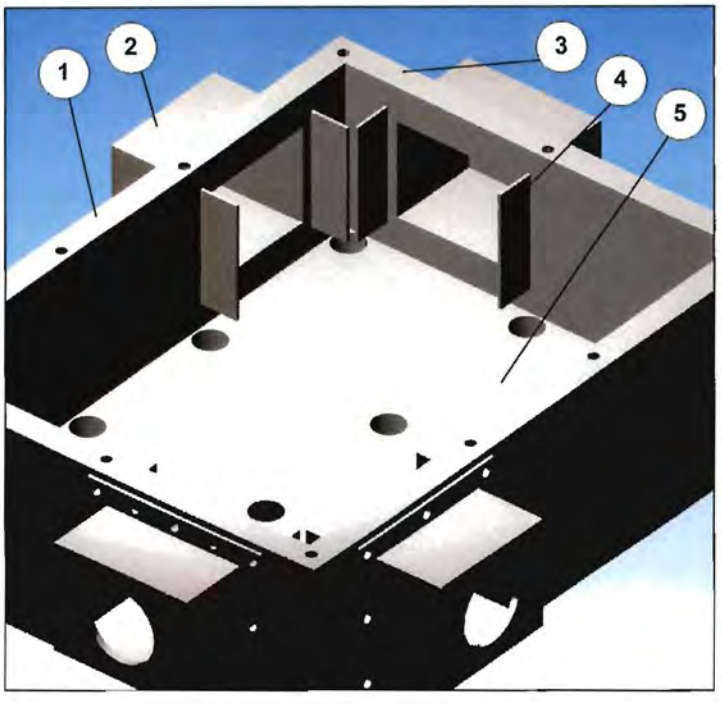

Figure 4-7: *Schematic illustration of the components that make up the integrated header box. (1 – Header Box side plate long, 2 – Recuperator headers, 3 – Header Box side plate short, 4 – Slotted plate inserts, 5 – Header Box base plate).*

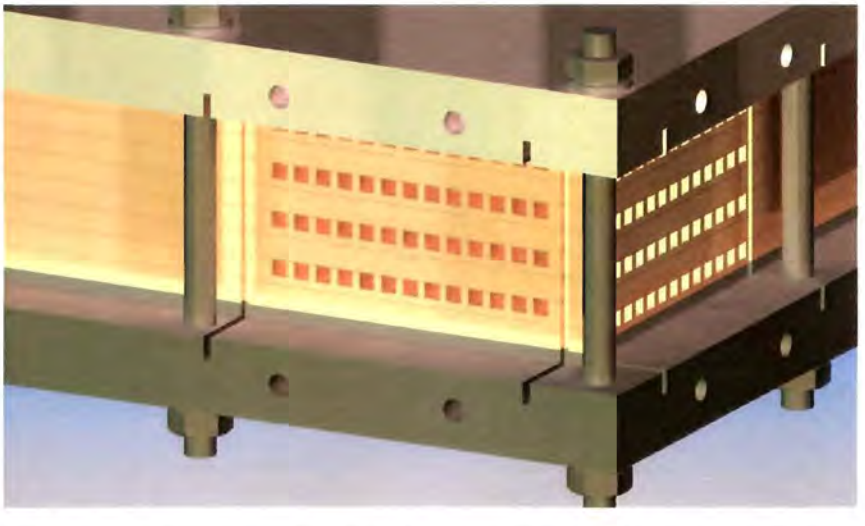

Figure 4-8: *Schematic illustration of the point of location for the slotted plate inserts in the recuperator unit.*

5 EVALUATION OF FABRICATED RECUPERATOR

5.1 Introduction

The objective of this chapter is to evaluate the fabricated W-Cu recuperator. Primary aspects that require attention involve the evaluation of the fabricated recuperator components as well as evaluation of the recuperator assembly integrity. These will be elaborated upon next.

5.2 Evaluation of Fabricated Recuperator

5.2.1 Evaluation of Fabricated Components

5.2.1.1 Evaluation areas for components

Different areas have been identified for evaluation of each recuperator component after it has been fabricated. These areas are shown in Table 5.1 and include:

- The flatness of critical parts – refers to the maximum deviation present in the direction perpendicular to a flat reference plane (i.e recuperator assembly planes) at any location on the fabricated component.
- Roughness of profiles – gives an indication of the quality of the material used in the design (specifically with reference to machined heat transfer profiles on recuperator plate geometries).
- Precision of machined parts – indication of whether the desired precision levels were achieved or whether the precision levels were affected by the manufacturing process.
- Surface finish of interfacing components – refers to the size of the bandwidth in which a specific surface dimension varies.

These areas are rated from (1) to (4) for the respective recuperator components in Table 5.1. The ratings used are denoted as follows:

- 1 - All in order: No non-conformances in evaluation area for specific component.
- 2 - Average/can be improved: End product derived from the identified method can be improved, but deviation should not be detrimental to the design.
- 3 - Not in order/might jeopardize the design: End product deviates from the specified requirements and may well influence the design negatively and fundamentally.
- 4 - Not applicable: Not applicable to the fabricated part.

Component	Evaluation areas for components							
	Flatness deviation of critical parts		Roughness of machined profiles		Precision of machined parts		Surface finish of interfacing components	
	Rating	Approx Deviation Value (mm)	Rating	Approx Measured Value	Rating	Approx Precision Value (mm)	Rating	Approx S.F. Value (mm)
Plate Geometry A	**3**	**±2mm**	4	n/a	**2**[5]	**±1 to ±2**	**2**	**±0.1mm**
Plate Geometry B	**3**	**±2mm**	4	n/a	**2**[6]	**±1 to ±2**	**2**	**±0.1mm**
Channel Profile A	4	n/a	**2**	**n/a**	1	±0.1mm	4	n/a
Channel Profile B	4	n/a	**2**	**n/a**	1	±0.1mm	4	n/a
Fastening frame	1	<0.1mm	1	n/a	1	±0.2mm	**2**	**±0.1mm**
Header Box Plates	1	<0.1mm	1	n/a	1	±0.2mm	**2**	**±0.1mm**
Headers	1	<0.1mm	1	n/a	1	±0.2mm	**2**	**±0.1mm**

Table 5.1: *Rating of evaluation areas for the manufactured recuperator components. All scores in bold are addressed below.*

5.2.1.2 Areas outside specification

The following areas are outside specification:

- Flatness deviation of recuperator plate geometries A and B - The flatness tolerance of the tungsten-copper plates used in the recuperator has changed dramatically from that set out in the concept design owing to the nature of the design and the residual stresses induced by the manufacturing process used. Due to these residual stresses and the little amount of material left at the base of the

[5] All in order except for slots machined for slotted plate inserts.
[6] All in order except for slots machined for slotted plate inserts.

plates after machining, a permanent flatness deviation of ±2mm of the plates has occurred in the z-direction relative to the x and y planes of the plates, resulting in a warped recuperator plate. The deviation of the manufactured recuperator plate geometry is shown in Figure 5-1 and Figure 5-2. All other plates manufactured for the header box have not shown this phenomenon due to the little amount of machining done on relatively thick work pieces compared to the recuperator plate geometries, where a large amount of machining was done on relatively thin work pieces.

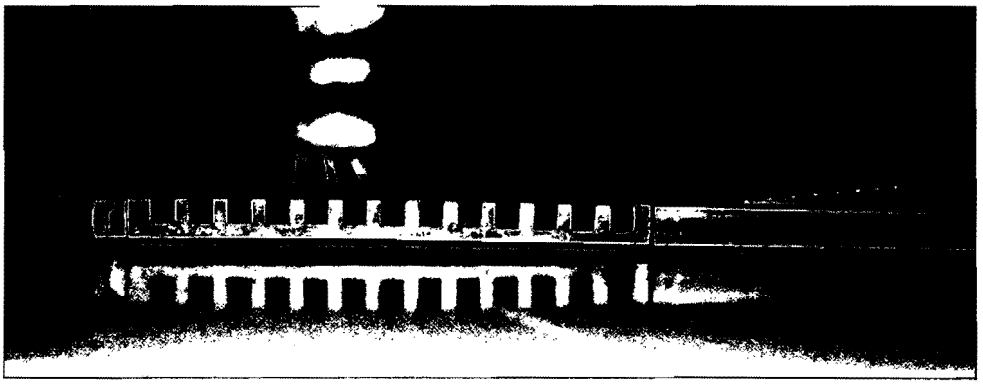

Figure 5-1: *Flatness deviation of recuperator plate geometry as a result of residual stresses induced by the manufacturing procedure used..*

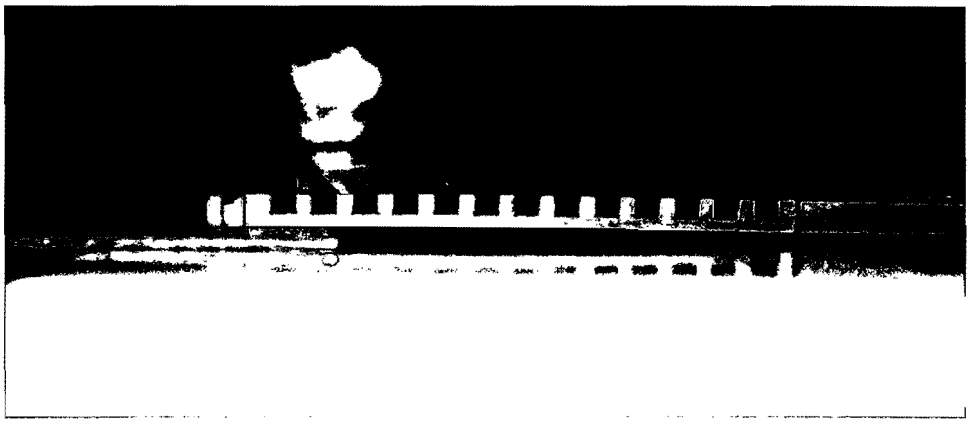

Figure 5-2: *Spacer with approximate width of 2mm to illustrate the deviation in the z-direction of the manufactured profile.*

5.2.1.3 Areas requiring improvement

The following areas require improvement (functional and non-functional improvements):

- Surface finish of plate geometries: Although C23000 Red Brass (0.1mm) is used to seal off the adjacent recuperator plate geometries, the ideal would have been to improve the surface finish of the respective plate geometries in such a way as to ensure a vacuum seal between adjacent plate geometries, without having to use the C23000 Red Brass sheets. Attempts to improve the surface finish of the plate geometries after manufacturing were hampered firstly by the size of the plates and secondly by the extent of the deformation experienced by the plates due to residual stresses induced by the machining of the channel profiles. As a result, it was impossible to manually implement a better surface finish. Automated surface treatment machines were also not an option since the fundamental bases upon which these equipment function, require the material to be treated to be a magnetic material, which tungsten-copper is not.
- Roughness of heat transfer channel profiles (Plate geometry A and B) – The roughness of the machined channel profiles varies in regions for each recuperator plate. This roughness is not, at any rate, attributable to wear experienced by the drill bits used over time, since this "variable roughness" phenomena was also present with the utilization of new drill bits. The variation in roughness might be attributable to a non-uniform material composition or homogeneity in the recuperator plate geometries, i.e. a region where material ductility is higher than in other regions. This higher ductility region would then be the cause of a rougher machined surface. In terms of design fabrication, a rougher heat transfer profile will only influence the design incrementally, since a rougher heat transfer profile can only cause a much larger pressure drop through the recuperator as a whole.
- Precision of machined slots (for slotted inserts in recuperator plate geometries) – The precision of the size and location of the machined slots could not be fixed within the initially specified tolerance of ±0.1mm due to the slight variations in the size of the raw tungsten-copper material plates received. Variation in the machined slot position for all recuperator plates assembled was as much as 2mm, where each plate's slot was manufactured individually according to the manufacturing drawings. The slots had to be remanufactured with all recuperator plates assembled, which consequently left only a larger tolerance in which the slots could be positioned accurately. Figure 5-3 shows this variation in size and position of the machined slots and Figure 5-4, the preferred tolerance needed.

Figure 5-3: *Variation in size and position of the machined slots of the W-Cu plate geometries (deviation outside specified tolerance).*

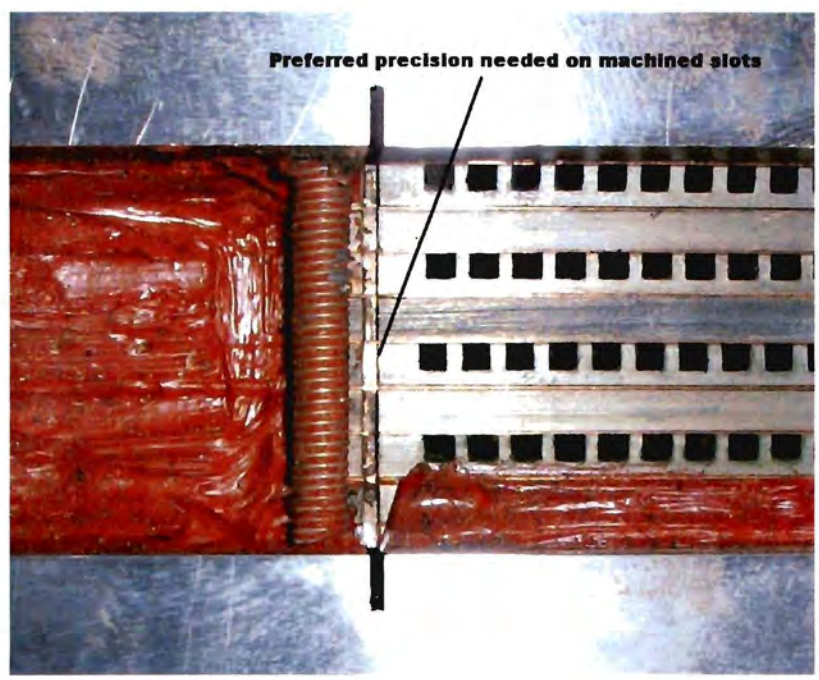

Figure 5-4: *Preferred precision needed on the machined slots.*

- Surface finish of fastening frame and header box: The ideal would be to improve the surface finish of the header box components to ensure that all joints are leak

tight. Conducting of tests on the recuperator assembly will reveal whether this will be necessary.

5.2.1.4 Possible drawbacks

Possible drawbacks that might arise from the non-conforming and improvement areas stated above are as follows:

- The deviation in the flatness tolerance for the recuperator plate geometries resulting in non-conforming flatness tolerances between recuperator plate geometries and the header box plates. This may well result in a leak path being present throughout the assembly. To counteract the latter and to limit the non-conforming flatness tolerances to a certain extent, the clamping force of the fastening frame should be increased inside the safe range as identified in Chapter 4.
- The larger-than-anticipated tolerance for the machined slots (location of slotted inserts) might create a leak path inside the overall assembly (from high pressure inlet header A to low pressure exit header B). This aspect will be evaluated with the first series of tests.
- Deviation in the flatness tolerance for adjacent recuperator plate geometries might also create various leak paths in the overall assembly. This can probably be limited to some extent by increasing the clamping force inside the safe range as identified in Chapter 4.
- The surface finish of all components forming part of the recuperator header box might not prevent Nitrogen leakage to the outside. This possible drawback will only be analyzed after the first series of leak tests to be conducted on the assembled recuperator unit.

5.2.2 Evaluation of Recuperator Integrity

5.2.2.1 Methods utilized for testing

Nitrogen Test Bank

The manufactured tungsten-copper recuperator was assembled and implemented into a test bank that made use of Nitrogen gas to determine if any leaks were present in the assembly. A schematic illustration of the experimental setup is shown in Figure 5-5. The Nitrogen used during all leak tests was regulated at 500kPa, and the recuperator was assembled with a clamping force as stipulated in Figure 5-5. All leak tests were conducted in a well ventilated environment and all Nitrogen gas used in the system was safely emitted to atmosphere.

Leak Test Specification and Leak Detection

The following leak tests were applied in determining whether a leak existed in the assembled recuperator:

- Nitrogen gas was pumped into one header only (indicated by either H1 or H2 in Figure 5-5) while the other header was monitored for any signs of a leak.

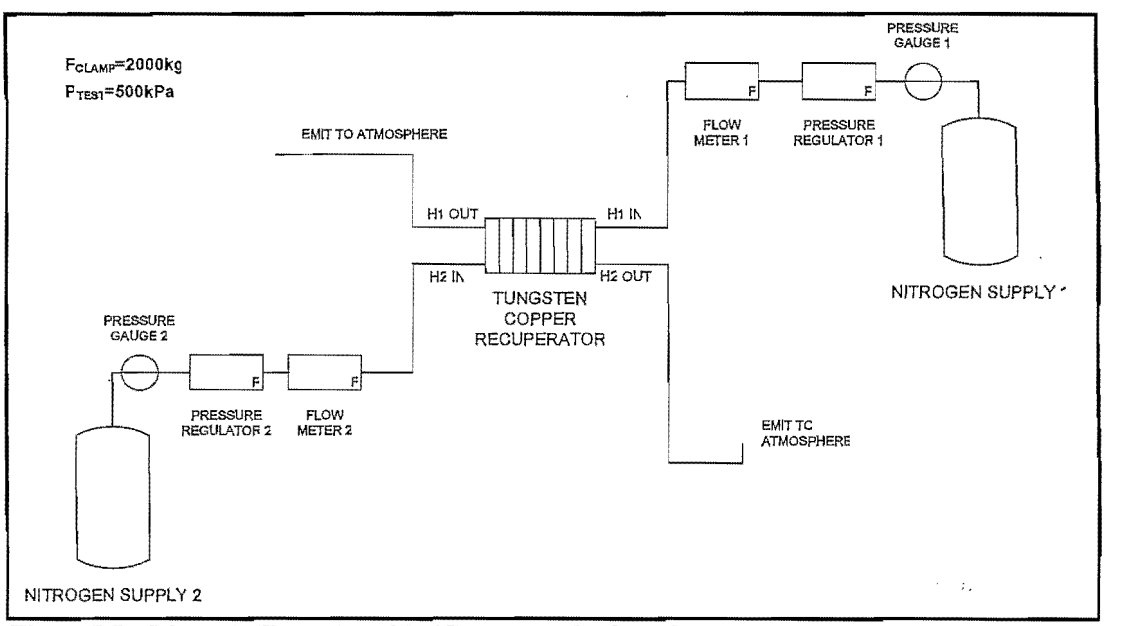

Figure 5-5: *Schematic illustration of the Nitrogen test bank in which the tungsten-copper recuperator was implemented. Leaks were either detected by i) pressurizing the 'hot' side of the recuperator (indicated by H1) and monitoring the 'cold side (indicated by H2) for leaks, or ii) pressurizing the 'hot' and 'cold' sides of the recuperator and monitoring the whole unit for leaks*

- Nitrogen was pumped through both headers (H1 together with H2 in Figure 5-5) and the unit was monitored as a whole for any signs of a leak.

Leakages in the recuperator unit were detected by the following methods:

- **Use of a standard handheld oxygen sensor:** The handheld sensor was held at points close to the recuperator headers and important sealing interfaces during testing as to pick up any Nitrogen emission that might come from the recuperator system. More detail regarding the sealing interfaces of importance is given in the following section.
- **Visual inspection of components after testing:** Mild steel components that are exposed to Nitrogen gas or any other gas with sufficient vapor content often form a light brown surface discoloration (slight surface corrosion) on the components themselves and give an indication where the working fluid had access throughout the whole assembly. By conducting this visual inspection after testing it was possible to trace and correct the areas on the header box (including all slotted inserts, headers and fastening frame) where Nitrogen seeped through/from the assembly.

Sealing Interfaces of Importance

As can be seen from Figure 5-6 and Figure 5-7, the following sealing interfaces of importance were identified before the leak tests were conducted:

- 'Slotted inserts' interface, indicated by '1'.
- Interface between recuperator plate geometries and the bottom/top plate of the fastening frame, indicated by '2'.
- Interface between bottom/top fastening frame plate and header box, shown by '3'.
- Interface between recuperator plate geometries A and B respectively, indicated by '4'.
- Interface between the side plates and the top / bottom plates of the header box, indicated by '5'.
- Interface between the header box side plates and the headers, indicated by '6'.

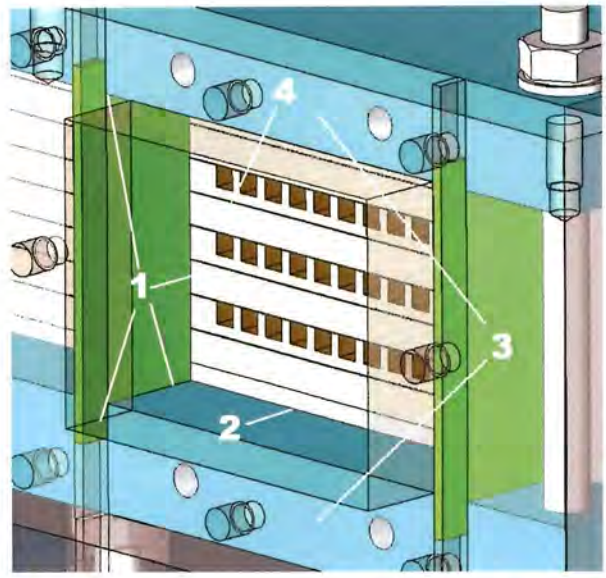

Figure 5-6: ***Indication of all the most important sealant interfaces on the recuperator.***
('1' – Slotted recuperator inserts interfacing with recuperator unit and header box; '2' – Recuperator plate geometries interfacing with bottom / top fastening frame plates; '3' – Bottom / top fastening frame plate interface with Header Box; '4' - Interface between respective recuperator plate geometries A and B).

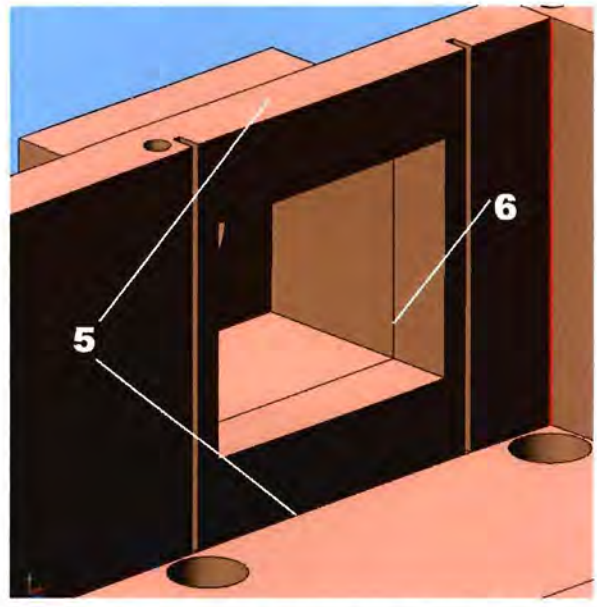

Figure 5-7: ***Indication of all the most important sealant interfaces on the recuperator.***
('5' – Interface of header box unit components with each other; '6' – Interface between header and header box side plates).

5.2.2.2 Leak testing of recuperator

Oxygen Sensor Analysis

With the first series of tests conducted, where Nitrogen gas was blown into one header set and the other header set monitored, the unit was not leak tight and Nitrogen gas seeped

from the system at a high rate. Also, when both header sets were pressurized with Nitrogen and the whole header box was monitored for leaks, several Nitrogen leaks occurred. These are elaborated upon next.

Visual Analysis

The following was observed after the first leak testing of the recuperator (observations made are linked to sealing interface locations on the recuperator as shown in Figure 5-6 and Figure 5-7):

- Interface #3 was a major contributor to the overall leak detected. As can be seen from Figures 5.9 (a) - 5.13 (a), interface #3 for all sides of the recuperator had a light brown surface discoloration, pointing out Nitrogen leaks, with the majority of gas leaking out at sides B and C.
- The bottom fastening frame plate also showed signs of Nitrogen leakage through interface #2 (between the bottom fastening plate frame and the recuperator profiled plate) by means of a light brown discoloration.
- Most of the slotted inserts (interfacing at #1) in the recuperator header box sealed off the path of flow efficiently except for those situated at header A and header D (indicated in Figures 5.9 (b) and 5.13 (b)).
- Interface #5 showed slight signs of leakages from the pressurized recuperator unit on the top and bottom surfaces of the header box side plates.
- Interface #6 also showed less signs of emitting Nitrogen from the pressurized system.

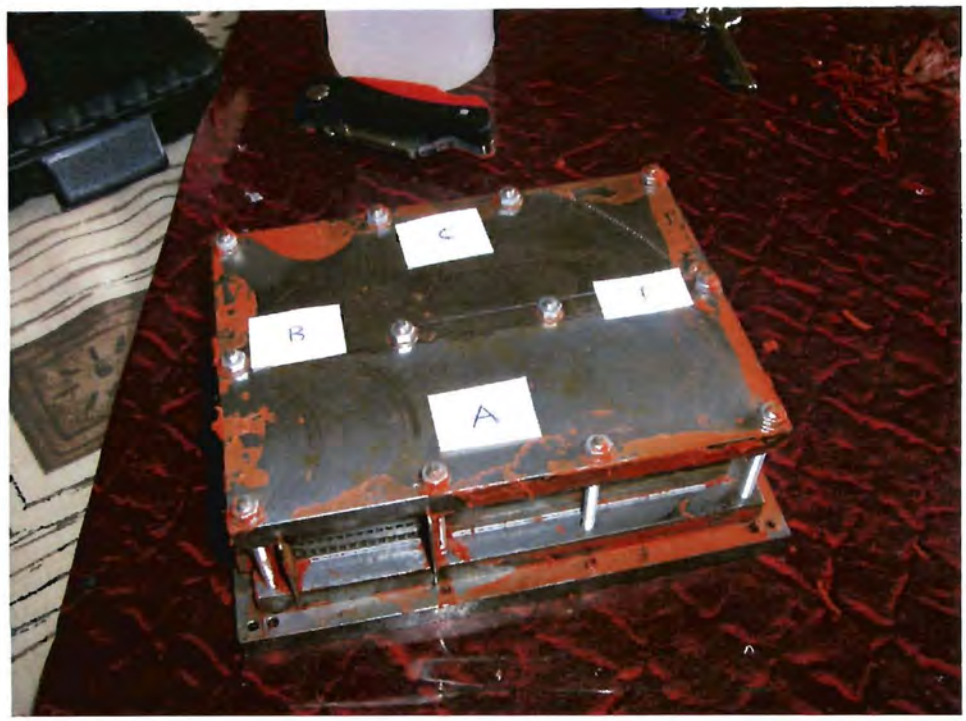

Figure 5-8: *The assembled recuperator as removed from the recuperator header box before inspection.*

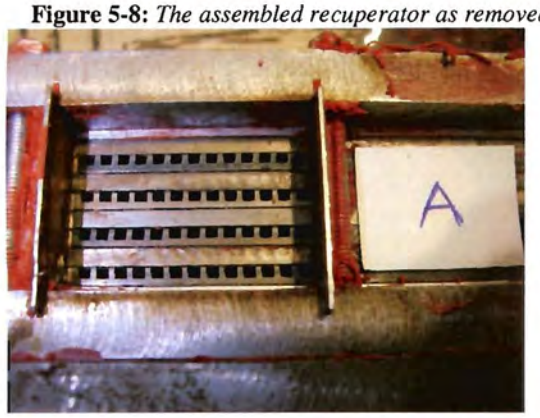

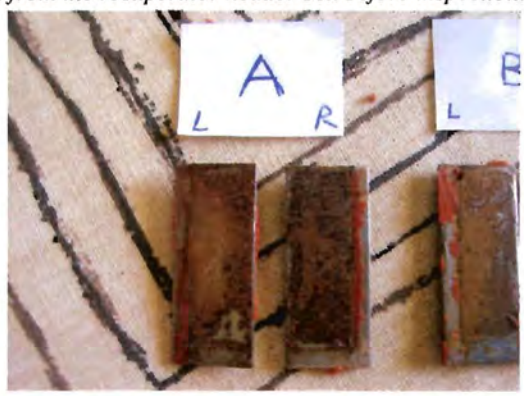

Figure 5-9: *(a), (b): Indication of the leaks that took place at header A's entrance (top / bottom fastening frame plate) and on the edges of the slotted plate inserts.*

Figure 5-10: *(a), (b): Indication of the excessive leak that took place at header B's bottom fastening frame plate. The edges of the slotted plate inserts as can be seen sealed off effectively.*

Figure 5-11: *(a), (b): Indication of the minor leaks that took place at header C, while the edges of the slotted plate inserts also show little evidence of Nitrogen emission.*

Figure 5-12: *(a), (b): Indication of the leaks that took place at header D's entrance (top / bottom fastening frame plate) and on the edges of the slotted plate inserts.*

From the observations made, it was not possible to determine whether any leak existed through interface #4 (i.e. through the recuperator plate geometries) since other leaks were already present. The other leaks therefore had to be resolved before addressing any leaks that might exist through the recuperator plate geometries themselves.

5.2.2.3 Corrective actions

Most interfaces that showed signs of Nitrogen leakages are part of the header box unit, wherein the recuperator unit is situated. These series of surfaces are identified as interfaces #3, #5 and #6 from Figure 5-6 and Figure 5-7, which can also be derived from the photographs above. To improve the leak tightness of the unit, it was of importance to generate a better sealing interface between firstly the relative header box components, secondly between the header box components and the slotted inserts and thirdly between the header box components and the fastening frame.

The corrective actions to improve the leak tightness entailed improving the surface finish of the header box components together with the fastening frame plates. Initial surface finishes entailed a general machining tolerance of 0.1mm. These components were now treated up to a surface finish of 20μm (0.02mm) for the second series of leak tests. By doing this the mating surfaces in the recuperator header box assembly would simulate more closely a vacuum tight seal and consequently ensure a joint assembly with higher integrity.

Even though the first series of tests couldn't reveal whether a leak existed through the deformed recuperator plates, it could be determined with the second series of tests if the modified header box unit sealed off the unit effectively. For the retesting of the recuperator, new 0.1mm C23000 seals were incorporated in the assembly together with the same clamp force utilized for the first series of tests. Retest results are noted hereafter.

5.2.2.4 Retesting of recuperator

Oxygen Sensor Analysis

With the second series of tests conducted, where Nitrogen gas was blown into one header set and the other header set monitored, traces of Nitrogen were present, indicating that leakage of Nitrogen gas was still present through recuperator plate geometries. Even though Nitrogen did leak from the headers as indicated, it took a lot longer for the oxygen sensor to pick up Nitrogen seeping from the system than it did with the previous set of tests. When both header sets were pressurized with Nitrogen and the whole header box was monitored for leaks, no Nitrogen leaks were noted. All the important sealing interfaces as mentioned previously were monitored for a time period of 10 minutes in which no Nitrogen seeped from the header box unit.

Visual Analysis

The following was observed after the second leak test was conducted on the recuperator:

- No sign of any Nitrogen leakage was picked up on Interface #3 throughout the whole unit. This is evident from the photos shown in Figure 5-13 (a)/(b) – Figure 5-14 (a)/(b).

- All slotted inserts have sealed off each flow path effectively; however, this was not the main concern since the first test run showed that little Nitrogen gas leaked through the slotted insert interfaces with the fastening frame and header box respectively.
- Interface #5 showed no signs of any Nitrogen leakages.
- Interface #6 also showed no signs of any Nitrogen leakages.

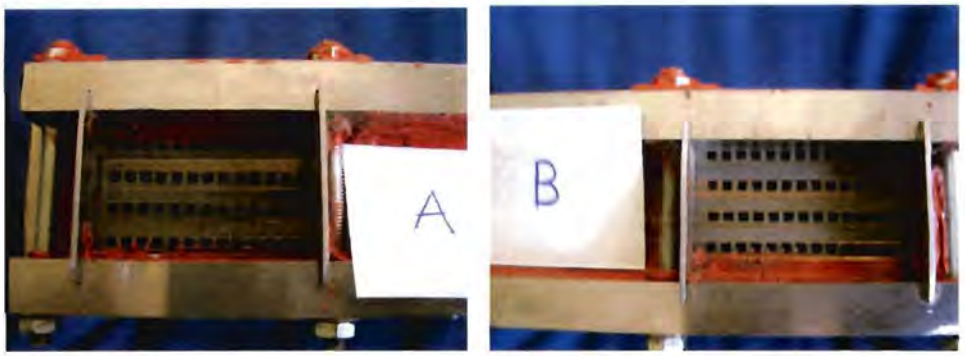

Figure 5-13: *(a) Condition of Interface #3 at header entrance A; No leaks present.(b) Condition of Interface #3 at header entrance B; No leaks present.*

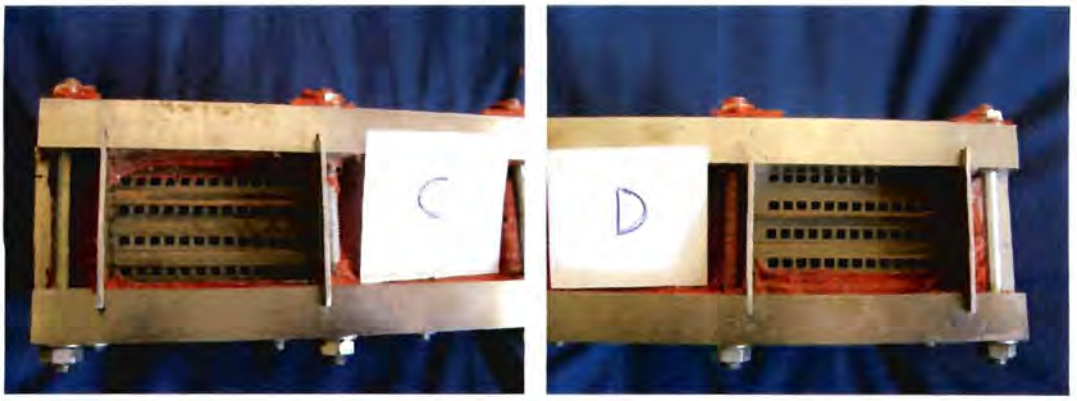

Figure 5-14: *(a): Condition of Interface #3 at header entrance C; No leaks present. (b) Condition of Interface #3 at header entrance D; No leaks present.*

A summary of all important aspects as noted in the evaluation of the fabricated recuperator unit together with accompanying recommendations will be presented in the closing chapter of this document.

6 SUMMARY, RECOMMENDATIONS & CONCLUSION

6.1 Summary

A detailed and comprehensive review of existing recuperator technologies and design methodologies has been presented in this report. Together with this, a recuperator of limited size has been designed and manufactured from W-Cu by means of identified methods. These methods that are presented in the design entailed the use of 2mm tungsten carbide drill bits to machine the correct recuperator profile, while the recuperator unit was joined by utilizing a mechanical fastening system. Although diffusion bonding was initially identified as the applicable joining technique, restrictions and limitations relating to the implementation of this technique has lead to the identification of a fastening system as the technique used in this study.

Evaluation of the fabricated recuperator revealed that several factors were outside the initially specified values, *inter alia*:

- Flatness tolerance of recuperator plate geometries
- Machined slots precision

These factors contributed to a leaking recuperator structure when tested (although the recuperator header box sealed off completely, minor leaks were still present in the recuperator unit, notably through the plate geometries as well as the machined slots).

Attempts to improve the integrity of the design only had a partial effect on the leakage rate experienced by the recuperator (increased clamp force, improved surface finish of recuperator header box components). Attempts to derive a better surface finish for the

recuperator plate geometries were hampered by the size of the plates as well as the extent of deformation already experienced by the machined plates, making the manual and automated improvement of the surface finish very difficult.

Aspects that most probably contributed to the deviations shown in the fabricated recuperator have been identified as follows:

- Residual stresses induced by manufacturing of the heat transfer profiles.
- Design aspects relating to the recuperator plate geometries. Certain aspects in the design of the recuperator plate geometries might have assisted in the non-conforming flatness tolerances shown by the recuperator plate geometries (inadequate surface finish and thickness of plate geometries).
- Non-conforming precision levels achieved through the identified manufacturing procedures in the integrated design.

6.2 Recommendations for Similar Work

From the respective outcomes, various recommendations can be made to aid and improve similar work relating to the recuperator design presented in this study. For clarity, these recommendations will be discussed according to design aspects, material aspects as well as surface finish considerations.

6.2.1 Design Aspects

- A close-knit relationship between the proposed design and the material to be used is needed. When a certain design is approached/envisioned, care has to be taken to ensure that the design and material to be used are reconcilable, hence that the material can be used in the design.
- Better design tolerances/manufacturing tolerances are definite requirements for similar work (which fall short in certain areas of the current design, e.g., machined slot precision) which the manufacturing process should be able to meet. Manufacturing methodology should focus on the establishment of an integrated assembly at high precision values. Component precision is still important, but overall assembly precision (especially in the case of the manufactured recuperator assembly) is of greater importance.

- Slight modifications to the proposed design are recommended if similar designs are pursued. The nature of the design of the recuperator plate geometries can be as such that more allowance for the total thickness of each plate is given to minimize any form of bending that might be induced by the machining process.

6.2.2 Material Aspects

- To ensure a designed product of a high quality, care should also be taken to ensure that the design material to be used is in the least stressed condition before machining or reworking of any kind commences (annealing of components is recommended).

6.2.3 Advanced Surface Finishing Considerations

Advanced surface finishing has featured as a primary aspect that needs to be addressed in order to ensure higher precision and thus higher design quality being incorporated into similar designs. This is especially true for designs that rely on high integrity sealing at high temperatures and pressures. For non-magnetic materials, as with W-Cu, possible advanced surface finishing processes may be based on vacuum motion on a mandrel or base plate. This is an aspect that should be investigated in similar work.

6.3 Recommendations for Future Related Studies

From certain aspects addressed in the literature survey as well as limitations encountered in this study, possible related studies have been identified which would be a valuable addition to the specific field:

- Establish and analyze a similar recuperator design of high structural integrity using diffusion bonding as joining technique and W-Cu as recuperator material.
- Establish and analyze a similar design of high structural integrity for high temperature applications by means of explosion bonding. Aspects of importance can entail *inter alia* joint quality and integrity, channel profile analysis as well as channel blockage.
- Investigate the feasibility of implementing graphite into a similar design (with specific emphasis on permeable characteristics as well as machining and joining of graphites).

- Investigate in further detail the machinability of W-Cu alloy as well as its associated surface finish and tolerances achievable using other precision machining methods.

6.4 Conclusion

The design and fabrication of a recuperator of limited size using tungsten-copper as a heat transfer material, requires re-evaluation. Similar work will ensure a design of a high quality when provision is made for advanced surface finishing of machined parts (notably the recuperator plate geometries), modifications to the proposed design as well as stress relieving of machined components for the purpose of eliminating any residual stresses that might be present.

Ultimately, the most favorable design will be established when the design incorporates diffusion bonding as the joining procedure. The successful integration of the ideal performance characteristics of compact heat exchangers with the favorable thermal and structural characteristics of W-Cu will ensure a highly effective recuperator design with improved performance capabilities in industry.

A-1 Appendix A: Recuperator Design Calculations conducted in EES®

A-1.1 *Assumptions*

The following assumptions have been made in the creation of the recuperator design calculations:

1. The calculations done reflect the performance of 1 hot and 1 cold recuperator channel only.
2. The calculations have been conducted using Nitrogen gas.
3. A fin efficiency of 97% has been used as base value for the purpose of these calculations. By implementing the applicable values of *the thermal conductivity, convection coefficient, fin height* as well as *fin thickness* into equations *(2.11)* and *(2.12)*[1], the indicated fin efficiency was derived. For the purpose of current design, fin height approaches fin thickness, thus giving this high fin efficiency.
4. Since the focus of this study does not fall on the performance of the recuperator, the pressure drop attributable to losses (K) in the channel itself has been left out of these calculations. Losses for fluid entering and exiting the recuperator channels have been taken into account.

A-1.2 *EES® Design Calculations Sheet*

The calculations cited below have been conducted in EES® and have been derived from the EES® equations window. For convenience, the various sections of calculations have been split up, with each section displaying its relevant purpose.

[1] Equations (2.11) and (2.12) used under the assumption that fin is a thin fin with an adiabatic tip [37]

"PRE-DEFINED FUNCTIONS"

```
"Nusselt - Verhit"
Function Nusselt_verhit(Re, Pr, x, C)

        IF (Re<2000) THEN
                N_uh = C
        ELSE
        IF (Re>2000) THEN
                N_uh = 0.023*Re^0.8*Pr^x
        ENDIF
        ENDIF
        Nusselt_verhit = N_uh

END

"Nusselt - Verkoel"
Function Nusselt_verkoel(Re, Pr, x, C)

        IF (Re<2000) THEN
                N_uc = C
        ELSE
        IF (Re>2000) THEN
                N_uc = 0.023*Re^0.8*Pr^x
        ENDIF
        ENDIF
        Nusselt_verkoel= N_uc

END
```

"THERMAL CONDUCTIVITY EQUATION"

```
Function k_5W3(T)

        k = 224.215001+1.13349536*T-0.00499440337*T^2+0.0000145760248*T^3-
        2.38575590E-08*T^4+1.95516530E-11*T^5-6.28842581E-15*T^6

        k_5W3 = k

End
```

"GEOMETRY & GENERAL VALUES DEFINED"

```
j=19                                                    [increments]
fin_thickness = 0.001                                   [m]
base_thickness = 0.001                                  [m]
channel_width = 0.002                                   [m]
channel_height = 0.002                                  [m]
channel_length = 0.295                                  [m]
channel_l_increment = channel_length/(j+1)
```

A_heat = 2*(channel_width+channel_height)*channel_length
A_fflow = channel_width*channel_height
A_fin = 2*channel_height*channel_length
D_hyd = 2*(channel_width*channel_height)/(channel_width+channel_height)
epsilon = 0.00005
epsilon_Dh = epsilon/D_hyd

"INLET ENVIRONMENT - HOT & COLD - DEFINED"

T_hi[0] = 400+273.15	[K]
p_hi[0] = 200000	[Pa]
m_dot_h = 0.0001	[kg/s]
T_ce[j] = 20+273.15	[K]
p_ce[j] = 500000	[Pa]
m_dot_c = 0.0001	[kg/s]

"e-NTU CALCULATIONS SUMMARIZED"

C_min[0] = MIN(C_h[0], C_c[0])
C_max[0] = MAX(C_h[0], C_c[0])

DUPLICATE i = 1, j-1
C_min[i] = MIN(C_h[i], C_c[i])
C_max[i] = MAX(C_h[i], C_c[i])
END

C_min[j] = MIN(C_h[j], C_c[j])
C_max[j] = MAX(C_h[j], C_c[j])

T_bar = (T_hi[0] + T_ce[j])/2

"CALCULATIONS FOR PRIMARY INLET - HOT"

"0th INCREMENT"

"Properties"
CP_h[0] = CP(N2,T=T_bar_h[0])
CV_h[0] = CV(Nitrogen,T=T_bar_h[0],P=p_bar_h[0])
gamma_h[0] = CP_h[0]/CV_h[0]
R_h[0] = (CP_h[0] - CV_h[0])/1000
k_h[0] = CONDUCTIVITY(N2,T=T_bar_h[0])
Pr_h[0] = PRANDTL(N2,T=T_bar_h[0])
rho_h[0] = DENSITY(N2,T=T_bar_h[0],P=p_bar_h[0])
mu_h[0] = VISCOSITY(N2,T=T_bar_h[0])

"Calculations"
C_h[0] = m_dot_h*CP_h[0]

```
"Fin efficiency"
eta_oh[0] = 1 - (A_fin/A_heat)*(1-eta_fh[0])
eta_fh[0] = 0.97

"Heat Transfer Coefficient"
Nu_h[0] = (h_h[0]*D_hyd)/k_h[0]
Nu_h[0] = Nusselt_verkoel(Re_h[0], Pr_h[0], 0.3, 2.98)

"Pressure Drop Equations"
v_h[0] = m_dot_h/(rho_h[0]*A_fflow)

Re_h[0] = abs((rho_h[0]*v_h[0]*D_hyd)/mu_h[0])
f_h[0] = MoodyChart(Re_h[0], epsilon_Dh)
DELTAP_h[0] = ((f_h[0]*channel_length)/D_hyd
+(0.8))*((abs(m_dot_h)*m_dot_h)/(2*rho_h[0]*A_fflow^2))
p_he[0] = p_hi[0] - DELTAP_h[0]
p_bar_h[0] = (p_hi[0]+p_he[0])/2

"Percentage Pressure Loss"
DELTAP_h_t[0]=DELTAP_h[0]

"Overall Heat Transfer Coefficient"
UA_h[0] = (eta_oh[0]*h_h[0]*A_heat)
L[0] = channel_l_increment


"i'th INCREMENT (i = 1,j-1)"

DUPLICATE i = 1,j-1

"Properties"
CP_h[i] = CP(N2,T=T_bar_h[i])
CV_h[i] = CV(Nitrogen,T=T_bar_h[i],P=p_bar_h[i])
gamma_h[i] = CP_h[i]/CV_h[i]
R_h[i] = (CP_h[i] - CV_h[i])/1000
k_h[i] = CONDUCTIVITY(N2,T=T_bar_h[i])
Pr_h[i] = PRANDTL(N2,T=T_bar_h[i])
rho_h[i] = DENSITY(N2,T=T_bar_h[i],P=p_bar_h[i])
mu_h[i] = VISCOSITY(N2,T=T_bar_h[i])

"Calculations"
C_h[i] = m_dot_h*CP_h[i]

"Fin efficiency"
eta_oh[i] = 1 - (A_fin/A_heat)*(1-eta_fh[i])
eta_fh[i] = 0.97

"Heat Transfer Coefficients"
Nu_h[i] = (h_h[i]*D_hyd)/k_h[i]
Nu_h[i] = Nusselt_verkoel(Re_h[i], Pr_h[i], 0.3, 2.98)

"Pressure Drop Equations"
p_hi[i] = p_he[i-1]
v_h[i] = m_dot_h/(rho_h[i]*A_fflow)
```

```
Re_h[i] = abs((rho_h[i]*v_h[i]*D_hyd)/mu_h[i])
f_h[i] = MoodyChart(Re_h[i], epsilon_Dh)
DELTAP_h[i] = ((f_h[i]*channel_length)/D_hyd)*((abs(m_dot_h)*m_dot_h)/(2*rho_h[i]*A_fflow^2))
p_he[i] = p_hi[i] - DELTAP_h[i]
p_bar_h[i] = (p_hi[i]+p_he[i])/2
DELTAP_h_t[i] = DELTAP_h_t[i-1]+DELTAP_h[i]

"Overall Heat Transfer Coefficients"
UA_h[i] = (eta_oh[i]*h_h[i]*A_heat)
L[i] = L[i-1] + channel_l_increment

END


"j'th INCREMENT"

"Properties"
CP_h[j] = CP(N2,T=T_bar_h[j])
CV_h[j] = CV(Nitrogen,T=T_bar_h[j],P=p_bar_h[j])
gamma_h[j] = CP_h[j]/CV_h[j]
R_h[j] = (CP_h[j] - CV_h[j])/1000
k_h[j] = CONDUCTIVITY(N2,T=T_bar_h[j])
Pr_h[j] = PRANDTL(N2,T=T_bar_h[j])
rho_h[j] = DENSITY(N2,T=T_bar_h[j],P=p_bar_h[j])
mu_h[j] = VISCOSITY(N2,T=T_bar_h[j])

"Calculations"
C_h[j] = m_dot_h*CP_h[j]

"Fin efficiency"
eta_oh[j] = 1 - (A_fin/A_heat)*(1-eta_fh[j])
eta_fh[j] = 0.97

"Heat Transfer Coefficients"
Nu_h[j] = (h_h[j]*D_hyd)/k_h[j]
Nu_h[j] = Nusselt_verkoel(Re_h[j], Pr_h[j], 0.3, 2.98)

"Pressure Drop Equations"
p_hi[j] = p_he[j-1]
v_h[j] = m_dot_h/(rho_h[j]*A_fflow)

Re_h[j] = abs((rho_h[j]*v_h[j]*D_hyd)/mu_h[j])
f_h[j] = MoodyChart(Re_h[j], epsilon_Dh)
DELTAP_h[j] = ((f_h[j]*channel_length)/D_hyd
+(1))*((abs(m_dot_h)*m_dot_h)/(2*rho_h[j]*A_fflow^2))
p_he[j] = p_hi[j] - DELTAP_h[j]
p_bar_h[j] = (p_hi[j]+p_he[j])/2
DELTAP_h_t[j] = DELTAP_h_t[j-1]+DELTAP_h[j]

"Overall Heat Transfer Coefficients"
UA_h[j] = (eta_oh[j]*h_h[j]*A_heat)
L[j] = L[j-1] + channel_l_increment
```

"CALCULATIONS FOR SECONDARY INLET - COLD"

"0th INCREMENT"

"Properties"
CP_c[0] = CP(N2,T=T_bar_c[0])
CV_c[0] = CV(Nitrogen,T=T_bar_c[0],P=p_bar_c[0])
gamma_c[0] = CP_c[0]/CV_c[0]
R_c[0] = (CP_c[0] - CV_c[0])/1000
k_c[0] = CONDUCTIVITY(N2,T=T_bar_c[0])
Pr_c[0] = PRANDTL(N2,T=T_bar_c[0])
rho_c[0] = DENSITY(N2,T=T_bar_c[0],P=p_bar_c[0])
mu_c[0] = VISCOSITY(N2,T=T_bar_c[0])

"Calculations"
C_c[0] = m_dot_c*CP_c[0]

"Fin efficiency"
eta_oc[0] = 1 - (A_fin/A_heat)*(1-eta_fc[0])
eta_fc[0] = 0.97

"Heat Transfer Coefficients"
Nu_c[0] = (h_c[0]*D_hyd)/k_c[0]
Nu_c[0] = Nusselt_verhit(Re_c[0], Pr_c[0], 0.4, 2.98)

"Pressure Drop Equations"
v_c[0] = m_dot_c/(rho_c[0]*A_fflow)

Re_c[0] = abs((rho_c[0]*v_c[0]*D_hyd)/mu_c[0])
f_c[0] = MoodyChart(Re_c[0], epsilon_Dh)
DELTAP_c[0] = ((f_c[0]*channel_length)/D_hyd
+(0.8))*((abs(m_dot_c)*m_dot_c)/(2*rho_c[0]*A_fflow^2))
p_ci[0] = p_ce[0] - DELTAP_c[0]
p_bar_c[0] = (p_ci[0]+p_ce[0])/2

"Percentage Pressure Loss"
DELTAP_c_t[0]=DELTAP_c[0]

"Overall Heat Transfer Coefficient"
UA_c[0] = (eta_oc[0]*h_c[0]*A_heat)

"i'th INCREMENT (i = 1,j-1)"

DUPLICATE i = 1,j-1

"Properties"
CP_c[i] = CP(N2,T=T_bar_c[i])
CV_c[i] = CV(Nitrogen,T=T_bar_c[i],P=p_bar_c[i])
gamma_c[i] = CP_c[i]/CV_c[i]
R_c[i] = (CP_c[i] - CV_c[i])/1000
k_c[i] = CONDUCTIVITY(N2,T=T_bar_c[i])
Pr_c[i] = PRANDTL(N2,T=T_bar_c[i])
rho_c[i] = DENSITY(N2,T=T_bar_c[i],P=p_bar_c[i])

```
mu_c[i] = VISCOSITY(N2,T=T_bar_c[i])

"Calculations"
C_c[i] = m_dot_c*CP_c[i]

"Fin efficiency"
eta_oc[i] = 1 - (A_fin/A_heat)*(1-eta_fc[i])
eta_fc[i] = 0.97

"Heat Transfer Coefficients"
Nu_c[i] = (h_c[i]*D_hyd)/k_c[i]
Nu_c[i] = Nusselt_verhit(Re_c[i], Pr_c[i], 0.4, 2.98)

"Pressure Drop Equations"
p_ci[i] = p_ce[i-1]
v_c[i] = m_dot_c/(rho_c[i]*A_fflow)

Re_c[i] = abs((rho_c[i]*v_c[i]*D_hyd)/mu_c[i])
f_c[i] = MoodyChart(Re_c[i], epsilon_Dh)
DELTAP_c[i] = ((f_c[i]*channel_length)/D_hyd)*((abs(m_dot_c)*m_dot_c)/(2*rho_c[i]*A_fflow^2))
p_ci[i] = p_ce[i] - DELTAP_c[i]
p_bar_c[i] = (p_ci[i]+p_ce[i])/2
DELTAP_c_t[i] = DELTAP_c_t[i-1]+DELTAP_c[i]

"Overall Heat Transfer Coefficients"
UA_c[i] = (eta_oc[i]*h_c[i]*A_heat)

END


"j'th INCREMENT"

"Properties"
CP_c[j] = CP(N2,T=T_bar_c[j])
CV_c[j] = CV(Nitrogen,T=T_bar_c[j],P=p_bar_c[j])
gamma_c[j] = CP_c[j]/CV_c[j]
R_c[j] = (CP_c[j] - CV_c[j])/1000
k_c[j] = CONDUCTIVITY(N2,T=T_bar_c[j])
Pr_c[j] = PRANDTL(N2,T=T_bar_c[j])
rho_c[j] = DENSITY(N2,T=T_bar_c[j],P=p_bar_c[j])
mu_c[j] = VISCOSITY(N2,T=T_bar_c[j])

"Calculations"
C_c[j] = m_dot_c*CP_c[j]

"Fin efficiency"
eta_oc[j] = 1 - (A_fin/A_heat)*(1-eta_fc[j])
eta_fc[j] = 0.97

"Heat Transfer Coefficients"
Nu_c[j] = (h_c[j]*D_hyd)/k_c[j]
Nu_c[j] = Nusselt_verhit(Re_c[j], Pr_c[j], 0.4, 2.98)

"Pressure Drop Equations"
p_ci[j] = p_ce[j-1]
v_c[j] = m_dot_c/(rho_c[j]*A_fflow)
```

```
Re_c[j] = abs((rho_c[j]*v_c[j]*D_hyd)/mu_c[j])
f_c[j] = MoodyChart(Re_c[j], epsilon_Dh)
DELTAP_c[j] = ((f_c[j]*channel_length)/D_hyd
+(1))*((abs(m_dot_c)*m_dot_c)/(2*rho_c[j]*A_fflow^2))
p_ci[j] = p_ce[j] - DELTAP_c[j]
p_bar_c[j] = (p_ci[j]+p_ce[j])/2
DELTAP_c_t[j] = DELTAP_c_t[j-1]+DELTAP_c[j]

"Overall Heat Transfer Coefficients"
UA_c[j] = (eta_oc[j]*h_c[j]*A_heat)
```

"WALL PROPERTIES"

```
"0th Increment"

k[0] = k_5W3(T_wp[0])
R_w[0] = base_thickness/(k_w[0]*A_heat)
k_w[0] = k[0]
T_bar_w[0] = (T_wp[0]+T_wc[0])/2

"i'th increment (i=1,j-1)"

DUPLICATE i=1,j

k[i] = k_5W3(T_wp[i])
R_w[i] = base_thickness/(k_w[i]*A_heat)
k_w[i] = k[i]
T_bar_w[i] = (T_wp[i]+T_wc[i])/2

END
```

"TOTAL HEAT TRANSFER AND TEMPERATURES"

```
Q_p[0] = m_dot_h*Cp_h[0]*DELTAT_h[0]
Q_pw[0]=UA_h[0]*(T_wp[0]-T_bar_h[0])
Q_w[0]=(1/R_w[0])*(T_wc[0]-T_wp[0])
Q_cw[0]=UA_c[0]*(T_bar_c[0]-T_wc[0])
Q_c[0]=m_dot_c*Cp_c[0]*DELTAT_c[0]

Q[0] = Q_p[0]
Q[0] = Q_pw[0]
Q[0] = Q_w[0]
Q[0] = Q_cw[0]
Q[0] = Q_c[0]

DELTAT_h[0]=T_he[0]-T_hi[0]
DELTAT_c[0]=T_ce[0]-T_ci[0]
T_bar_h[0]=(T_hi[0]+T_he[0])/2
T_bar_c[0]=(T_ci[0]+T_ce[0])/2
```

```
Q_total[0] = Q[0]


DUPLICATE i=1,j

T_he[i-1]=T_hi[i]
T_ci[i] = T_ce[i-1]

Q_p[i] = m_dot_h*Cp_h[i]*DELTAT_h[i]
Q_pw[i]=UA_h[i]*(T_wp[i]-T_bar_h[i])
Q_w[i]=(1/R_w[i])*(T_wc[i]-T_wp[i])
Q_cw[i]=UA_c[i]*(T_bar_c[i]-T_wc[i])
Q_c[i]=m_dot_c*Cp_c[i]*DELTAT_c[i]

Q[i] = Q_p[i]
Q[i] = Q_pw[i]
Q[i] = Q_w[i]
Q[i] = Q_cw[i]
Q[i] = Q_c[i]

DELTAT_h[i]=T_he[i]-T_hi[i]
DELTAT_c[i]=T_ce[i]-T_ci[i]
T_bar_h[i]=(T_hi[i]+T_he[i])/2
T_bar_c[i]=(T_ci[i]+T_ce[i])/2
Q_total[i] = Q_total[i-1]+Q[i]

END
```

A-1.3 *EES® Results*

$A_{fflow} = 0.000004$ [m^2]	$A_{fin} = 0.00118$ [m^2]	$A_{heat}=0.00236$ [m^2]
$base_{thickness} = 0.001$ [m]	$channel_{height} = 0.002$ [m]	$channel_{length}=0.295$ [m]
$channel_{l\_increment} = 0.01475$ [m]	$channel_{width} = 0.002$ [m]	$D_{hyd}=0.002$ [m]
Epsilon = 0.00005	$epsilon_{Dh} = 0.025$	$fin_{thickness}=0.001$ [m]
j = 19 [increments]	$m\_dot_c = 0.0001$ [kg/s]	$m\_dot_h=0.0001$ [kg/s]
$T_{bar} = 483.2$ [K]	$k_{5W3} = 389.5$ [W/Mk]	$Q_{total} = 38.24$ W[A]

[A] Note that this value is for one representative channel only.

Increment	CP_c[i]	CP_h[i]	CV_c[i]	CV_h[i]	C_c[i]	C_h[i]	C_max[i]	C_min[i]	DELTAP_c[i] [Pa]	DELTAP_c_t[i] [Pa]
0	1089	1094	790	794	0.1089	0.1094	0.1094	0.1089	816.9	816.9
1	1086	1090	786.9	790.9	0.1086	0.109	0.109	0.1086	692.8	1510
2	1082	1087	783.9	787.8	0.1082	0.1087	0.1087	0.1082	667.8	2177
3	1079	1083	781	784.8	0.1079	0.1083	0.1083	0.1079	643.5	2821
4	1076	1080	778.2	781.9	0.1076	0.108	0.108	0.1076	619.7	3441
5	1073	1077	775.5	779.1	0.1073	0.1077	0.1077	0.1073	596.5	4037
6	1069	1074	772.9	776.4	0.1069	0.1074	0.1074	0.1069	573.9	4611
7	1066	1071	770.4	773.8	0.1066	0.1071	0.1071	0.1066	551.8	5163
8	1064	1068	768.1	771.3	0.1064	0.1068	0.1068	0.1064	530.4	5693
9	1061	1065	765.8	768.9	0.1061	0.1065	0.1065	0.1061	509.5	6203
10	1058	1062	763.7	766.7	0.1058	0.1062	0.1062	0.1058	489.1	6692
11	1056	1060	761.7	764.5	0.1056	0.106	0.106	0.1056	469.4	7161
12	1054	1057	759.8	762.5	0.1054	0.1057	0.1057	0.1054	450.2	7611
13	1051	1055	758.1	760.6	0.1051	0.1055	0.1055	0.1051	431.6	8043
14	1049	1052	756.1	758.3	0.1049	0.1052	0.1052	0.1049	409.2	8452
15	1045	1048	752.9	754.8	0.1045	0.1048	0.1048	0.1045	806.6	9259
16	1042	1044	749.7	751	0.1042	0.1044	0.1044	0.1042	736.3	9995
17	1041	1042	747.3	748.1	0.1041	0.1042	0.1042	0.1041	667.9	10663
18	1042	1041	745.9	746.1	0.1042	0.1041	0.1042	0.1041	601.6	11265
19	1042	1042	745.2	744.8	0.1042	0.1042	0.1042	0.1042	594.9	11859

T_hi[i]	T_wc[i]	T_wp[i]	UA_c[i]	UA_h[i]	v_c[i]	v_h[i]
[K]	[K]	[K]	[W/K]	[W/K]	[m/s]	[m/s]
673.2	657.5	657.5	0.1634	0.1667	9.849	24.85
659.6	644	644	0.1609	0.1642	9.628	24.59
646.2	630.6	630.6	0.1584	0.1618	9.412	24.31
632.9	617.4	617.4	0.1559	0.1593	9.198	24.02
619.7	604.2	604.2	0.1534	0.1569	8.988	23.72
606.7	591.2	591.2	0.1509	0.1544	8.78	23.42
593.8	578.4	578.4	0.1485	0.152	8.575	23.12
581	565.7	565.7	0.146	0.1495	8.374	22.8
568.4	553.1	553.1	0.1435	0.1471	8.175	22.49
555.9	540.6	540.6	0.141	0.1447	7.979	22.17
543.5	528.3	528.3	0.1385	0.1422	7.786	21.84
531.3	516.2	516.2	0.1361	0.1398	7.596	21.51
519.3	504.2	504.2	0.1336	0.1374	7.409	21.18
507.4	492.4	492.4	0.1312	0.135	7.226	20.84
495.7	473.2	473.2	0.3783	0.132	7.002	20.38
478.4	452.2	452.2	0.374	0.3907	6.608	19.43
444.3	418.2	418.2	0.3682	0.3848	6.091	18.18
410.5	384.6	384.6	0.3624	0.3788	5.581	16.95
377	351.4	351.4	0.3564	0.3726	5.082	15.7
344.2	318.9	318.9	0.3499	0.3661	4.592	14.45

Appendix B: Manufacturing Drawings of Recuperator

#	DESCRIPTION	QTY.
1	W-Cu Plate Geometry -Profile A	4
2	Red Brass - 0.5mm Seal	8
3	W-Cu Plate Geometry - Profile B	4
4	Top Frame Clamper	1
5	Bottom Frame Clamper	1
6	M4 Hexagon Nut	24
7	M4 Threaded Rod	12
8	M4 Washer	24
9	Slotted Plate Inserts	8
10	Header Box - Side Plate #2	2
11	Header Box - Side Plate #1	2
12	Header Inlet - B	2
13	Header Inlet - A	2
14	Header Box - Bottom Plate	1
15	Header Box - Top Plate	1

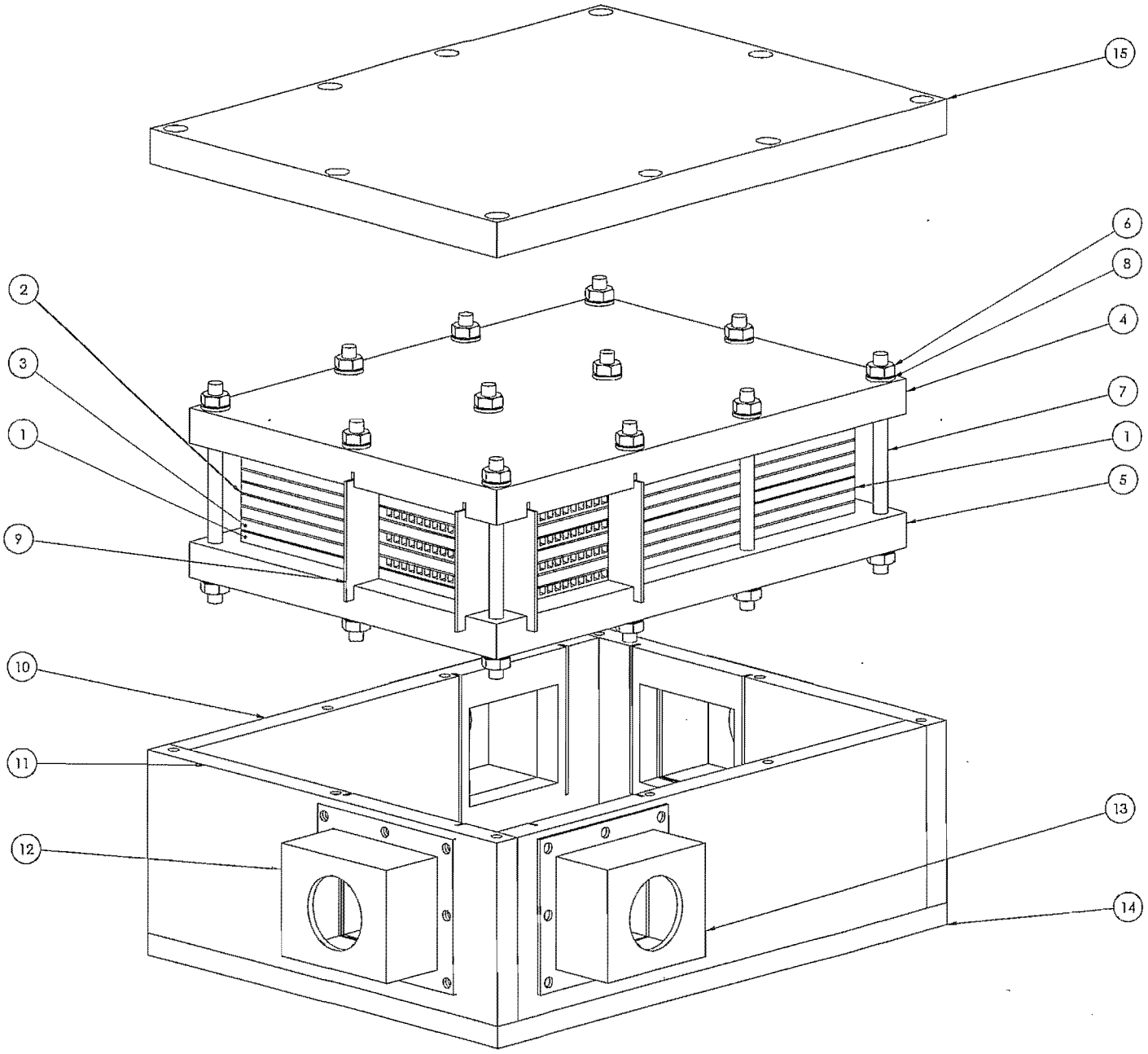

Illustration

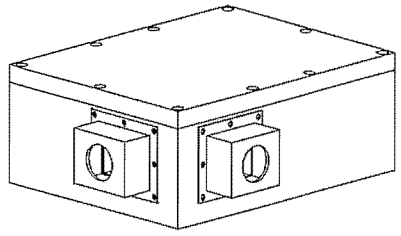

DO NOT SCALE DRAWING | REVISION

UNLESS OTHERWISE SPECIFIED:
DIMENSIONS ARE IN MILLIMETERS
SURFACE FINISH:
TOLERANCES:
LINEAR: +-0.1MM
ANGULAR:

MATERIAL: N/A

TITLE: W-Cu Recuperator Assembly

DWG NO. M.ING01-5W3-FR01-01

A2

SCALE:1:2 | QUANTITY

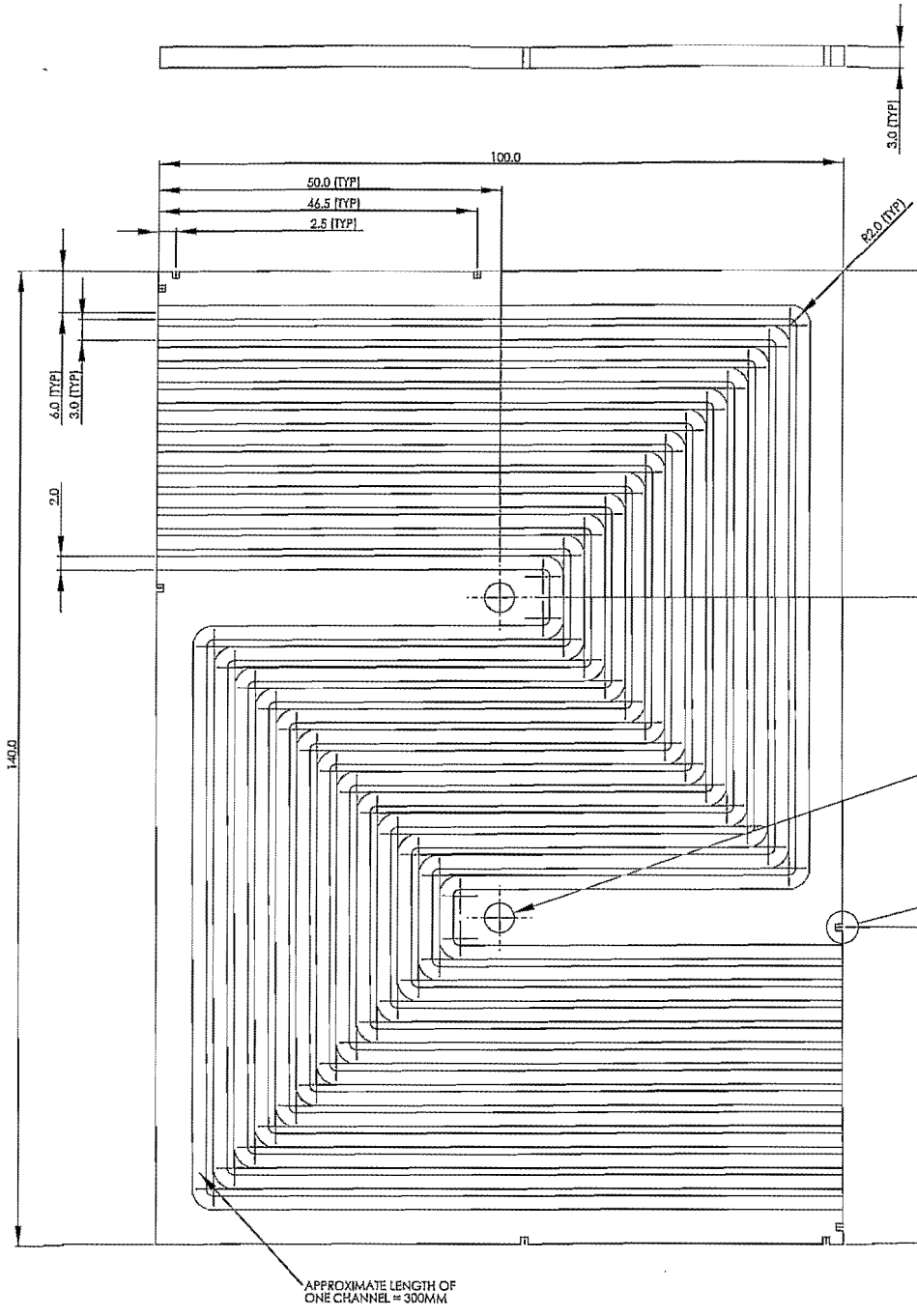

ILLUSTRATION

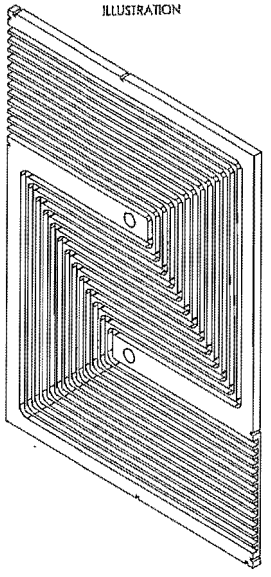

DETAIL A
SCALE 2 : 0.15

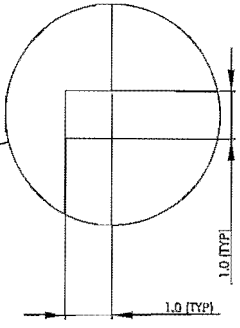

DO NOT SCALE DRAWING	REVISION
UNLESS OTHERWISE SPECIFIED: DIMENSIONS ARE IN MILLIMETERS SURFACE FINISH: TOLERANCES: LINEAR: +- 0.1MM ANGULAR:	TITLE: W-Cu : Profile A
MATERIAL: W-Cu	DWG NO. M.ING01-5W3-FR01-02 A2
	SCALE:2:2 QUANTITY

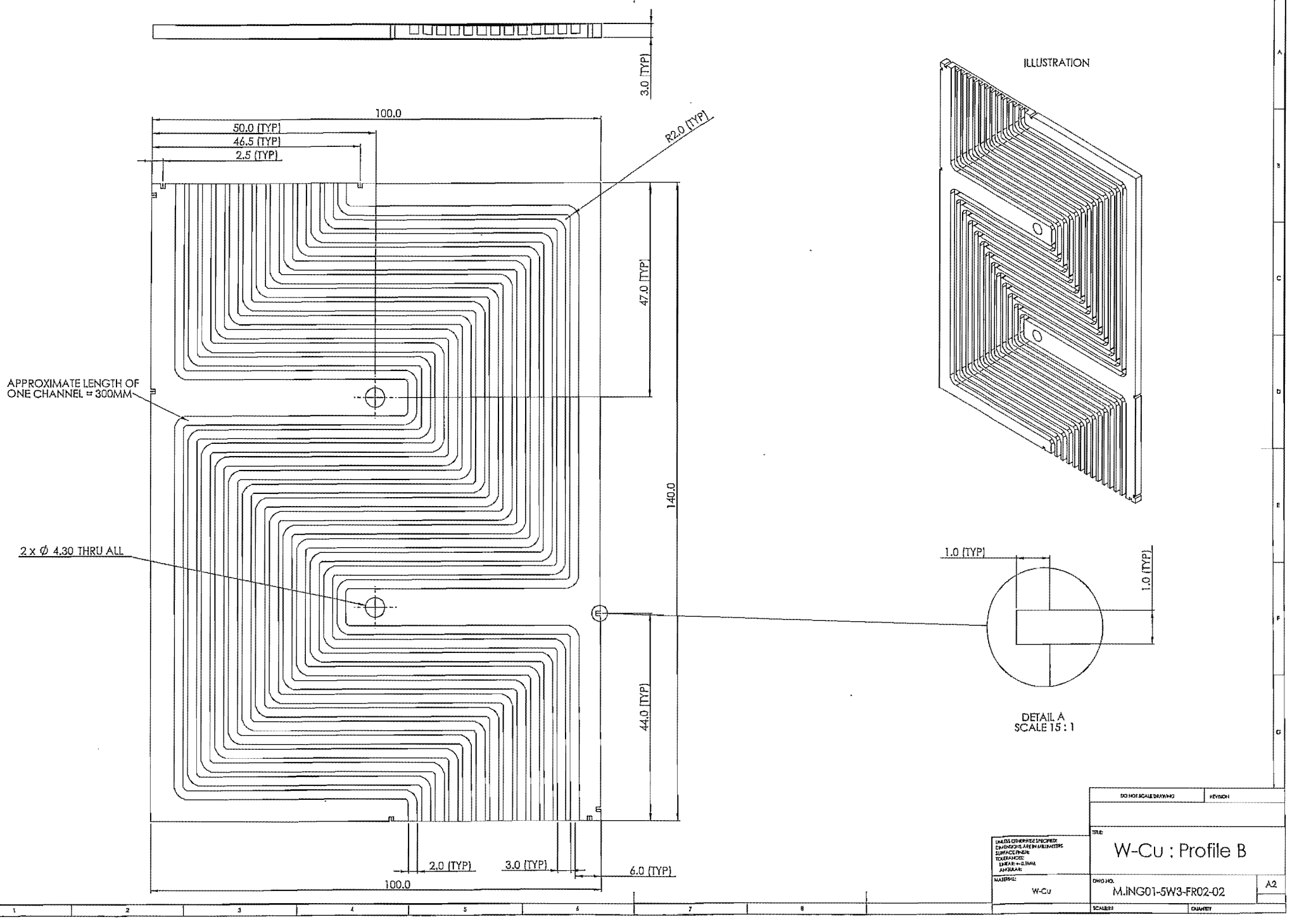
3.0 (TYP)
100.0
50.0 (TYP)
46.5 (TYP)
2.5 (TYP)
R2.0 (TYP)
47.0 (TYP)
140.0
APPROXIMATE LENGTH OF ONE CHANNEL = 300MM
2 x Ø 4.30 THRU ALL
44.0 (TYP)
2.0 (TYP)
3.0 (TYP)
6.0 (TYP)
100.0
ILLUSTRATION
1.0 (TYP)
1.0 (TYP)
DETAIL A
SCALE 15 : 1
DO NOT SCALE DRAWING
REVISION
UNLESS OTHERWISE SPECIFIED:
DIMENSIONS ARE IN MILLIMETERS
SURFACE FINISH:
TOLERANCES:
LINEAR: +- 0.1 MM
ANGULAR:
MATERIAL:
W-Cu
TITLE:
W-Cu : Profile B
DWG NO.
M.ING01-5W3-FR02-02
A2
SCALE:1:1
QUANTITY

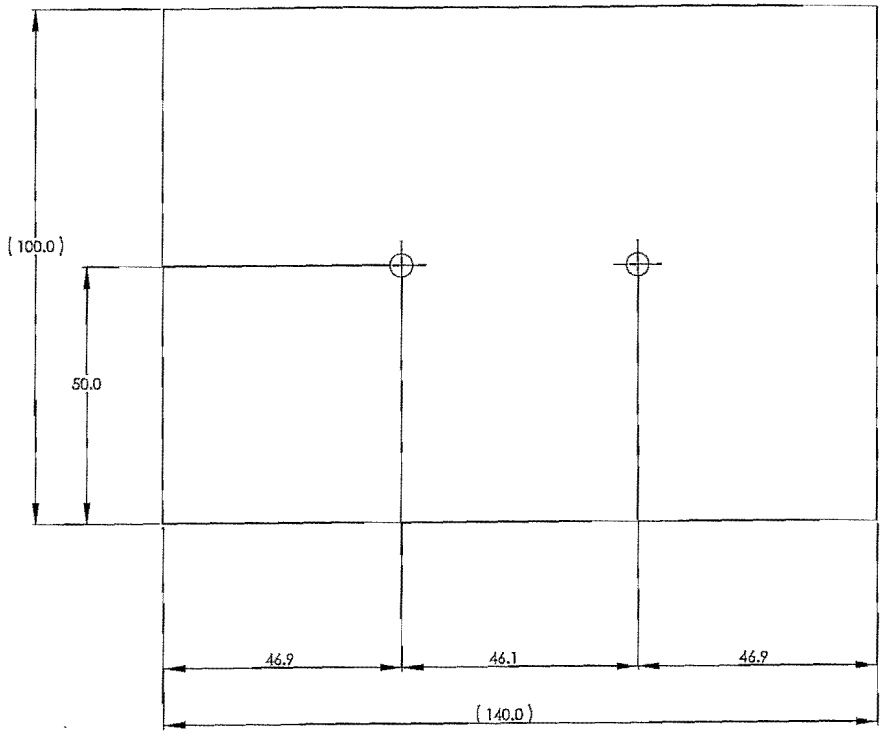

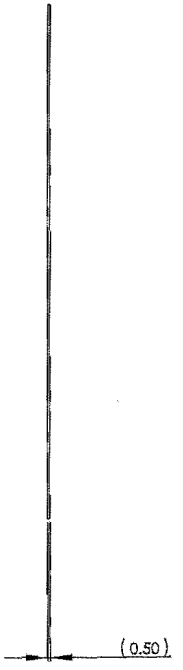

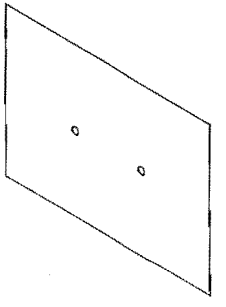

ILLUSTRATION

NOTE:
- RED BRASS SHEETS TO BE SUPPLIED
- QUANTITY = 8

DO NOT SCALE DRAWING	REVISION A
UNLESS OTHERWISE SPECIFIED: DIMENSIONS ARE IN MILLIMETERS SURFACE FINISH: TOLERANCES: LINEAR: ± 0.5MM ANGULAR:	TITLE: Red Brass 0.5mm Seal
MATERIAL: MILD STEEL	DWG NO. M.ING01-5W3-FR03-02 A2
SCALE:1:1	QUANTITY: 10

DETAIL A
SCALE 2 : 0.7

NOTE:
- DEPTH OF SLOTTED CUTS INTO MATERIAL = 4MM
- DIMENSIONS GIVEN IN DETAIL VIEW A IS TYPICAL FOR ALL SLOTS THAT ARE TO BE MACHINED.
- MATERIAL SUPPLIED (MILD STEEL)

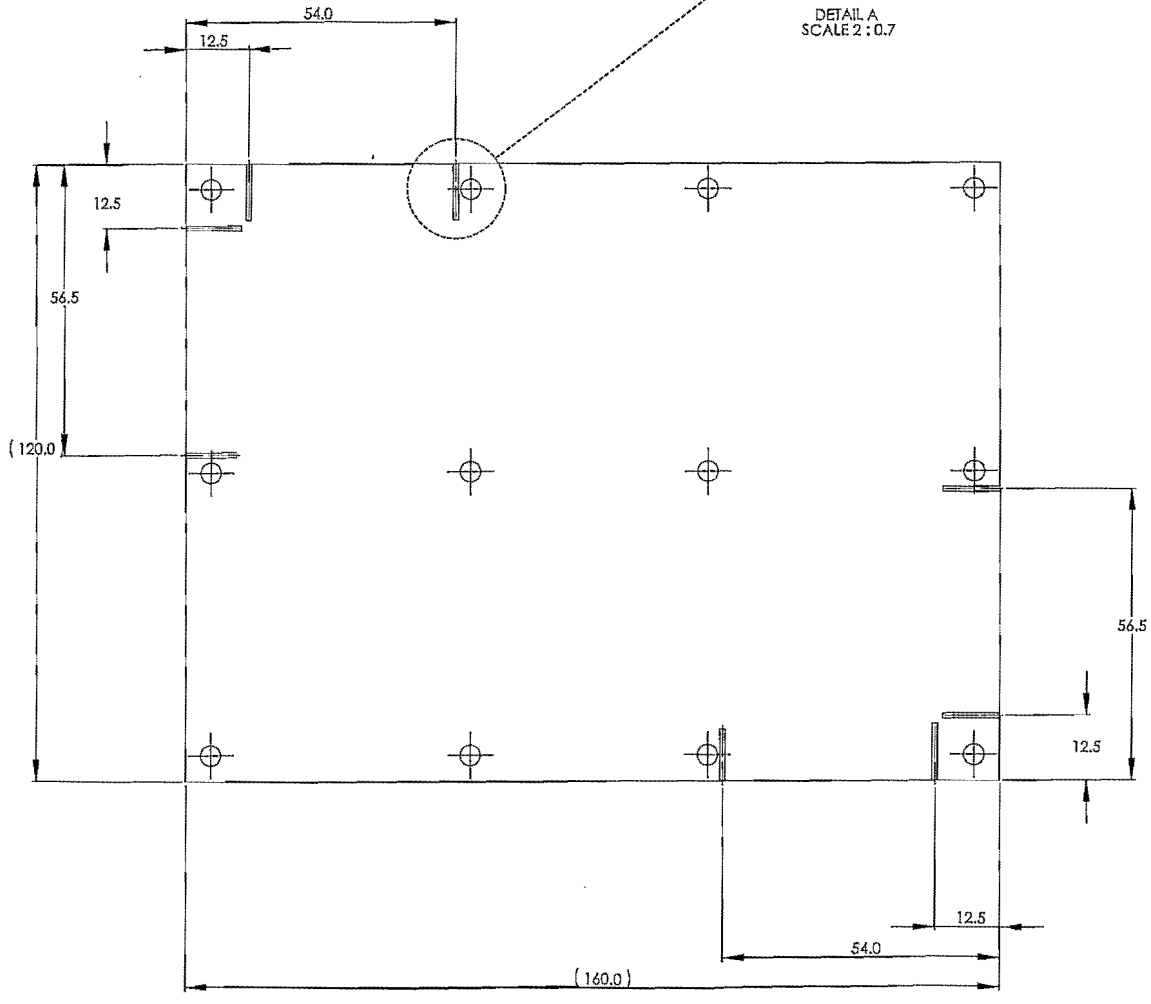

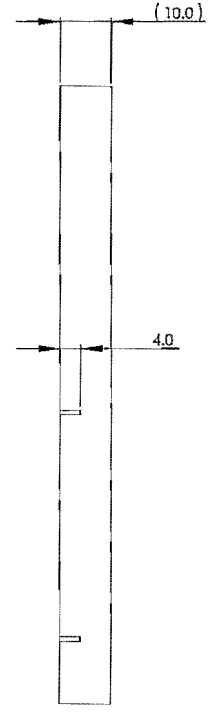

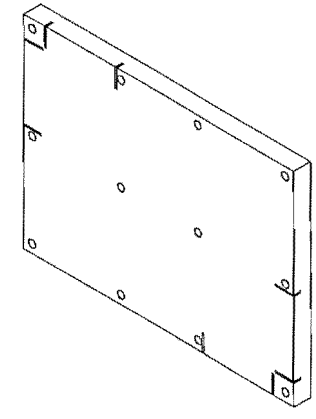

ILLUSTRATION

DO NOT SCALE DRAWING	REVISION A
UNLESS OTHERWISE SPECIFIED: DIMENSIONS ARE IN MILLIMETERS SURFACE FINISH: TOLERANCES: LINEAR: +- 0.1MM ANGULAR:	TITLE: Top Frame Clamper
MATERIAL: MILD STEEL	DWG NO. M.ING01-SW3-FR04-02 A2
SCALE:1/2	QUANTITY 1

NOTE:
- DEPTH OF SLOTTED CUTS INTO MATERIAL = 4MM
- DIMENSIONS GIVEN IN DETAIL VIEW A IS TYPICAL FOR ALL SLOTS THAT ARE TO BE MACHINED.
- MATERIAL SUPPLIED (MILD STEEL)

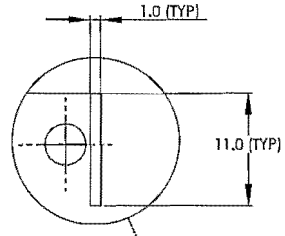

DETAIL A
SCALE 2 : 0.7

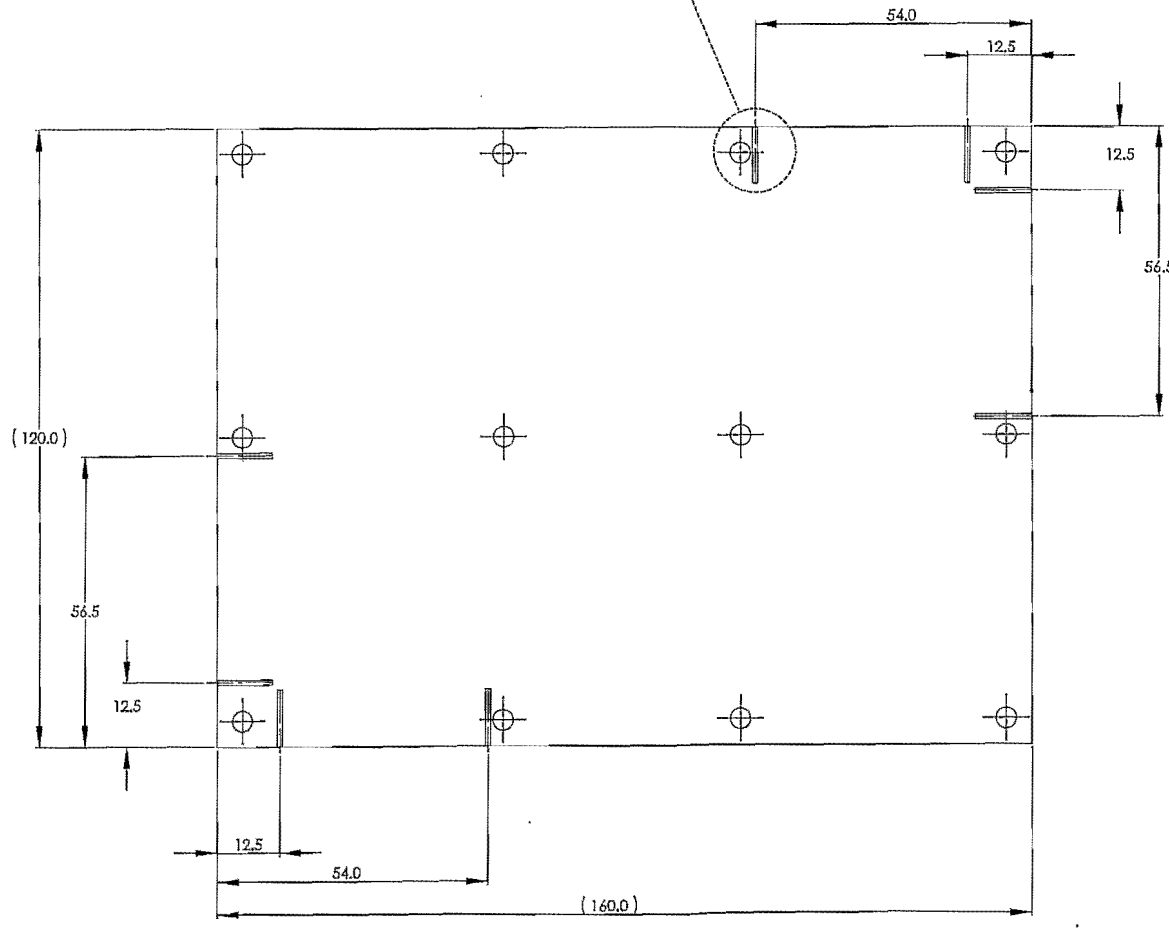

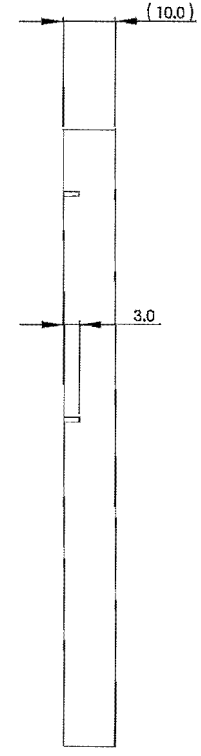

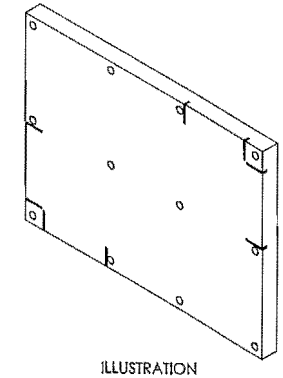

ILLUSTRATION

DO NOT SCALE DRAWING	REVISION A
UNLESS OTHERWISE SPECIFIED: DIMENSIONS ARE IN MILLIMETERS SURFACE FINISH: TOLERANCES: LINEAR: +-0.1MM ANGULAR:	TITLE: Bottom Frame Clamper
MATERIAL: MILD STEEL	DWG NO. M.ING01-5W3-FR05-02 A2
	SCALE:1:2 QUANTITY 1

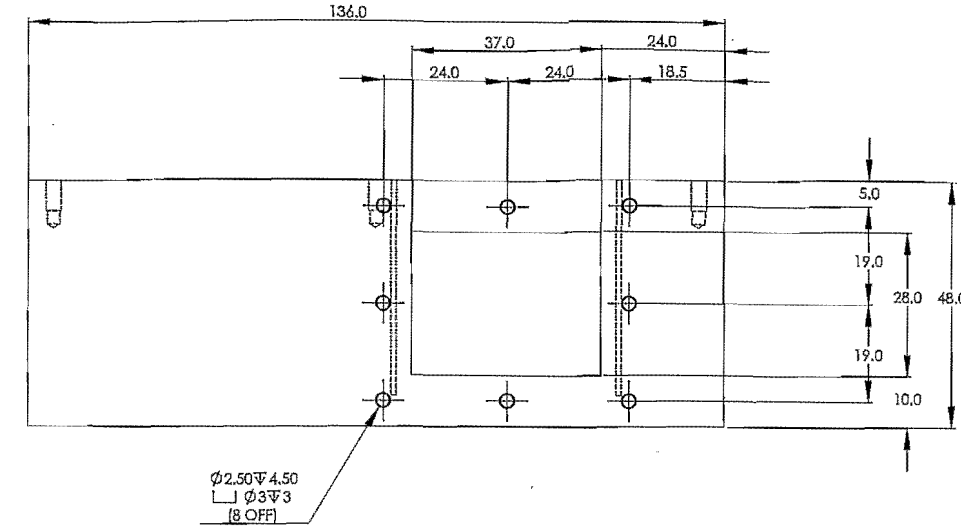

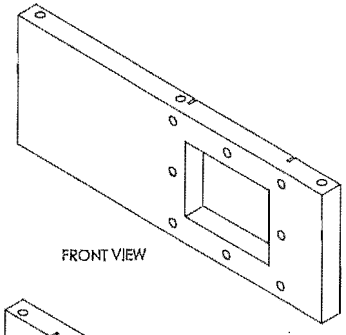

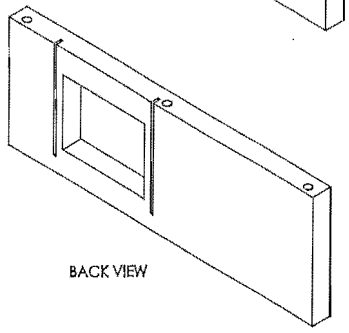

ILLUSTRATION

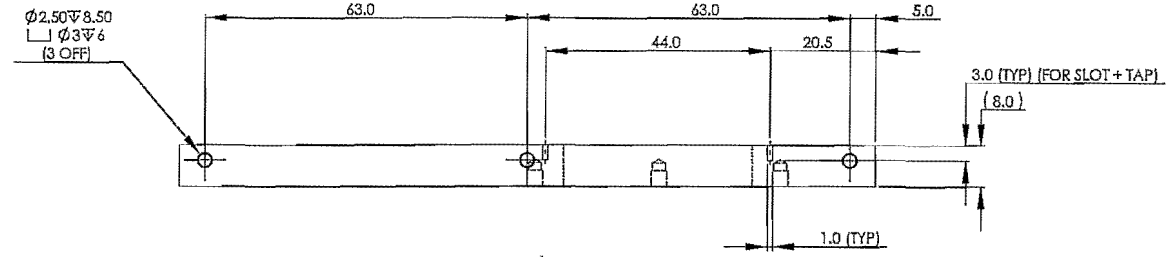

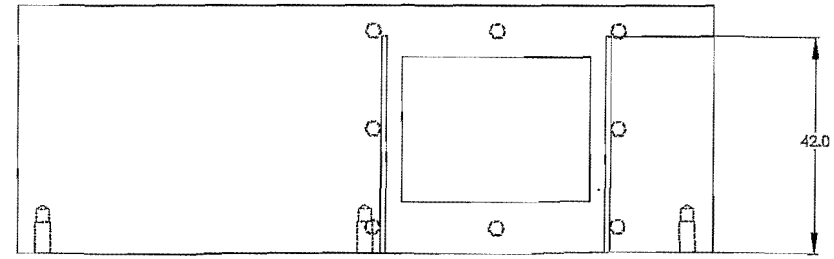

DO NOT SCALE DRAWING | REVISION A

UNLESS OTHERWISE SPECIFIED:
DIMENSIONS ARE IN MILLIMETERS
SURFACE FINISH:
TOLERANCES:
LINEAR: +/- 0.1MM
ANGULAR:

MATERIAL: MILD STEEL (MM)

TITLE: Header Box Plate -1

DWG NO. M.ING01-5W3-FR06-02 | A2

SCALE:1:1 | QUANTITY: 2

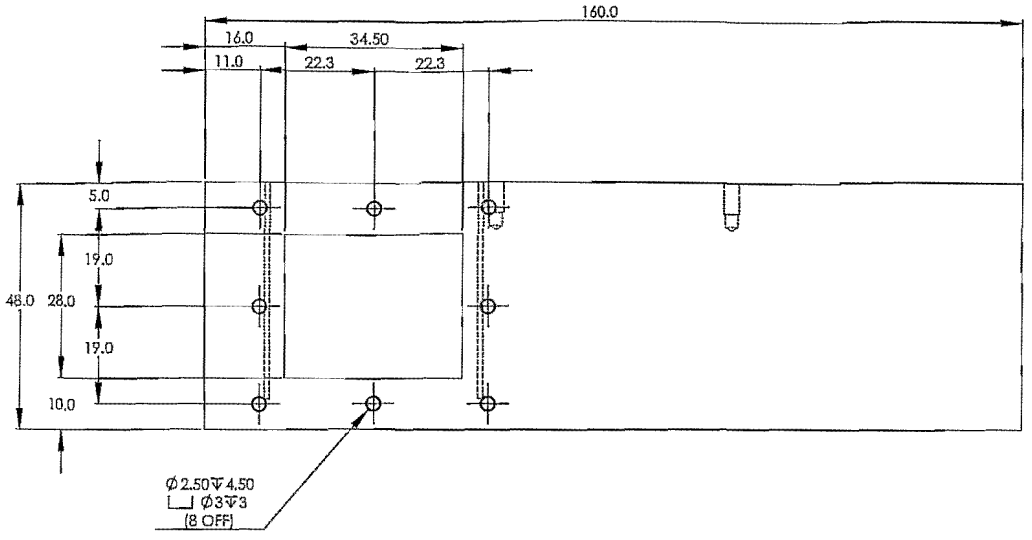

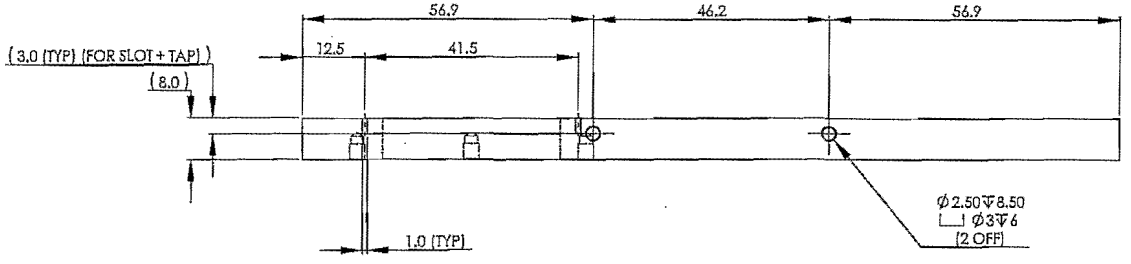

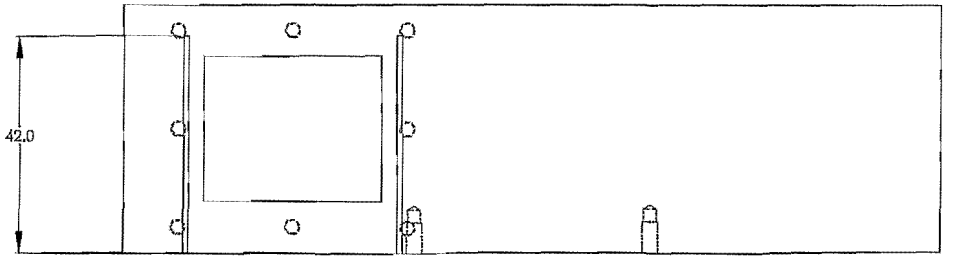

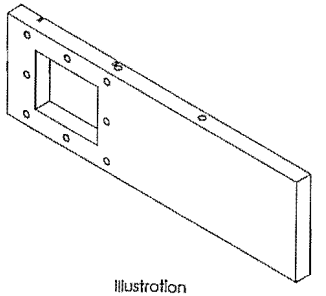

Illustration

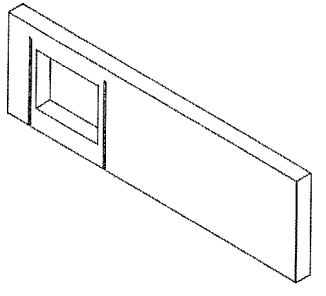

DO NOT SCALE DRAWING | REVISION A

UNLESS OTHERWISE SPECIFIED:
DIMENSIONS ARE IN MILLIMETERS
SURFACE FINISH:
TOLERANCES:
LINEAR: +/- 0.5MM
ANGULAR:

MATERIAL: MILD STEEL (8MM)

TITLE: Header Box Plate -2

DWG NO. M.ING01-5W3-FR07-02

A2

SCALE:1:1 | QUANTITY: 2

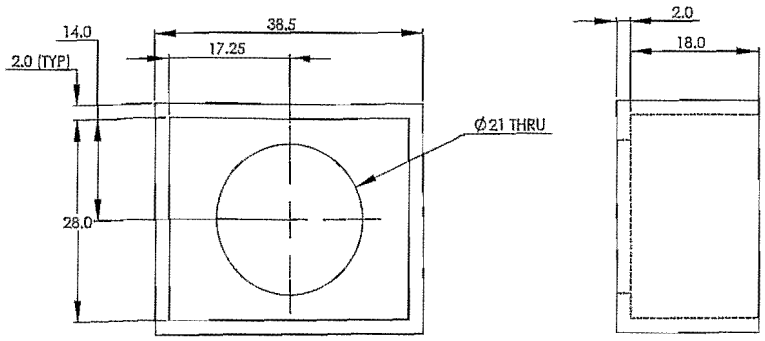

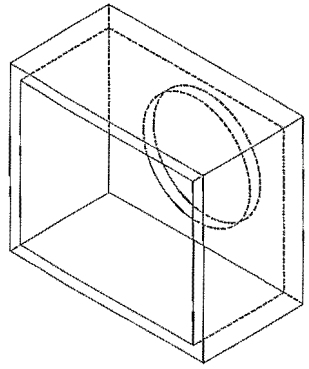

HEADER INLET A - PART 1

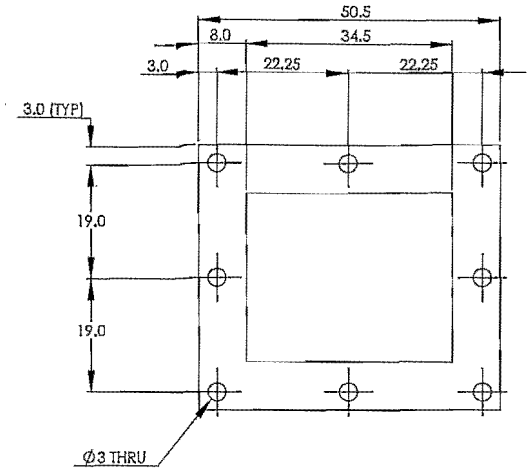

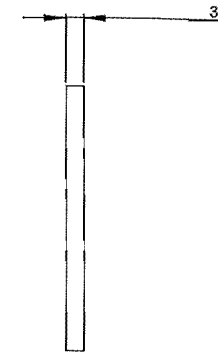

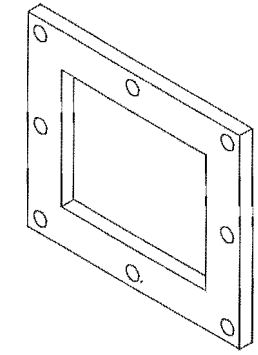

HEADER INLET A - PART 2

NOTE:

- WELD PARTS 1 & 2 TO EACHOTHER ON INTERFACE AS SHOWN.
- QUANTITY = 2
- SURFACE A SHOULD BE MAINTAINED FLAT
- WELD OCCURS ON SURFACE B

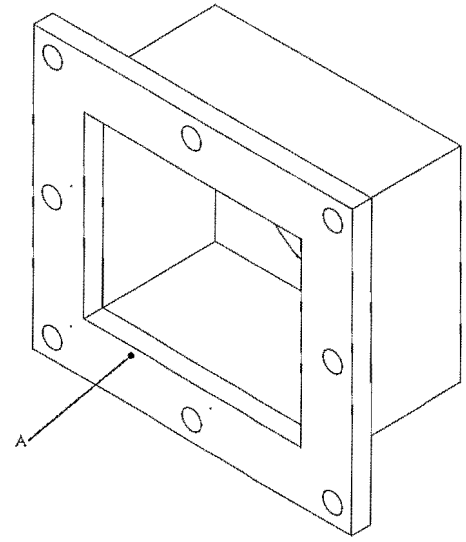

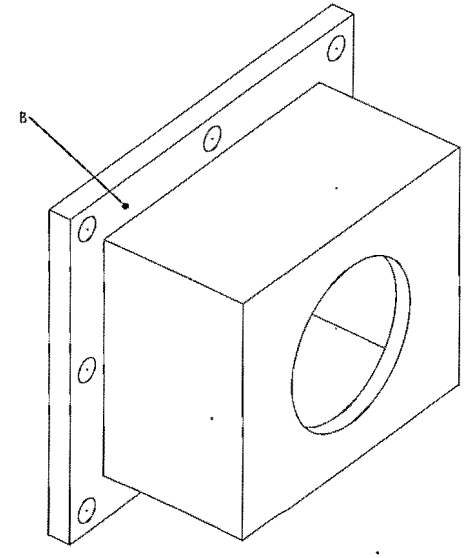

DO NOT SCALE DRAWING	REVISION A
UNLESS OTHERWISE SPECIFIED: DIMENSIONS ARE IN MILLIMETERS SURFACE FINISH: TOLERANCES: LINEAR +-0.1MM ANGULAR:	TITLE: Header Inlet - A
MATERIAL: MILD STEEL	DWG NO. M.ING01-5W3-FR08-02 A2
SCALE:2:3	QUANTITY: 2

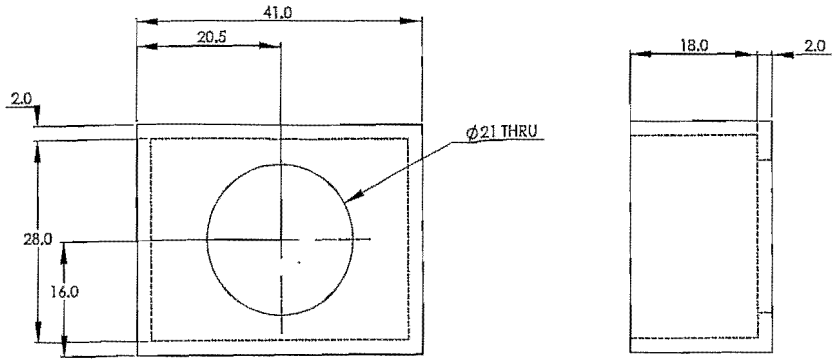

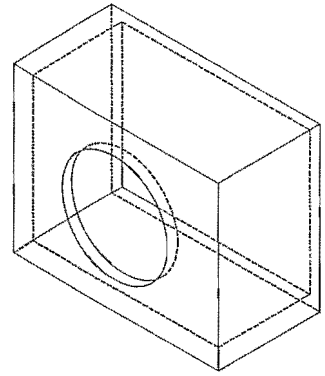

HEADER INLET B - PART 1

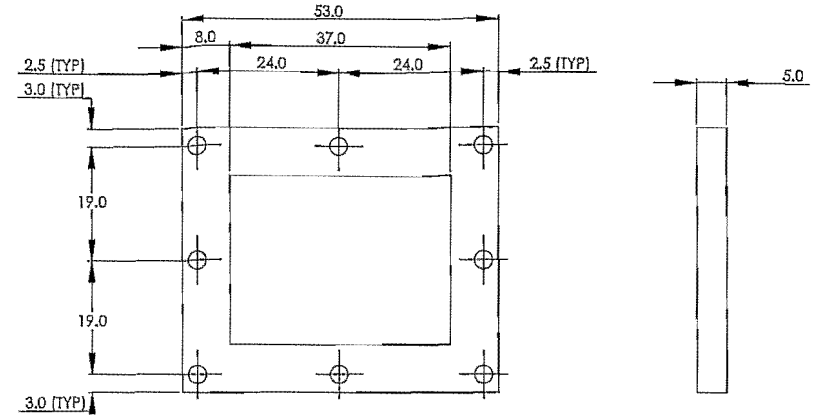

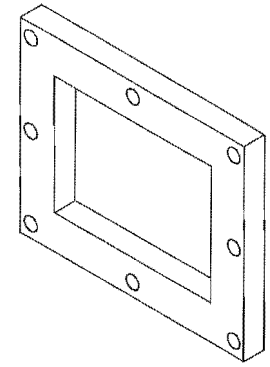

HEADER INLET B - PART 2

NOTE:
- WELD PARTS 1 & 2 TO EACH OTHER ON INTERFACE AS SHOWN
- QUANTITY = 2
- SURFACE A SHOULD BE MAINTAINED FLAT
- WELD OCCURS ON SURFACE B

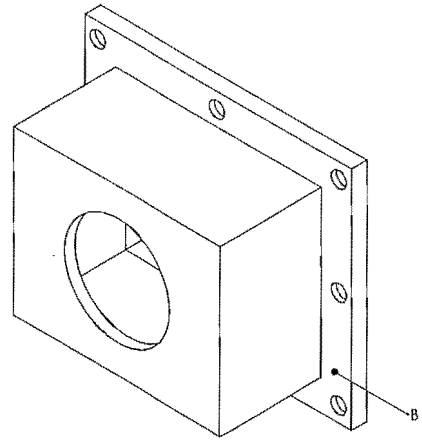

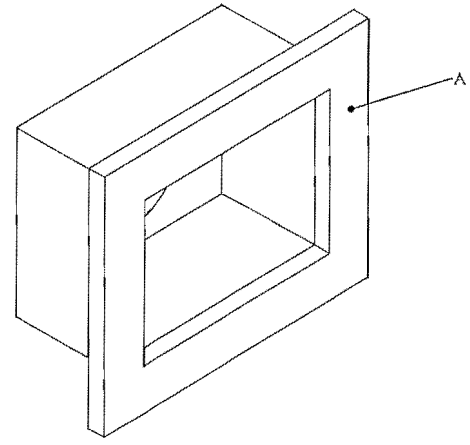

DO NOT SCALE DRAWING | REVISION A

UNLESS OTHERWISE SPECIFIED:
DIMENSIONS ARE IN MILLIMETERS
SURFACE FINISH:
TOLERANCES:
LINEAR: +-0.1MM
ANGULAR:

MATERIAL: MILD STEEL

TITLE: Header Inlet - B

DWG NO. M.ING01-5W3-FR09-02

A2

SCALE: 1 | QUANTITY: 2

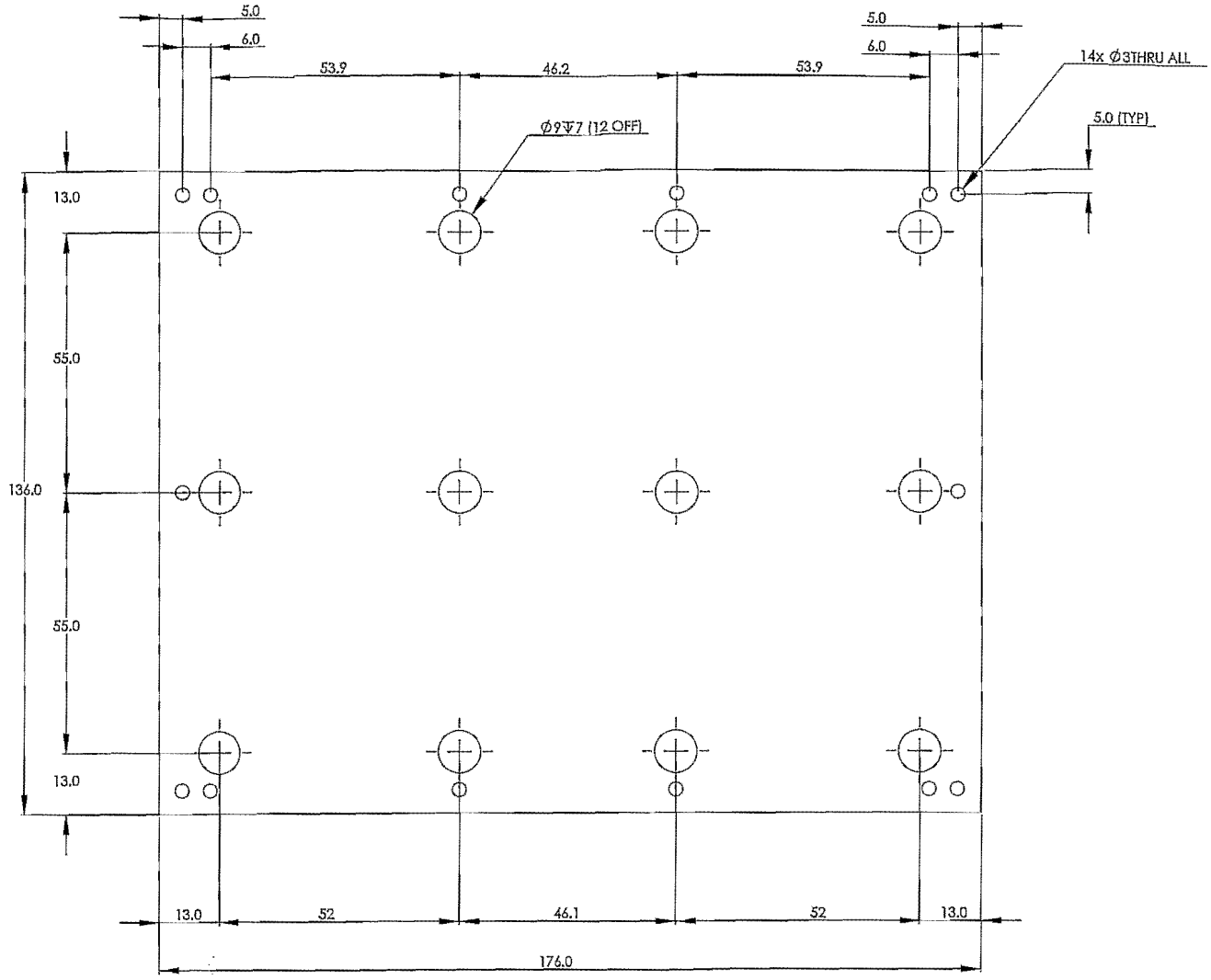

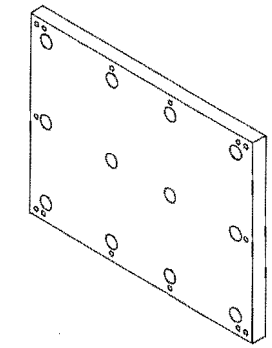

ILLUSTRATION

DO NOT SCALE DRAWING | REVISION A

UNLESS OTHERWISE SPECIFIED:
DIMENSIONS ARE IN MILLIMETERS
SURFACE FINISH:
TOLERANCES:
LINEAR: +/- 0.1MM
ANGULAR:

MATERIAL: MILD STEEL (10MM)

TITLE: Header Box Bottom Plate

DWG NO. M.ING01-5W3-FR 10-02

A2

SCALE: 1:1 | SHEET 1

FRONT VIEW OF 'HEADER BOX TOP'

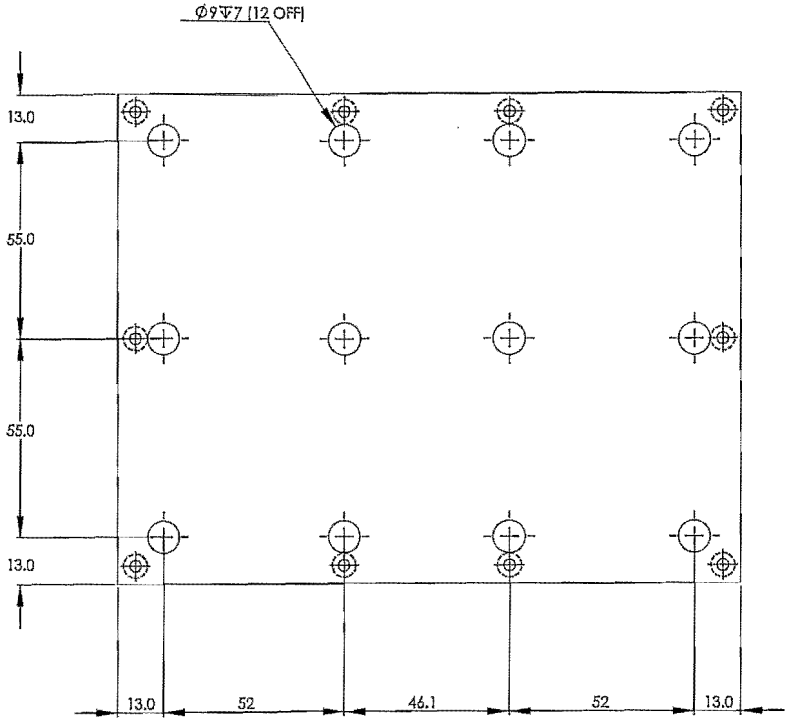

BACK VIEW OF 'HEADER BOX TOP'

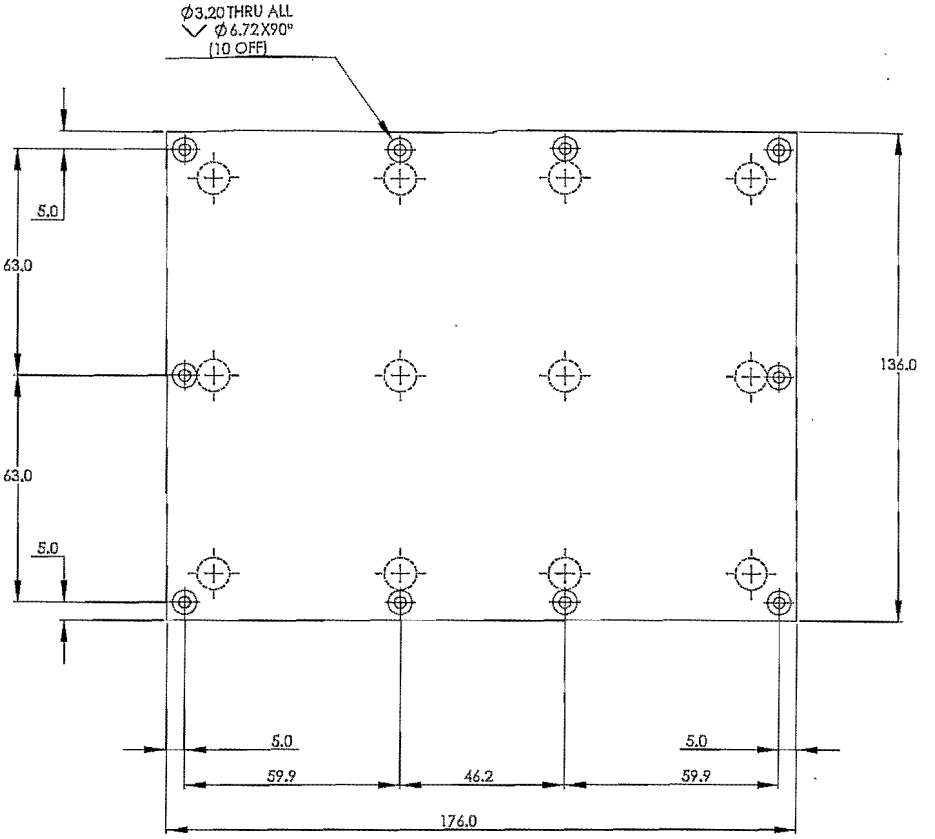

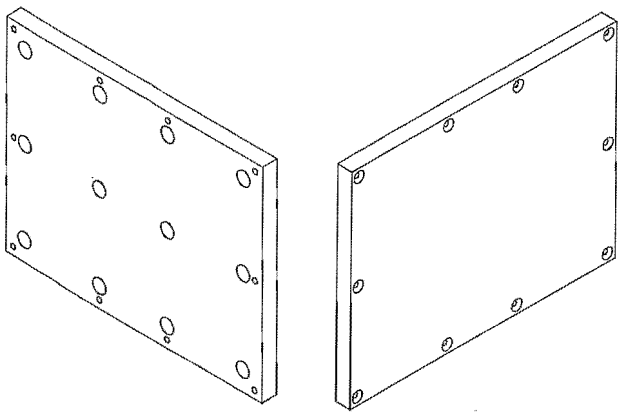

ILLUSTRATION

DO NOT SCALE DRAWING	REVISION A
UNLESS OTHERWISE SPECIFIED: DIMENSIONS ARE IN MILLIMETERS SURFACE FINISH: TOLERANCES: LINEAR: ±0.1MM ANGULAR:	TITLE: Header Box Top
MATERIAL: MILD STEEL (10mm)	DWG NO. M.ING01-5W3-FR11-02
	A2
	SCALE:1:2 QUANTITY: 1

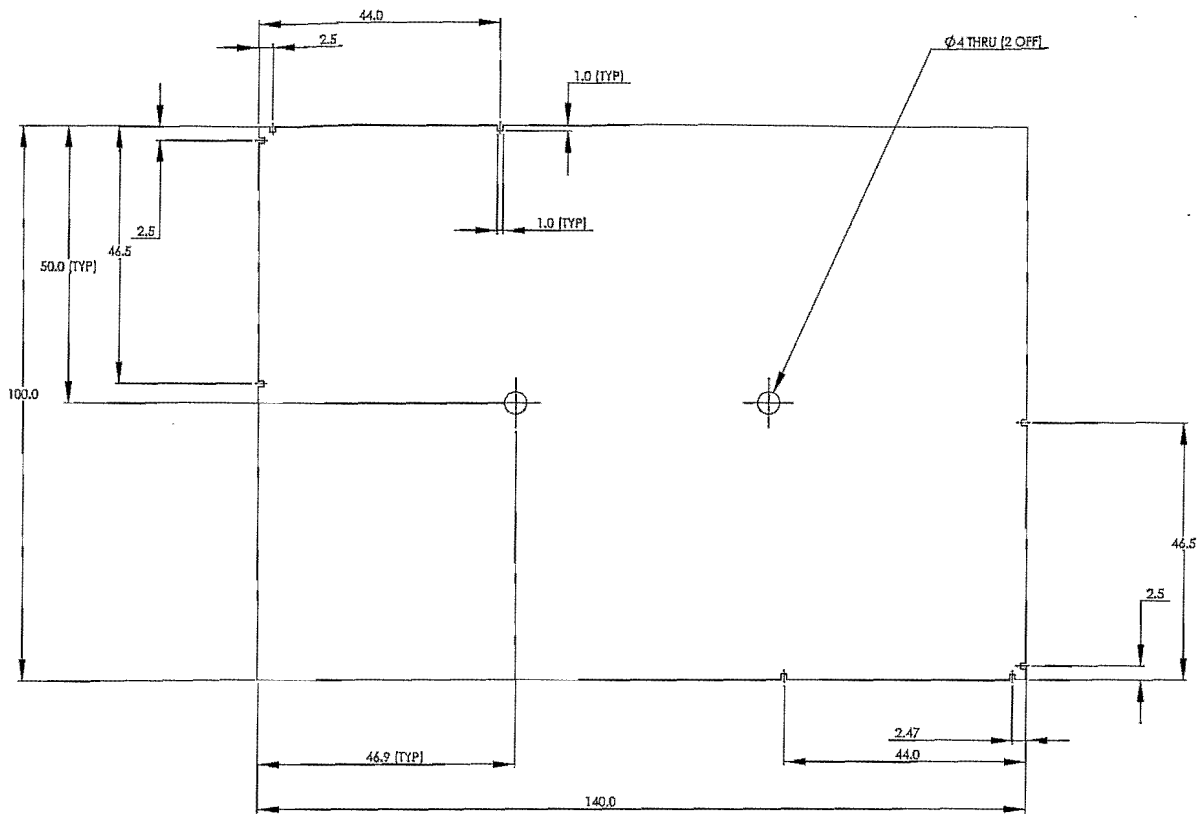

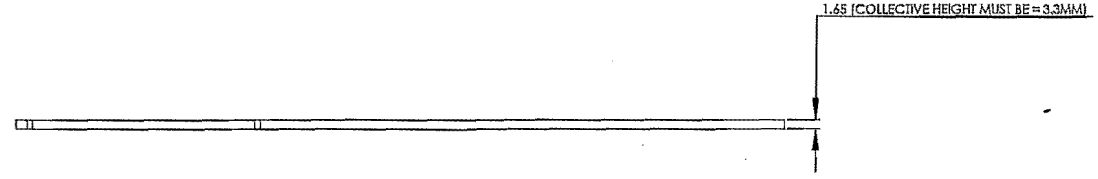

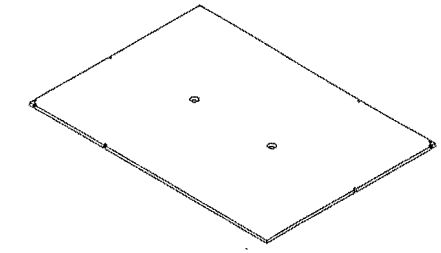

ILLUSTRATION

DO NOT SCALE DRAWING	REVISION
UNLESS OTHERWISE SPECIFIED: DIMENSIONS ARE IN MILLIMETERS SURFACE FINISH: TOLERANCES: LINEAR: +- 0.1MM ANGULAR:	TITLE: SLOTTED HEIGHT INSERTS
MATERIAL: ALUMINUM	DWG NO. M.ING01-5W3-FR 12-02
SCALE: 1/1	QUANTITY: 2

Bibliography

[1] Schleicher, R., Raffray, A.R. & Wong, C.P. An Assessment of the Brayton Cycle for High Performance Power Plants. *Fusion Technology*, Vol. 39 (2), 2001.

[2] McDonald, C.F. Recuperator Considerations for Future Higher Efficiency Microturbines. *Journal of Applied Thermal Engineering,* Vol.23, 2003.

[3] *Diffusion Bonded Heat Exchangers.* URL: www.heatric.com/diffusion_bonded_ exchangers.htm Retrieved July 2005.

[4] Krishnan, J., Bhanumurthy, K., Gawde, P.S., Derose, J., Kale, G.B. & Srikrushnamurthy, G. Manufacture of a matrix heat exchanger by diffusion bonding. *Journal of Materials Processing Technology.* Vol.66, 1997.

[5] Van Greuning, J. *Material Selection and Optimization of a High-Temperature Compact Heat Exchanger.* M.Eng. dissertation, North-West University, 2006.

[6] McDonald, C.F. Low-cost compact primary surface recuperator concept for microturbines. *Journal of Applied Thermal Engineering*, Vol. 20, 2000.

[7] McDonald, C.F. & Wilson, D.G. The Utilization of Recuperated and Regenerated Cycles for High Efficiency Gas Turbines in the 21st Century. *Journal of Applied Thermal Engineering,* vol. 16, no. 8/9, 1996.

[8] Utriainen, E. Investigation of Some Heat Transfer Surfaces for Gas Turbine Recuperators. Phd.Eng dissertation, Department of Heat and Power Engineering Division of Heat Transfer; Division of Heat Transfer. 2001.

[9] Reay, D. Compact Heat Exchangers, Enhancement and Heat Pumps. *International Journal of Refrigeration,* Vol. 25, 2002.

[10] Gezelius, K. Design of Compact Intermediate Heat Exchangers for Gas Cooled Fast Reactors. MSc.Eng dissertation. Department of Nuclear Engineering, Massachussetts Institute of Technology, 2004.

[11] Anxionnaz, A., Cabassud, M., Gourdan, C & Tochon, P. Heat exchanger/reactors (HEX reactors): Concepts, technologies: State-of-the-art. Chemical Engineering and processing, Vol. 47, 2008.

[12] Phillips, C.H. & Symonds, K.T. Development of a novel integrated chemical reactor-heat exchanger, Paper presented at Sixth HEXAG (Heat Exchanger Action Group) meeting, 1996

[13] Omatete, O.O., Pint, B.A., Stinton, D.P. & Maziasz, P.J. Assessment of Recuperator Materials for Microturbines. Metals and Ceramics Division, Oak Ridge National Laboratory. Oak Ridge, Tennessee. 2000.

[14] Pint, B.A. Recuperator Alloys - Composition Optimization for Corrosion Resistance. Metals and Ceramics Division, Oak Ridge National Laboratory . Oak Ridge, Tennessee. 2003.

[15] Maziasz, P., Pint, B.A., Swindeman, R.W., More, K.L., & Santella, M.L. Advanced alloys for high temperature recuperators. Metals and Ceramics Division, Oak Ridge National Laboratory. Oak Ridge, Tennessee. 2003.

[16] Natesan, K., Purohit, A. & Tam, S.W. Materials Behavior in HTGR Environments. Manuscript prepared for Engineering Technology. 2003.

[17] PYROID® Pyrolytic Graphite. URL: www.minteq.com/our-products/minteq-pyrogenics-group/pyroidR-pyrolytic-graphite/ Retrieved August 2005.

[18] Carbon-Carbon composites: Fiber Materials.Inc. URL: http:///www.fibermaterialsinc.com/index.html/ Retrieved August 2007.

[19] Cook, J.L. & Crawford, J.A. "Multidirectional substrates for advanced composites". 76th Annual Meeting of the American Ceramic Society, March.1975.

[20] Das, J., Chakraborty, A., Bagchi, T.P. & Sarma, B. Improvement of machinability of tungsten by copper infiltration technique. *International Journal of Refractory Metals and Hard Materials,* Vol. 26, 2008.

[21] Todd, R.H. Manufacturing Processes Reference Guide. 1994. (Retrieved by agreement with Industrial Press Inc on 2 November 2006).

[22] Electrical Discharge Machining (EDM) Design Considerations Process Capabilities. URL: http://www.engineersedge.com/edm.shtml. Retrieved 10 February 2007.

[23] Electrical Discharge Machining. URL: www.answers.com/topic/electrical-discharge-machining.html. Retrieved 10 February 2007.

[24] Electrical Discharge Machining and Surface Alloying – The Process, Parameters and State of Play. URL: http://www.azom.com/details.asp?ArticleID=2082. Retrieved 10 February 2007.

[25] About Electrical Discharge Machines (EDM). URL: www.process-equipment.globalspec.com Retrieved 10 February 2007.

[26] Nobili, A. *Explosion Bonding Process.* Nobelclad Technical Bulletin NT 200, Nobelclad Rivesaltes plant – France. 2002.

[27] Joshi, A. Introduction to Explosion Welding. Department of Metallurgical Engineering & Material Science, Indian Institute of Technology - Bombay. 2003.

[28] Explosive welding and manufacturing process and product features. URL: http:///www.asahi-kasei.co.jp/baclad/en/process.html. Retrieved 15 August 2007.

[29] Garret, B.R., Blank, G.F. & Ranadive, A.J. Broad Applications of Diffusion Bonding. NASA Contractor Report. National Aeronautics & Space Administration, 1966.

[30] Lee, H-S., Yoon, J-H., Yi, Y-M. Solid State Diffusion Bonding of Titanium alloys. Solid State Phenomena Vol. 124-126. 2007.

[31] Wittenborn, G. Diffusion Bonding. 1st Annual KU Aerospace Materials and Processes "Virtual" Conference. University of Kansas, 2001.

[32] Friedrich, C. Designing Fastening Systems. RIBE Verbindungstechnik GmbH, Schwabach, Germany. 2002.

[33] Incropera, F.P. & De Witt, D.P. Fundamentals of Heat and Mass Transfer. Fifth Edition. New York, London, Sydney: John Wiley and Sons Inc. 2002.

[34] Naterer, G.F. Heat Transfer in Single and Multiphase Systems. Boca Raton, Fla.: CRC Press. 2003.

[35] Pitts, D. & Sissom, L. *Schaum's Outline of Theory and Problems of Heat Transfer*, Second Edition. New York: McGraw-Hill, 1998.

[36] Rousseau, P.G. *Thermal Fluid Systems Modelling.* Faculty of Engineering, North-West University. 2005.

[37] Ramesh, K.S. & Dusan, P.S. *Fundamentals of Heat Exchanger Design,* New Jersey; John Wiley & Sons, Inc., 2003.